HOKKAIDO UNIVERSITY

Title	Future projection on Siberian wildfire and its aerosol emissions by the improved fire module of Spatially Explicit Individual Based Dynamic Global Vegetation Model
Author(s)	Nurrohman, Reza Kusuma
Degree Grantor	北海道大学
Degree Name	博士(農学)
Dissertation Number	甲第16101号
Issue Date	2024-09-25
DOI	https://doi.org/10.14943/doctoral.k16101
Doc URL	https://hdl.handle.net/2115/93890
Type	doctoral thesis
File Information	Reza_Kusuma_Nurrohman.pdf

Hokkaido University Collection of Scholarly and Academic Papers : HUSCAP

Future projection on Siberian wildfire and its aerosol emissions by the improved fire module of Spatially Explicit Individual Based Dynamic Global Vegetation Model

空間明示的個体ベース動的全球植生モデルの改良型火災モジュールによるシベリア林野火災とそれによるエアロゾル排出量の将来予測

Hokkaido University　Graduate School of Agriculture

Frontiers in Environmental Sciences　Doctoral Course

Reza Kusuma Nurrohman

ABSTRACT

Wildfire is one of the most significant disturbances, globally affecting biogeochemical cycles, atmospheric chemistry, carbon cycle, and ecosystem structure and function. The effects of wildfires are becoming increasingly severe due to climate change, it is estimated that the global mean CO_2 emission intensity has increased by 0.9 ± 0.9% $year^{-1}$ from 2000 to 2019. Siberia has the largest forest biome and one-third of global forest cover and one of among the regions impacted by intense wildfires annually that affects the atmosphere–land interactions of the global climate. Modeling of fire regimes using dynamic global vegetation models (DGVMs) is a key approach to analyzing these factors. However, including interactive fire disturbances in vegetation models is critical for accurately simulating vegetation dynamics. Therefore, in this study, the widely used process based SPread and InTensity of FIRE (SPITFIRE) module was integrated into the spatially explicit individual-based dynamic global vegetation model (SEIB-DGVM) to predict fire, vegetation, and burned biomass emission variables in Siberia in the future.

The SEIB-DGVM was modified to add two new input variables for fire ignition: population and lightning data, and then integrated the complete SPITFIRE equation. The model was run in three phases under fire-on and fire-off mode and each phase repeated 5 time: 1) a 1000-year spin-up phase to bring the soil and vegetation carbon pools into equilibrium using daily baseline Climatic Research Unit Time Series (CRU TS)3.22 climate data, 2) a 156-year historical phase also using daily baseline CRU TS3.22 climate data, and 3) a 95-year future phase using daily MIROC-AR5 base V3 RCPs 8.5, 6.0, 4.5, and 2.6 climate data. Finally, to ensure that the simulation results and the projections data are in line with the observational data, the model outputs validated by using Global Fire Emissions Database 4 (GFED4), GFED4s, European Space Agency's (ESA) Biomass Climate Change Initiative (CCI) and Global Biomass Burning Emissions Inventory (GBEI) benchmark datasets.

The model is able to reproduce historical data that well compared to the benchmark datasets. Overall, on spatial comparison, the model is able to produce data with the same distribution pattern with a value of 70.7% compared to the benchmark datasets. Numerically and on a long-term average, the model is able to produce values with very high accuracy of around 99% compared with the benchmark datasets. The model estimated that until 2100, Siberia will continue to experience an increase in the frequency of forest fires. Under the RCP8.5 climate scenario, the CO_2, CO, $PM_{2.5}$, total particulate matter (TPM), and total particulate carbon (TPC) emissions in Siberia will continue to increase annually until 2100 by 0.295 ± 0.08 % $year^{-1}$ or individually by 189.66 ± 6.55, 15.18 ± 0.52, 2.47 ± 0.09, 1.87 ± 0.06, 1.30 ± 0.04 Tg species $year^{-1}$, respectively. Under the same climate scenario and period

comparison, we estimated that the number of trees burnt increased by 100 %, resulting in a 385.19 ± 40.4 g C m^{-2} $year^{-1}$ loss of net primary production (NPP).

The model modifications have led to a more realistic depiction of fire frequency, intensity, and extent, aligning the model outputs more closely with benchmark datasets. The major variables reached an agreement of 70.7% or greater with the observations. Additionally, the improved model accurately simulated forest structure, increasing the agreement between the simulated and observed dataset patterns and further emphasizing the reliability of the model and its emission projections.

TABLE OF CONTENTS

1. INTRODUCTION

1.1. Background

Fires are among the most significant disturbances affecting biogeochemical cycles, atmospheric chemistry, the carbon cycle, and ecosystem structure and function worldwide (Pickett et al., 1999). Wildfires are also the dominant climate-driven disturbance agent in boreal forests (Goldammer and Furyaev, 1996; Shorohova et al., 2011; De Groot et al., 2013), shaping major forest cover in Russia (Krylov et al., 2014) and rapidly increasing burned area and emission intensity in Canada and Alaska (Zheng et al., 2021). Fires influence vegetation dynamics by enabling plants to adapt to fire regimes, which in turn affects vegetation productivity, litter, and fuel load (Cochrane, 2003; Bergeron et al., 2004; Whelan, 2009). The intensity and frequency of large-scale boreal forest fires are expected to increase in the future due to increased global temperatures, drier conditions, and longer fire seasons, which will cause more emissions from biomass burning (Flannigan et al., 2009; Gauthier et al., 2015) and human activity by using fire for land management (e.g. use of fire as a tool in the deforestation process) (Hantson et al., 2016; Archibald et al., 2013; Morton et al., 2008). Globally, from 2000 to 2019, satellites detected a decrease in the burned area of grassland, while there was a slight increase in the area of forest fires in Russia (Zheng et al., 2021). Europe, France, Spain, Portugal, and Greece are already experiencing larger and more devastating fires (Carnicer et al., 2022). Not only large fires but also small fires have a significant impact: Areas burned by small fires contributed 35% to the total burnt area, from 345 Mha $year^{-1}$ to 464 Mha $year^{-1}$, and related carbon emissions increased from 1.9 Pg C $year^{-1}$ to 2.5 Pg C $year^{-1}$ from 2001-2010 (Randerson et al., 2012). This finding is in line with current studies reporting that the global mean CO_2 emission intensity has increased by 0.9 ± 0.9% $year^{-1}$ from 2000 to 2019 (Zheng et al., 2021) and that the Fire Weather Index (FWI) reached levels above 30, corresponding to high, very high, and extreme levels of fire frequency, causing CO_2 emissions to increase in Europe since 1980 (Carnicer et al., 2022).

Forest fires are important ecological factors that influence both the establishment and succession of vegetation (Abaimov and Sofronov, 1996). Climate-driven large fires are responsible for rapid changes in vegetation (Cleve and Viereck, 1981), soil properties (Pastor and Post, 1986; Pellegrini et al., 2021), biogeochemical cycling, microclimate, forest ecosystems (Crutzen and Goldammer, 1993), productivity, stability, and many other ecological properties (Melillo et al., 1993). Forest fires also indirectly affect vegetation

dynamics by increasing CO_2 levels in the atmosphere (Seiler and Crutzen, 1980; Nguyen and Wooster, 2020), as CO_2 is one of the primary products of biomass combustion and is emitted in all phases of fire (ignition, flaming, glowing, pyrolysis, and extinction) (Andreae and Merlet, 2001), with the flaming phase leading to emissions (Lobert et al., 1991; Ward and Hardy, 1991). Thus, it is challenging to estimate CO_2 emissions due to the forest fires because they are generated in large quantities during biomass combustion and because of the different emission timelines produced during each combustion stage. Increasing atmospheric CO_2 concentrations alter the global carbon cycle by causing global warming (Van Der Werf et al., 2006, 2010, 2017; Neto et al., 2009; Kaiser et al., 2012; Lin et al., 2013), and the resulting global warming is expected to intensify extreme fire seasons, leading to further surges in carbon emissions that significantly contribute to the global burden of greenhouse gases (fire-climate feedbacks) (Bowman et al., 2009). This event also affect the agricultural sector positively and negatively depending on the region, environment, and crop types (Kimball and Idso, 1983). Additionally, prolonged exposure to very high CO_2 concentrations at ground level has negative impacts on health (Jacobson et al., 2019). Therefore, accurate modeling of future wildfires and their emissions is required to understand the associated risks.

Boreal vegetation store between 17% of the world's carbon, yet encompasses almost 30% of all terrestrial carbon stocks (Kasischke, 2000; Gauthier et al., 2015), and two-thirds are located in Siberia, Russia (Shvidenko and Nilsson, 2003). In Siberia, burned biomass emissions approached 0.4 Gt C $year^{-1}$ in 2021, three times the average value between 1997 and 2020, according to GFED4s (Friedlingstein et al., 2020). Kharuk et al., (2022) also stated that the decadal frequency of wildfires tripled between 2001–2010 and 2011–2020. Catastrophic boreal forest fires are expected to continue to increase in the future due to increased global temperature, drier conditions, and longer fire seasons, and these fires will increase the severity and emissions produced from biomass burning (Flannigan et al., 2009). Burning vegetation is a major source of black carbon (BC), carbon monoxide (CO) (Forster, P. et al., 2018), and particulate matter (PM) (Reddington et al., 2016). According to records from the Copernicus Atmosphere Monitoring Service (CAMS), Russia experienced a drastic increase to 8 megatons (Mt) in $PM_{2.5}$ emissions in 2021, which is 78% higher than the average level between 2004 and 2021 (4.5 Mt) (Romanov et al., 2022). Furthermore, an increase in atmospheric emissions negatively affects the climate by contributing to global warming and climate change (Randerson et al., 2006; Westerling et al., 2006; Bowman et al.,

2009) and affect weather systems by modulating solar radiation and cloud properties (Schultz et al., 2008).

Understanding how long-term climate change, fire regimes, and forest vegetation interact under multiple climate scenarios is critical for forecasting forest succession trends (Clark and Richard, 1996). Modeling of fire regimes using dynamic global vegetation models (DGVMs) is a key approach to analyzing these factors. However, including interactive fire disturbances in vegetation models is critical for accurately simulating vegetation dynamics (Thonicke et al., 2001). A well-structured process-based fire module can accurately assess fire activity, consumed biomass due to fire, and biomass burning emissions. The assessment of each fire-related variable is interconnected with another variable, so the module must be well constructed because the amount of consumed biomass during forest fires can vary significantly. Several factors affect burned biomass, such as spatial and temporal variations in burned area based on ignition factors, the quantity and quality of the fuels available, and vegetation or plant functional type (PFT); additionally, every PFT reacts differently to fire disturbance (Cramer et al., 2001; Ito, 2011). Since the first global fire models were integrated into dynamic global vegetation models (DGVMs) two decades ago, the variety and complexity of fire models have expanded (Hantson et al., 2016). The Fire Modeling Intercomparison Project (FireMIP) compared eleven current fire models by structure and simulation protocols, using a benchmarking system to evaluate the models (Rabin et al., 2017). The results indicate that models that explicitly distinguish ignition factors, such as lightning and human-caused “ignition events”, as well as physical properties and processes that determine fire spread and intensity by plant functional type (PFT), performed better. One such fire module is SPITFIRE (an upgrade of GlobFIRM) (Thonicke et al., 2010), which has been used in several DGVMs: LPJ-GUESS-SPITFIRE, ORCHIDEE-SPITFIRE, JSBACH-SPITFIRE, and LPJ-LMfire. In this study, we integrated the SPITFIRE fire module into the spatially explicit individual-based dynamic global vegetation model (SEIB-DGVM) to predict fire, vegetation, and burned biomass emission variables in Siberia in the future. We selected the SEIB-DGVM because of its high-quality biogeochemical model coupled with a three-dimensional representation of forest structure where individual trees compete for light and space (Sato et al., 2007). The SEIB-DGVM processes physical, physiological, and vegetation dynamics and was previously used for reconstructing the geographical distributions of fundamental plant productivity properties (Sato et al., 2020), evaluating the geographic and environmental heterogeneity of larch forests with a special focus on

topography (Sato and Kobayashi, 2018), and assessing the impacts of global warming on Siberian larch forests and their interactions with vegetation dynamics and thermohydrology (Sato et al., 2016). The SEIB-DGVM accurately simulates forest ecology after typhoon disturbances (Wu et al., 2019), nonstructural carbohydrate dynamics (Ninomiya et al., 2023), and masting in a temperate forest (Végh and Kato, 2024).

The original fire module of the SEIB-DGVM utilizes the Glob-FIRM fire module from Thonicke et al., (2001), which has several limitations. For instance, it does not account for human-altered fire regimes or other land use impacts (Thonicke et al., 2001). In addition, Glob-FIRM derives the burnt fractional area of a grid cell from the simulated length of the fire season and from the minimum annual fuel load; this method does not specify ignition sources and assumes a constant fire-induced mortality rate for each plant functional type (PFT) (Thonicke et al., 2010). Therefore, updating from Glob-FIRM to SPITFIRE, which explicitly considers ignition factors such as lightning and human-caused ignition, is essential for accurately estimating fire dynamics and the resulting burned biomass emissions. To improve the fire simulations with the SEIB-DGVM, we replaced its fire module with the SPITFIRE model (Thonicke et al., 2010) by adding complete ignition factors (human and lightning ignitions), and all SPITFIRE variables completely. Furthermore, the module included a calculation mechanism for trace gas and aerosol emissions (Andreae and Merlet, 2001) and was adjusted to produce monthly outputs for all variables in the SEIB-DGVM. In this study, we integrated the SPITFIRE fire module into the spatially explicit individual-based dynamic global vegetation model (SEIB-DGVM) to predict fire, vegetation, and burned biomass emission variables in Siberia in the future. These improvements allowed us to simulate fire activity and aboveground biomass dynamics and spatiotemporally assess the projected burned biomass and its emissions for the 21st century in Siberia under representative concentration pathways (RCPs).

1.2. Objectives

This study has developed the SEIB-DGVM model by integrating the latest widely used fire module SPITFIRE. The model development includes full integration of all SPITFIRE variables, improvement of model output from annual to monthly, addition of Net Biome Production (NBP) variable calculation, and addition of burned biomass emission calculation. Our detailed research objectives were separated into several sections below.

1. To produce accurate forest fire simulations by comparing simulation results from improved models: SEIB-DGVM SPITFIRE, default model: SEIB-DGVM GlobFIRM and observed data from benchmark datasets.
2. To analyze and estimate the impact of forest fires on forest ecosystems by analyzing tree allometry, NPP, and NBP variables in fire-on and fire-off simulations under different RCPs climate scenarios.
3. To project burned biomass emissions from forest fires and their distribution patterns under different RCPs climate scenarios in Siberia.

2. METHODS

2.1. Study sites

Boreal forests represent the largest forest biome and one-third of global forest cover (De Groot et al., 2013) and play an important role in the atmosphere–land interactions of the global climate system (Randerson et al., 2006; Bonan, 2008). Geographically, boreal forests are found in Canada, Alaska, and Siberia, of which Siberia has the largest forested area. Siberia is largely covered by deciduous needleleaf conifers (Figure 1), which consist mostly of the larch species *Larix sibirica, L. decidua,* and *L. dahurica* (Abaimov et al., 1998), which are categorized as pyrophytic species, meaning that they require periodic fires to persist on the landscape (Kharuk et al., 2011). The Siberian land cover has changed very little over the last century (Ivanov et al., 2022), and the boreal forest covers approximately >15 million km^2, and contain a large amount of carbon that is comparable to the combined carbon storage in tropical and temperate forests (Dixon et al., 1994; Kasischke, 2000).

The main external factors affecting Siberian boreal forests are fires and climate change (Goldammer and Furyaev, 1996; Shorohova et al., 2009). Climate change increased the frequency of forest fires, which in turn amplified the impacts of climate change locally. In the Arctic, a rapid warming trend has been observed, and the increase in temperature over the last 20 years of the 20th century was 2 to 3 times higher than the global average, while in the first 20 years of the 21st century, it exceeded four times (Chylek et al., 2022). This enormous increase in temperature in Siberia, affecting the duration and speed of snowmelt and accelerates thawing of carbon-rich permafrost (Natali et al., 2019; Schuur et al., 2015; Nitzbon et al., 2020), which results in drier ground cover, an increased frequency of wildfires, longer fire seasons, and increased ignition sources (Kharuk et al., 2022). These changes may result in a new climate state in which heatwaves as well as the associated the occurrence of wildfires may become routine and more severe (Hantemirov et al., 2022; Landrum and Holland, 2020). Produced emissions from thawing permafrost and from wildfire are likely to feed into the global carbon cycle's feedback on climate change (Schuur et al., 2015), and triggering further warming trends globally (Schimel et al., 2001; Kharuk et al., 2011; Krylov et al., 2014).

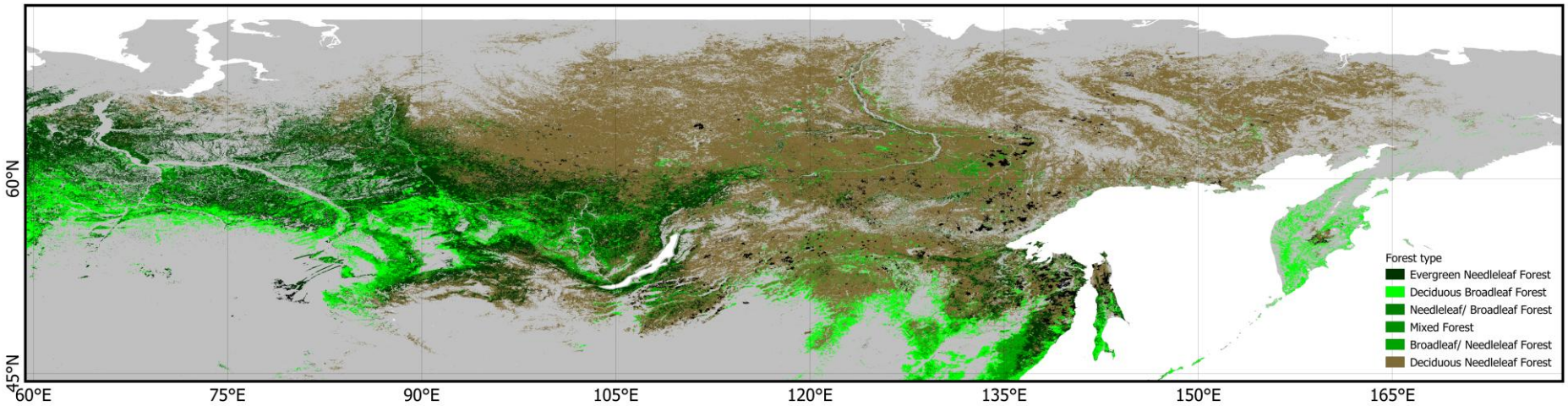

Figure 1. Study site (black rectangle: 60^{o}-180^{o}E and 45^{o}-80^{o}N). Green and brown color indicate the forest types in Siberia are provided from Global Land Cover dataset (GLC 2000): Northern Eurasia (Bartalev et al., 2003). Grey color indicate other vegetation types in the Siberian area provided by Database of Global Administrative Areas (GADM).

2.2. Improved fire module principles

We improved the SEIB-DGVM fire module by replacing Glob-FIRM (Thonicke *et al.*, 2001) with the SPITFIRE model (Thonicke *et al.*, 2010). First, we added two new input variables for fire ignition: population and lightning data. Second, we incorporated the complete SPITFIRE equations (Thonicke *et al.*, 2010): including new variables, PFT parameters, local parameters, and improved the output to be able to produce on a monthly scale (Figure 4). The variable integration between the default and improved fire model requires several parameter-specific PFTs (Table 3).

The default SEIB–DGVM uses annual time steps for vegetation dynamics and disturbance, which we improved to monthly time step outputs. The basic equation of fire disturbance is the area burnt, which we adjusted with the SPITFIRE equation (Thonicke *et al.*, 2010) by including fire probability and area of the grid cell:

$$A_b = P_b \times A \tag{1}$$

Where A_b is the area burnt in a grid cell per month (ha month^{-1}), P_b is the product of the probability of fire per month at any point inside the grid cell (month^{-1}) and A is the area of the grid cell (ha). P_b is the fire probability, and it is the product of the fuel load (litter + aboveground biomass) and its moisture factor. We used the same P_b mechanism as the default fire module, where if the fuel load satisfies the minimum fuel threshold (200 gC m^{-2}), random fire can occur at any point location inside the grid cell. In this fire module improvement, P_b was modified by considering the ignition event $E(n_{ig})$ (ha^{-1}) by anthropogenic (human population density) and natural (lightning strikes) ignition possibilities, fire danger index (FDI), and mean fire area $\bar{a}f$(ha). Thus, equation 2 can be represented as:

$$A_b = E(n_{ig}) \times FDI \times \bar{a}f \times A \tag{2}$$

Technically, the SEIB-DGVM simulation of each grid is carried out independently among the surrounding grids, so the fire cannot spread to other grids without those grids meeting the ignition requirements (fuel load and fuel moisture). Further changes in the the input and output of the new SEIB-DGVM SPITFIRE are shown in Appendix A.1, while Appendix A.2

summarizes the improvement processes represented in this study, which can be classified into two groups: disturbance, and biogeochemical dynamics. Appendix A.3 lists the symbols used in the model's equations.

After all SPITFIRE variables were installed, we also conducted a verification process for all variables. The verification process included assessing the new input data (lightning and population data), as well as all new variables by testing their outputs and units. The module verification process is very important to ensure that the module produces the right outputs but not for the wrong reasons (Rabin et al., 2017).

2.2.1. Burned area calculation input variable

Mean fire area can be calculated as equation 3 as fires tend to take on an elliptical reform and spread at varying speeds both with and against the direction of the wind (Albini, 1976; Forestry Canada Fire Danger Group, 1992).

$$\underline{af} = \frac{\frac{\pi}{4 \times L_B} \times (D_T)^2}{10000} \tag{3}$$

Dt is the length of major axis (m), in SEIB-DGVM we use the resolution of establishment site for woody PFTs (Dived) variable. L_B is the length-to-breadth ratio of the elliptical form of fires (Forestry Canada Fire Danger Group, 1992) and calculated PFTs specific, for woody and grass PFTs. L_B can be estimated as a weighted average of $L_{B,tree}$ and $L_{B,grass}$.

$$L_{B,tree} = 1.0 + 8.729 \times (1 - e^{-0.03 \times U_{forward}})^{2.155} \tag{4}$$

$$L_{B,grass} = 1.1 + \left(U_{forward}\right)^{0.464} \tag{5}$$

Ignition event $E(n_{ig})$ is the sum of independent calculations of lightning-caused (n_{il}) and human-caused (n_{ih}) fire ignition events, ignoring stochastic variations (Thonicke *et al.*, 2010).

$$E(n_{ig}) = n_{ih} + n_{il} \quad (6)$$

2.2.2. Ignition events

The LIS/OTD High-Resolution Full Climatology (HRFC) V2.3.2015 (Cecil and Daniel, 2001) data provided frequency of lightning-caused ignition events (n_{il}), actual unit is count/km^2/year then converted into count/ha/year, and gives the annual frequency of total lightning flash rates. Human-caused ignition events (n_{ih}) used population density data obtained from Gridded Population of the World (GPWv4) (CIESIN, 2018), as the default unit is person/km^2, we converted it into person/ha. The population density and lightning flash data detailed information are shown in Table 1.

Table 1. Population and lightning input data information

Variable	Unit	Product	Spatial resolution	Temporal resolution	Temporal coverage	Reference
Population density	person km^{-2}	Gridded Population of the World (GPWv4)	2.5 arc-minute	Annual	2000-2020	(CIESIN, 2018)
OTD Flash Rate	count km^{-2} year^{-1}	LIS/OTD High Resolution Full Climatology (HRFC) V2.3.2015	0.5 degree	Annual	2015	(Cecil and Daniel, 2001)

As the first improvement step, we modified the data format, the GPWv4 (netCDF) and LIS/OTD HRFC (hdf5) data are gridded into 1^o grid mesh (360×180) as the SEIB-DGVM requirements for land property (land_prop.txt) input, then converted into text format (.txt), and make sure that the sequence is N90W180, N90W179, ..., N89W180, ..., S90E180, each line corresponds to one grid mesh, so the data structure will be 1 column and 64800 rows, text format files.

The SEIB-DGVM fire module improvement workflow was shown in Figure 5 in the main article, and the orange color inside the dashed box indicates the new input and there is absolute certainty to add another new input that might be considered in the further improvement of SEIB-DGVM. Interestingly, we found a novel discovery in this model improvement process that there will be a huge possibility improvement of SEIB-DGVM in the near future for many research areas because SEIB-DGVM is able to accept any new input as long as it meets the input data requirements and able to process well and can be integrated with the variables in it, so we believed that SEIB-DGVM has a high potential to be a rapid-growing model for analyzing and simulating global vegetation dynamics from many perspectives, needs, and scientific focus areas.

To ensure that the data can be read and processed well by SEIB-DGVM, we visualize it on a global scale and in Siberia, according to the research area as shown in Figure 2, prepared the data in (netCDF) format in 0.5^{o} spatial resolution to be able to compare with the output results of the data in SEIB-DGVM (as the data output from SEIB-DGVM is in 0.5^{o} spatial resolution).

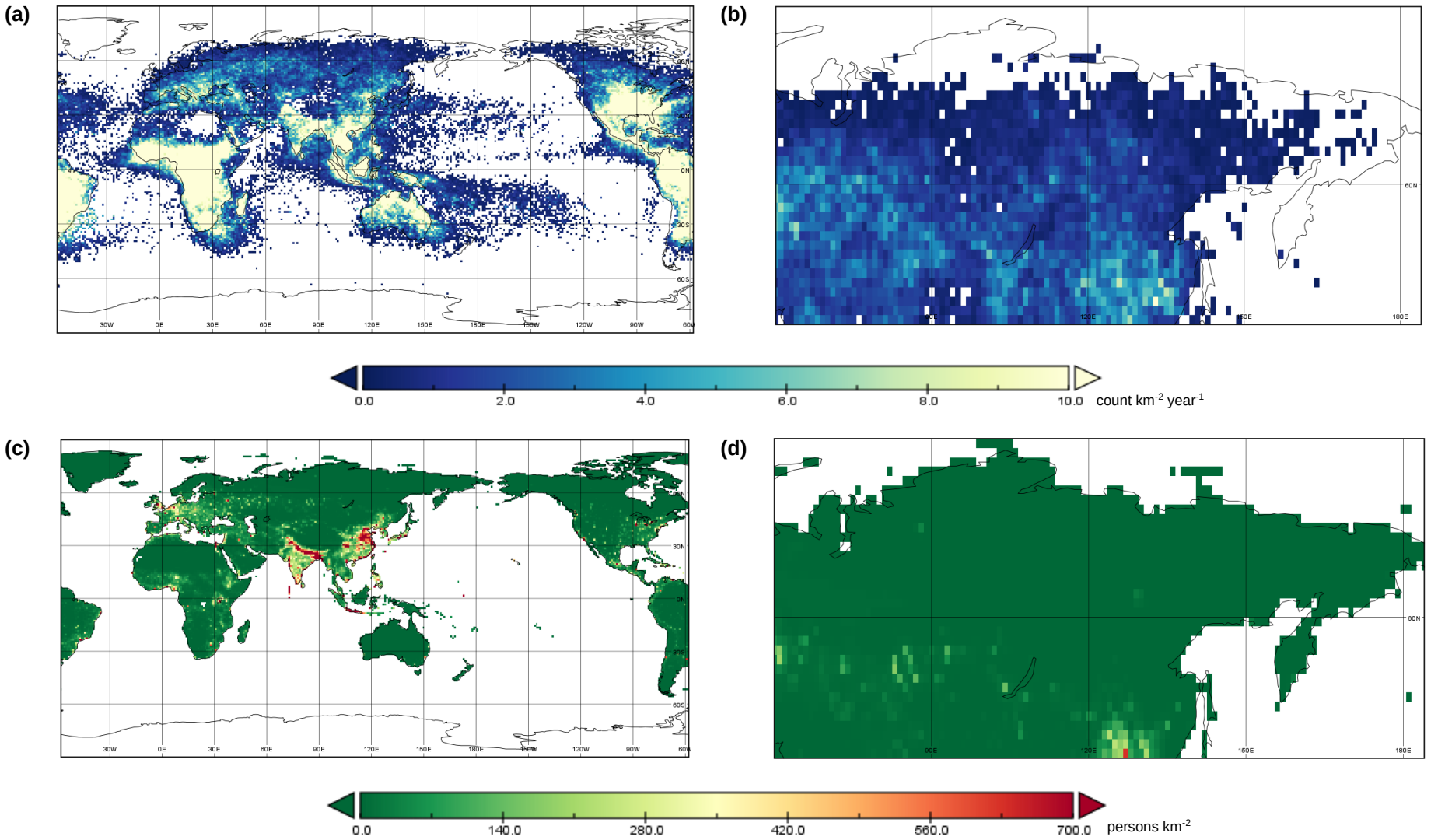

Figure 2. Spatial distribution of lightning flash rate (LIS/OTD HRFC) and population density (GPWv4) input data: **(a)** LIS/OTD HRFC global, **(b)** LIS/OTD HRFC Siberian, **(c)** GPWv4 global, **(d)** GPWv4 Siberian

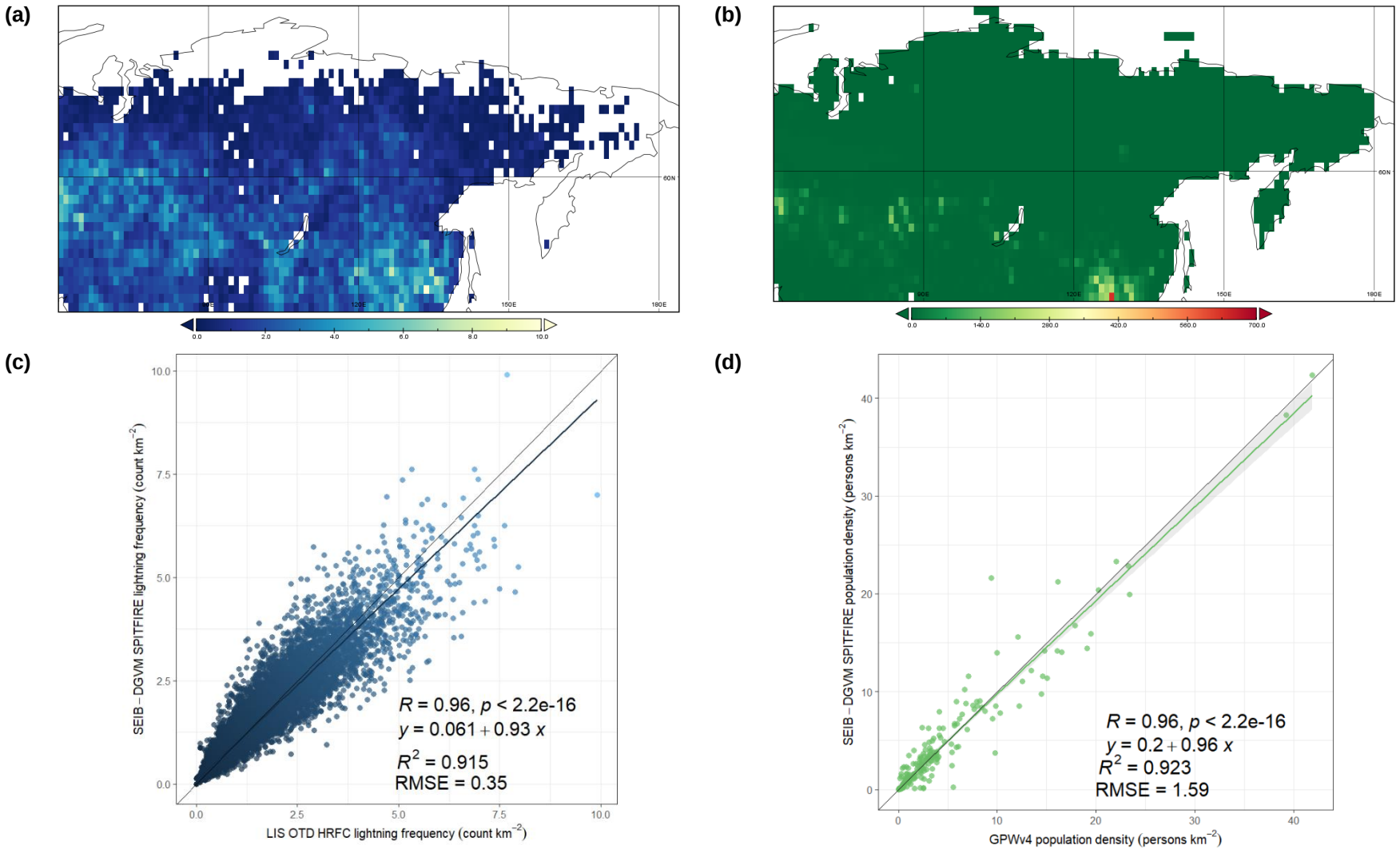

Figure 3. (a) Spatial distribution of lightning flash rate model output, **(b)** Spatial distribution of population density model output, **(c)** Comparison between simulated lightning flash rate and observational lightning flash rate (LIS/OTD HRF), **(d)** Comparison between simulated population density and population density (GPWv4)

Figure 3 shows the SEIB-DGVM output of Lightning flash rate and Population density and it's the comparison with the original input GPWv4 and LIS/OTD HRFC data. Based on the comparison results we get the high value of coefficients determination *(R^2)* and correlation coefficients *(R)* for both data comparison, the value of lightning flash rate comparison is R^2=0.97, and for population density data is R^2=0.93. Although it doesn't produce 100% comparison results, but 97% and 93%, followed by 0.99 and 0.97 correlation coefficients, for lightning flash rate and population density data comparison shows a strong relationship between the input and output, and these results proved that the SEIB-DGVM was able to read and process the new input well.

Further explanation of the input-output comparison is: the input data has different formats and spatial resolutions, then the first thing we did is data transformation, transformed the data format and regridding the data to 1^o grid for SEIB-DGVM input and to 0.5^o grid for output comparison, this process we used the Climate Data Operator (CDO) software (Schulzweida, 2019) remapcon operators, first-order conservative remapping that remaps all fields conservatively to a Gaussian N32 grid. We know that the process of remapping or regridding data will produce a bias, moreover multiple-time regridding the same data, and the size of the bias depends on the technique and method used. The method we used in this study is the best method for regridding compared to other methods, as the first- and second-order conservative methods provide an accurate and conservative machine accuracy, completely general, weights can be computed for any type of grid on a sphere, enabling component model developers to use any grid that is suitable for a specific component without being restricted by compatibility with other component model grids in a connected model environment (Jones, 1999).

After the new input is confirmed able to be read and processed properly by SEIB-DGVM, we implement the complete ignition events equation from SPITFIRE (Thonicke *et al.*, 2010) with some model configuration adjustments and environmental factor parameters.

$$N_{il} = I_p \times Lightning\ Flash\ Rate \quad (7)$$

Latham and Williams, (2001) stated that 0.20 of these are cloud-to-ground flashes (CG), and under ideal conditions for igniting fires, their effectiveness is 0.04 (Latham and Schlieter,

1989; Latham and Williams, 2001). *Ip* is an ignition parameter (0.0 – 1.0), and in this study, we used 1.0 because lightning strikes are the primary source of wildfire ignition in Siberia (Sofronov *et al.*, 1998; Ivanova and Ivanov, 2005; Kharuk *et al.*, 2016), with continued regional warming, the role of lightning as a source of wildfire ignition is likely to increase both because of the increased availability of dry fuel as well as from a direct increase in lightning frequency (Kharuk *et al.*, 2022). Research in areas with similar environmental conditions about lightning strikes in the continental USA projects that an increase in air temperature by 1^{o}C leads to an increase in lightning frequency of ~12% (Romps *et al.*, 2014), and for Alaska and northern Canada, lightning ignition was estimated to increase by 90–230% by the end of this century (Hessilt *et al.*, 2021).

Regarding the lightning input dataset on the module, we used one-year and annual data of LIS/OTD HRFC as interannual variability in lightning is generally small (Thonicke *et al.*, 2010).

$$N_{ih} = P_D \times k(P_D) \times \frac{a(N_D)}{100} \tag{8}$$

$$k(P_D) = 30.0 \times e^{-0.5 \times \sqrt{P_D}} \tag{9}$$

After climatic sensitivity ignition, human activity grew to become a stronger factor in controlling fire regimes also due to the construction of the Trans-Siberian Railway and the subsequent development of settlements in remote areas (Ivanova and Ivanov, 2005). Thus, in this improvement, we considered the population density ignition factor also. P_D is the population density (persons km^{-2}), and $a(N_D)$ (ignitions individual^{-1}) is a parameter expressing a person's probability of causing an ignition event (Thonicke *et al.*, 2010). The function forms is supported by Archibald *et al.*, (2009) analysis, that the number of fires in southern Africa tends to rise as population density rises up to roughly 10 kilometers and declines thereafter. At the global scale analysis, Knorr *et al.*, (2014) also discovered that fire frequency rises by 10 to 20% in areas with less than 0.1 persons per km^2 compared to its value in areas with no population. In the SEIB-DGVM, $a(N_D)$ is and user-definable parameter, with a scale of 0.0 – 1.0, and in this study we adjust the value to 0.7 or 70% (total

of human and unknown caused fire), as the recent research in eastern Siberia Xu *et al.*, (2022), shown that fires over Yakutia, 31.4 ± 6.8% caused by lightning ignitions, 51.0 ± 6.9% caused by anthropogenic ignitions, and the last 14.4% unknown cause.

2.2.3. Fuel moisture content

Default SEIB-DGVM already has a fuel moisture content equation, and according to Thonicke *et al.*, (2001) we made variable name adjustments as GlobFIRM to make tracking and improvement easier. The fuel moisture content fraction calculation *(m)*, is as follows:

$$m = \frac{frac\ moisture\ litter \times pool\ w1\ runningrecord(1)}{Depth * Wfi} \tag{10}$$

$$m = 0.4994 \times \tilde{m} + 1.02 \tag{11}$$

Fuel moisture content fraction (unitless) calculation inside SEIB-DGVM (Equation 10) is based on the fuel moisture content calculation in the LPJ-DGVM (Equation 11), where $frac\ moisture\ litter$ is a local parameter of the fraction of litter moisture to soil moisture at the top layer and the default value is 0.5, $pool\ w1\ runningrecord(1)$ is annual soil water content of first soil layer, *Depth* is soil depth (there are 3 soil layers and the depth of each layer is 500 mm, 1000 mm, and 1500 mm, respectively) and *Wfi* is field capacity (Sato *et al.*, 2007). Equation 11 obtained from equation 8 on Viegas *et al.*, (1992), that used to predict the fuel load on the Moisture module inside the BEHAVE system.

In the fire module improvement, we added the equation of relative moisture content *(ω_o)* of the fuel load:

$$\omega_o = e^{(-(\alpha_{av} \times fuel\ load) \times NI)} \tag{12}$$

The values of α_{av} ($^oC^{-2}$) are average of inverse proportion to their surface-area-to-volume ratios of each fuel classes, with $\alpha_{1h} = 1.0 \times 10^{-3}$, $\alpha_{10h} = 5.42 \times 10^{-5}$, and $\alpha_{100h} = 1.49 \times 10^{-5}$. We used the average value of $(\alpha_{1h}, \alpha_{10h}, and\ \alpha_{100h})$ because SEIB-DGVM classifies fuel load by biomass type: litter trunk, litter leaf, and aboveground biomass, and for LPJ-DGVM SPTIFIRE allocated among four fuel classes: 1-h (leaves and twigs, i.e. leaf mass plus 4.5% of the carbon stored as heartwood (HW) and the sapwood (SW), respectively), 10-h (small branches, i.e. 7.5% of HW and SW), 100-h (large branches, i.e. 21% of HW and SW) and 1000-h (boles or trunks, i.e. 67% of HW and SW) (Thonicke *et al.*, 2010). The consumption of 1000-h fuels is not considered in the calculation of moisture content because does not influence fire spread or intensity (Pyne *et al.*, 1996).

NI is an abbreviation of Nesterov Index ($^\circ C^2$), is a cumulative function of daily maximum temperature T_{max} and dew-point temperature T_{dew} ($^\circ C$):

$$NI = \sum T_{max} \times (T_{max} - T_{dew}) \tag{13}$$

$$NI = \sum T_{max} \times \left(T_{max} - (T_{min} - 4.0)\right) \tag{14}$$

We approximate T_{dew} by (T_{min}−4), where T_{min} is the daily minimum temperature (Running *et al.*, 1987), same approach used by (Venevsky *et al.*, 2002), and (Thonicke *et al.*, 2010).

2.2.4. Fire Danger Index

Fire Danger Index *(FDI)* is the probability that an ignition event will start a fire and can be calculated by combining the relative moisture content equation *(ω_o)* (Equation 12), the fire spread probability equation *(P_{spread})* (Equation 15), and also depends on fire weather conditions as described by NI (Equation 13). Moisture extinction (m_e) is PFT-specific disturbance parameter that indicates the proportion of litter moisture extinction due to fire.

$$P_{spread} = \left\{1 - \frac{\omega_o}{m_e}, \omega_o \leq m_e\ 0, \omega_o > m_e\ \right\} \tag{15}$$

$$FDI = max\left(0, \left(1 - \frac{1}{m_e} \times e^{-((\alpha_{av} \times fuel\ load) \times NI)}\right)\right) \quad (16)$$

Equation 16 will produce the Fire Danger Index *(FDI)* value if there is enough fuel load that satisfies the minimum threshold (200 g C m^{-2}), and FDI will be zero if there is no fuel or the fuel has a high moisture content that is unable to be ignited.

2.2.5. Rate of spread

The rate of Spread (ROS) is the predicted speed of the fire in the front or head of the fire, where it spreads the fastest, is known as which accounts for both crowning and spotting and can be obtained using Rothermels equations (Rothermell, 1972; Wilson, 1982; Pyne *et al.*, 1996). We also implemented the complete rate of spread equations as SPITFIRE (Thonicke *et al.*, 2010) as we were able to add all of the needed parameters, integrate it, and create new variables on SEIB-DGVM.

The forward and backward fire rate of spread $ROS_{f,surface}$ and $ROS_{b,surface}$ (m min^{-1}) respectively, can be obtained by:

$$ROS_{f,surface} = \frac{I_R \times \xi \times (1 + \phi_w)}{p_b \times \varepsilon \times Q_{ig}} \quad (17)$$

$$ROS_{b,surface} = ROS_{f,surface} \times e^{-0.012 \times U_{forward}} \quad (18)$$

I_R is the reaction intensity, the energy that is released per unit fire front area (kJm^{-2} min^{-1}); ξ is the propagating flux ratio, the percentage of I_R that causes nearby fuel particles to heat up and ignite; ϕw is a multiplier that takes into consideration how wind affects the effective value of ξ; ρb is the fuel bulk density (kgm^{-3}), assigned by PFT-specific parameter (Table 3); ε is the effective heating number, the percentage of a fuel particle that reaches ignition temperature at the beginning of flame combustion; and Q_{ig} is the heat of pre-ignition, the heat needed to ignite a specific mass of fuel (kJ kg^{-1}). The ROS variable calculation details are explained in more detail in Appendix A.

The estimated fire duration can also be calculated based on the fire danger index, using the following equation:

$$t_{fire} = \frac{241}{1 + 240 \times e^{-11.06 \times FDI}} \quad (19)$$

2.2.6. Fire fraction and intensity

The surface fire intensity, $I_{surface}$ (kW m^{-1}) is the product of the forward rate of fire spread $ROS_{f,surface}$, fuel consumption FC, fuel heat content h, and area burnt fraction $A_{b,frac}$ (Byram, 1959).

$$I_{surface} = h \times \frac{\sum FC}{1000 \times A_{b,frac}} \times \frac{ROS_{f,surface}}{60} \quad (20)$$

$$A_{b,fraction} = \frac{A_b}{A} \quad (21)$$

FC is fuel consumption in a surface fire (gDM m^{-2}), and calculated using empirical equations as fuel moisture function of the fuel load (Peterson and Ryan, 1986), this equation has been adjusted for SEIB-DGVM as there is no fuel classification based on the length of combustion, described in the Appendix A.

2.2.7. Fire damage to plants

The SPITFIRE module is very detailed in its classification of fire spread, ranging from surface fires to crown scorch caused by surface fire. The scorch height SH of the fire can be obtained by the following equation (Peterson and Ryan, 1986; Agee, 1997; Dickinson and Johnson, 2001):

$$SH = F \times \left(I_{surface}\right)^{0.667} \quad (22)$$

F is PFT-specific parameter of the crown scorch equation (Table 3). Assuming a cylindrical crown, the crown scorch fraction (CK) impacted by a fire can be obtained using the following formula:

$$CK = \frac{SH - T_H + CL}{CL} \quad (23)$$

T_H is the individual tree height of woody PFT, *CL* is crown length, and the value is provided by PFT-specific parameters (Table 3). Post-fire tree mortality is caused by the cambium damage, and crown damage is caused by bark heating. Those causes are assumed to act independently, so the total probability of mortality P_m *is* determined by the probability of crown damage mortality $P_m(CK)$ and cambial damage $P_m(\tau)$.

$$P_m = P_m(\tau) + P_m(CK) - \left(P_m(\tau) \times P_m(CK)\right) \quad (24)$$

The probability of crown damage mortality $P_m(CK)$ is obtained by:

$$P_m(CK) = r(CK) \times CK^p \quad (25)$$

r(CK) is the crown damage resistance factor, and *p* is Woody PFTs parameter, the values of each parameter are described in Table 3 (Peterson and Ryan, 1986; Williams *et al.*, 1998; Cochrane, 2003).

Probability of cambial damage mortality $P_m(\tau)$:

$$P_m(\tau) = \left\{0, \frac{\tau_l}{\tau_c} \leq 0.22\ 0.563 \times \frac{\tau_l}{\tau_c} - 0.125, \frac{\tau_l}{\tau_c} > 0.22\ 1, \frac{\tau_l}{\tau_c} \geq 2.0\right\} \quad (26)$$

τ_l is the residence time of the fire, τ_c is the critical time of cambial damage, so τ_l/τ_c is the ratio of fire residence time to the cambial damage (Peterson and Ryan, 1986). The value of τ_l is dependent on I_R, as provided by the fire spread model (Rothermell, 1972; Wilson, 1982), described in Appendix A. The critical time of cambial damage τ_c (min), depends on the bark thickness (cm) (Peterson and Ryan, 1986).

$$\tau_c = 2.9 \times BT^2 \tag{27}$$

$$BT = par_1 \times DBH + par_2 \tag{28}$$

BT calculated from the diameter at breast height, *DBH* (cm), and par_1 and par_2 are PFT-specific parameters (Table 3). Generally, during a fire, all leaf biomass of grass, all leaf biomass of dead and surviving trees, half of the trunk biomass of dead trees, and half of the litter pool are burned (classified into surface fire and crown scorch), while the remaining biomass of dead trees is transformed into litter. In response to fire, the phenology phase of all grass PFTs changes to dormant (they reenter the growth phase as described previously in the section titled 'Phenology'). If the stock resource of grass PFTs (*gmassstock*) does not satisfy the minimum value (50 g DM m–2) after fire, the deficit is supplemented by litter (Sato *et al.*, 2007). The fraction of individual trees killed in a fire also depends on PFT fire resistance (M3, Table 3).

2.2.8. Trace gas and aerosol emissions

Trace gas and aerosol emissions estimation is referred to the Fire Modeling Intercomparison Project (FireMIP) protocols (Li *et al.*, 2019), the comprehensive study comparison of nine dynamic global vegetation models (DGVMs) and produced important estimation for long-term and large-scale fire emissions. By using FireMIP protocol reference, SEIB-DGVM SPITFIRE improved to output PFT-level fire emissions.

Trace gas and aerosol emissions are the result of the total amount of burned biomass, the sum of dead and live fuel consumption as the result of surface fire and crown scorch. Trace gas emissions are estimated based on fire carbon emissions, vegetation characteristics from

DGVMs, and fire emissions factors. Fire emissions of trace gas and aerosol for each species i and PFT j, $E_{i,j}$ (g species m^{-2}) are estimated based on Andreae and Merlet, (2001):

$$E_{i,j} = EF_{i,j} \times \frac{CE_j}{C} \quad (29)$$

Where $EF_{i,j}$ is PFT specific emission factor (g species (kg DM)$^{-1}$), CE_j is the combusted biomass of PFT_j due to the fire (g C m^{-2}), and C is the unit conversion factor from carbon to dry matter, $C = 0.5 \times 10^3 gC(kg\ DM)^{-1}$. The Emission factors *(EF)* used in this study are based on Andreae and Merlet, (2001), and the updated pyrogenic emissions species by various types of biomass burning (Andreae, 2019) (Table 2).

DGVMs generally simulate vegetation as a combination of PFTs in a given grid location to represent plant function at a global scale, instead of land cover types (Li *et al.*, 2019). In this, we classified the PFTs with the LCTs to integrate the emission factors of each LCTs for trace gas and aerosol emissions estimation process. TrBE and TrBR are classified as Tropical Forest; TeNE, TeBE, and TeBS are classified as Temperate Forest; BoNE, BoNS, and BoBs are classified as Boreal Forest, and the last is Teh and TrH are classified as Grassland/ Savana, SEIB-DGVM didn't classify crop PFTs so cropland LCTs will not be used.

Detailed information about the integration of the SPITFIRE module in the SEIB-DGVM, which includes the improvement and adjustment of whole variables is describen in the Figure 4.

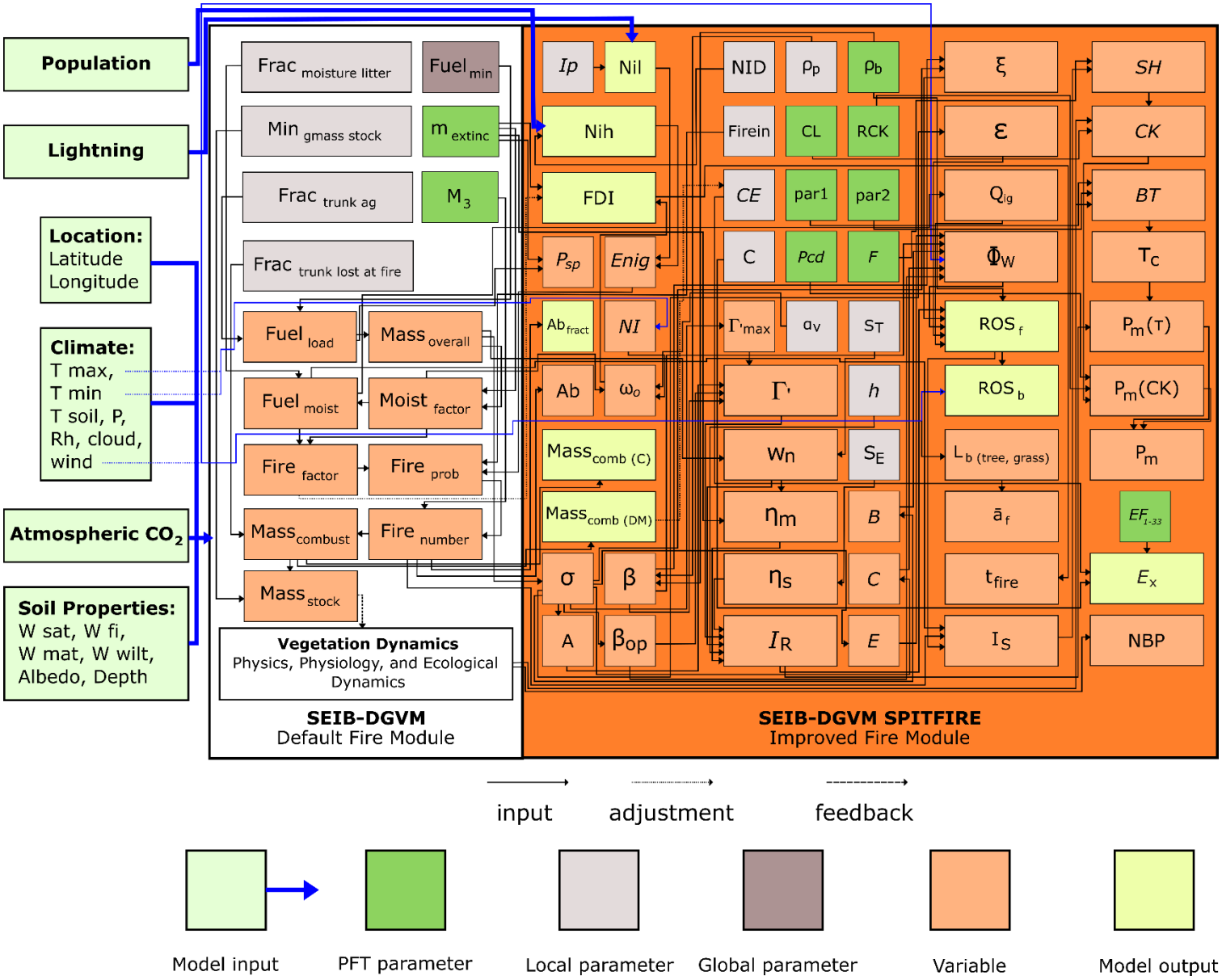

Figure 4. SEIB-DGVM SPITFIRE systems diagram. All variables are displayed, describing the improvements (SPITFIRE), the interaction between the previous fire module (Glob-FIRM). All original SPITFIRE variables were integrated: ignition factor (lightning and population), PFT parameters, and other fire-related variables. In addition to the default annual output, the improved module had monthly outputs of all variables depending on the user needs. For the meaning of abbreviations, refer to the Appendix A.3.

Table 2. Emission factors (g species (kg DM^{-1}) for land cover types (LCTs) (Andreae and Merlet, 2001; Andreae, 2019)

No.	Species	PFT parameter abbreviation	Grassland/ savana	Tropical forest	Temperate forest	Boreal forest	Cropland
1	CO_2	ES1	1647	1613	1566	1549	1421
2	CO	ES2	70	108	112	124	78
3	CH_4	ES3	2.5	6.3	5.8	5.1	5.9
4	NHMC	ES4	5.5	7.1	14.6	5.3	5.8
5	H_2	ES5	0.97	3.11	2.09	1.66	2.65
6	NO_x	ES6	2.58	2.55	2.9	1.69	2.67
7	N_2O	ES7	0.18	0.2	0.25	0.25	0.09
8	$PM_{2.5}$	ES8	7.5	8.3	18.1	20.2	8.5
9	TPM	ES9	8.5	10.9	18.1	15.3	11.3
10	TPC	ES10	3.4	6	8.4	10.6	5.5
11	OC	ES11	3.1	4.5	8.9	10.1	5
12	BC	ES12	0.51	0.49	0.66	0.5	0.43
13	SO_2	ES13	0.51	0.78	0.75	0.75	0.81
14	C_2H_6 (ethane)	ES14	0.42	0.94	0.71	0.9	0.76
15	CH_3OH (methanol)	ES15	1.48	3.15	2.13	1.53	2.63
16	C_3H_8 (propane)	ES16	0.14	0.53	0.29	0.28	0.2
17	C_2H_2 (acetylene)	ES17	0.34	0.43	0.35	0.27	0.32
18	C_2H_4 (ethylene)	ES18	1.01	1.11	1.22	1.49	1.14
19	C_3H_6 (propylene)	ES19	0.49	0.86	0.67	0.66	0.48
20	C_5H_8 (isoprene)	ES20	0.12	0.22	0.19	0.07	0.18
21	$C_{10}H_{16}$ (terpenes)	ES21	0.1	0.15	1.07	1.53	0.03
22	C_7H_8 (toluene)	ES22	0.2	0.23	0.43	0.32	0.18
23	C_6H_6 (benzene)	ES23	0.34	0.38	0.46	0.52	0.31
24	C_8H_{10} (xylene)	ES24	0.09	0.09	0.17	0.1	0.09
25	CH_2O (formaldehyde)	ES25	1.33	2.4	2.22	1.76	1.8
26	C_2H_4O (acetaldehyde)	ES26	0.86	2.26	1.2	0.78	1.82

No.	Species	PFT parameter abbreviation	Grassland/ savana	Tropical forest	Temperate forest	Boreal forest	Cropland
27	C_3H_6O (acetone)	ES27	0.47	0.63	0.7	0.61	0.61
28	$C_3H_6O_2$ (hydroxyacetone)	ES28	0.52	1.13	0.85	1.48	1.74
29	C_6H_5OH (phenol)	ES29	0.37	0.23	0.33	2.96	0.5
30	NH_3 (ammonia)	ES30	0.91	1.45	1	2.82	1.04
31	HCN (hydrogen cyanide)	ES31	0.42	0.38	0.62	0.81	0.43
32	MEK/2-butanone	ES32	0.13	0.5	0.23	0.15	0.6
33	CH_3CN (acetonitrile)	ES33	0.17	0.51	0.23	0.3	0.25

Table 3. SEIB-DGVM SPITFIRE Plant Functional Type (PFT)-specific model parameter values and their attribution to LCTs. This table was modified from (Thonicke et al., 2010).

PFTs	Land Cover Types (LCTs)	Fuel bulk density (kg m^{-3})		Scorch height parameter		Crown length parameter	Bark thickness parameters			Crown damage parameter		Fire resistance
		Pb	Reference	*F*	Reference	*CL*	par1	par2	Reference	*R(CK)*	*p*	*M3*
BoNE	Boreal Forest	25	(Miller and Urban, 1999; Hély et al., 2000)	0.11	(Hely et al., 2003)	1/3	0.0292	0.2632	(Reinhardt et al., 1997)	1	3	0.12
BoNS		22	(Keane et al., 1990)	0.094	(Dickinson and Johnson, 2001)	1/3	0.0347	0.1086	(Reinhardt et al., 1997)	1	3	0.12
BoBS		22	(Keane et al.,	0.09	(Dickinson	1/3	0.03	0.10	(Reinhardt	1	3	0.12

PFTs	**Land Cover Types (LCTs)**	**Fuel bulk density (kg m^{-3})**		**Scorch height parameter**		**Crown length parameter**	**Bark thickness parameters**			**Crown damage parameter**		**Fire resistance**
		Pb	Reference	*F*	Reference	*CL*	par1	par2	Reference	*R(CK)*	*p*	*M3*
			1990)	4	and Johnson, 2001)		47	86	et al., 1997)			

PFTs attributed to land cover types (LCTs) are needed to classify the fire emission factor (*EF*) (Table 2) to estimate trace gas and aerosol emissions (Andreae and Merlet, 2001).

2.3. Model calibration

We calibrate the improved model by using all of the benchmark datasets (Table 5). The calibration process is done sequentially for all of the major variables, from burned fraction, burned area, dry matter, aboveground biomass, burned biomass emissions, and the forest ecology variables (Figure 5). This calibration process involves comparing the average value of the output variable with the corresponding variable from the benchmark dataset, ensuring that both are aligned in terms of spatiotemporal resolution. The process is sequential because one variable is used for the calculation of another variable (such as burned fraction and burned area affecting aboveground biomass, forest structure, dry matter, and emissions). One calibration process is performed with multiple iterations until the output variable has similar numerical values and spatial distribution to the benchmark data, and the process is repeated for other variables once the previous variable has been calibrated.

2.4. Model application

The original SEIB-DGVM utilizes three computational time steps: a daily time step for all physical and physiological processes except for soil decomposition and tree growth, a monthly time step for soil decomposition and tree growth, and an annual time step for vegetation dynamics and fire disturbance (Sato et al., 2007). In this study, we improved the fire module to calculate natural and anthropogenic fire ignition factors (based on lightning flashes and population density) and adjusted it to produce monthly outputs using temporal resolution statistical downscaling methods with user-defined weighted monthly parameters (Table 4). The annual average ignition factor variables (population density and lightning flash rate) were used consistently throughout all simulation phases.

We ran the improved model (SEIB-DGVM SPITFIRE) and the default model (SEIB-DGVM GlobFIRM) under the same protocols to equally compare and assess their fire products (Figure 6 in the Supplement)[*]. Simulations were run in three phases (spin-up, historical and future) and the simulation was run with the fire mode on and fire mode off to compare and assess the vegetation products during fire, and also each phase was replicated 5 times to minimize bias due to random variables in the tree morality[1]. The model was run in three phases[2]: 1) a 1000-year spin-up phase to bring the soil and vegetation carbon pools into equilibrium with the climate using daily baseline CRU TS3.22 climate data, 2) a 156-year

historical phase also using daily baseline CRU TS3.22 climate data and spin-up simulation results as inputs, and 3) a 95-year future phase using daily MirocAR5 base V3 RCP8.5, RCP6.0, RCP4.5, and RCP2.6 climate data and historical simulation results as inputs (Figure 5). The MirocAR5 Base V3 dataset has been bias-corrected with CRU TS3.22 climate data, so using these two datasets consecutively in spin-up, historical, and future simulations ensures the harmony of the input climate data. Five different types of RCP scenario climate data were used to determine the impact of fire and climate on forest structure and their interactions.

In the previous SEIB-DGVM study, a 2000-year spin-up was needed to obtain the convergence amount of soil organic matter (Sato et al., 2010). However, we have conducted preliminary simulations with the same study area by setting the spin-up years to 1000 years and 2000 years. We confirmed that the outputs of the 1000-year and 2000-year spin-up simulations were very similar; thus, the 1000-year spin-up was enough to reach carbon stock equilibrium. This parameter setting is also in line with the simulation settings in other SEIB-DGVM studies: Sato et al. (2007) performed a 1000-year spin-up and combined it with all of the simulation phases to extract general trends of postfire succession. Another study by Arakida et al. (2021) also confirmed that a spin-up period of 100 years was sufficient for the equilibrium of the LAI, aboveground biomass, and GPP at all the study sites in Siberia.

In addition, we have verification stage[3] to ensures that the new input data can be read, produced, and processed properly (Rabin et al., 2017). Then, we calibrate all of the major emissions individually and sequentially with the benchmark dataset because each variable affects other variables, and we need to ensure the final output is comparable with the benchmark datasets[4]. After verifying that the new module was incorporated seamlessly, we validated the model outputs (fire, vegetation and emissions variables) by using GFED4, GFED4s, ESA Biomass CCI and GBEI benchmark datasets[5].

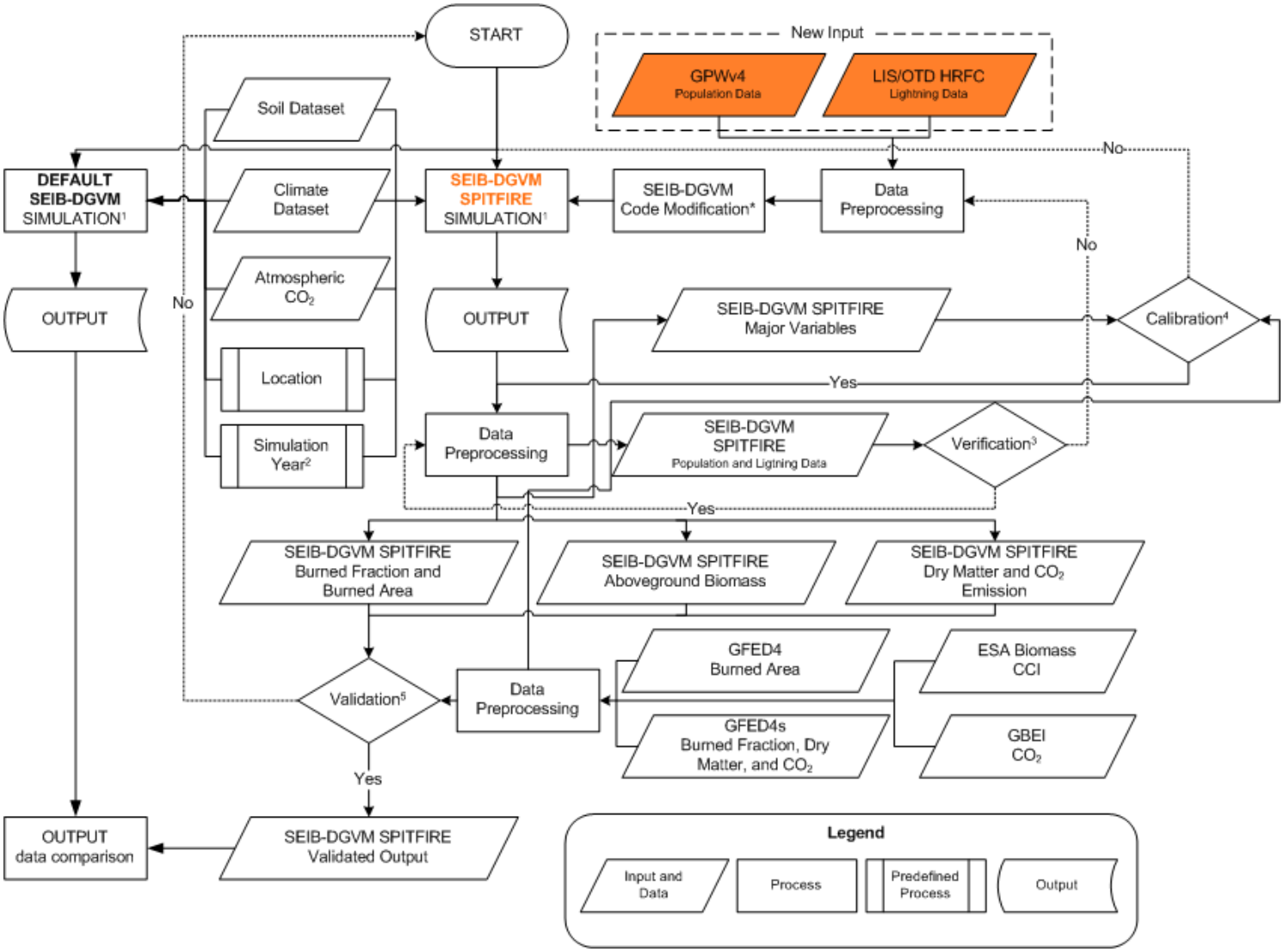

Figure 5. Workflow of improving the SEIB-DGVM fire module

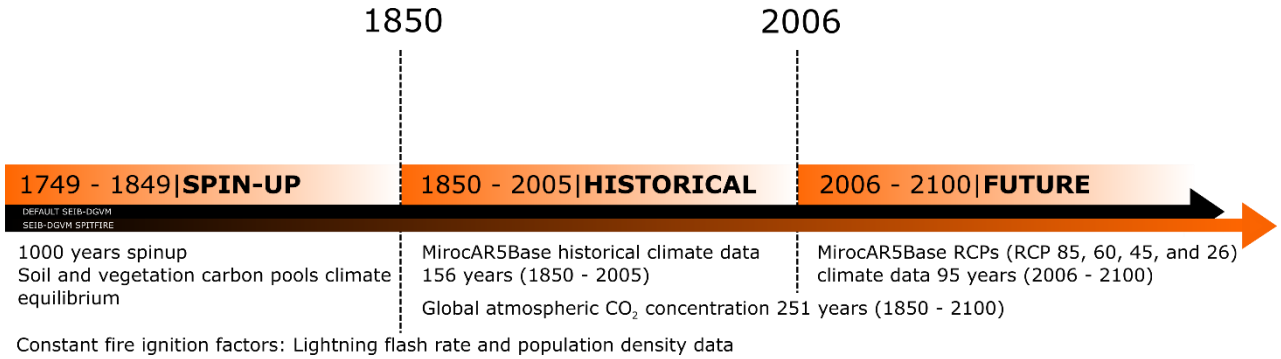

Figure 6. SEIB-DGVM SPITFIRE simulation protocols

Table 4. SEIB-DGVM SPITFIRE input data descriptions

Model Input	**Product**	**Variable**	**Spatial Resolution**	**Temporal Resolution**	**Temporal Coverage**	**Reference**
Climatic data	CRU TS3.22 High-Resolution Gridded Data of Month-by-month Variation in Climate	Cloud cover, diurnal temperature range, frost day frequency, PET, precipitation, daily mean temperature, monthly average daily maximum and minimum temperature, vapor pressure, and wet day frequency	0.5 degree	daily	1901 – 2013	(NCAS, 2014)

Model Input	**Product**	**Variable**	**Spatial Resolution**	**Temporal Resolution**	**Temporal Coverage**	**Reference**
	MirocAR5 base daily V3 (Historical, RCP8.5, RCP6.0, RCP4.5, and RCP2.6)	Air temperature, soil temperature, fraction of cloud cover, precipitation, humidity, and wind velocity	0.5 degree	daily	1850-2100	
CO_2	-	Global atmospheric Carbon dioxide concentrations (CO_2)	-	-	1850-2100	-
Soil properties	Global Soil Wetness Project 2	Soil moisture at saturation point, field capacity, matrix potential, wilting point, and albedo	1 degree (360 x 180)	time fixed	time fixed	www.iges.org/gswp
Ignition factors	LIS/OTD High-Resolution Full Climatology	Lightning flash rate	2.5 arc-minute	Annual	2015	(CIESIN, 2018)

Model Input	Product	Variable	Spatial Resolution	Temporal Resolution	Temporal Coverage	Reference
	(HRFC) V2.3.2015					
	Gridded Population of the World (GPWv4)	Population density	0.5 degree (720 x 360)	Annual	2000-2020	(Cecil and Daniel, 2001)

2.5. Model benchmarks

A common method for validating the outputs of dynamic global vegetation models (DGVMs) is to use satellite-based product datasets. For instance, direct observations of global fire occurrence by satellite-borne sensors can detect active fires, fire radiative power, and burned areas, and these observations have been available since the 1990s (Mouillot et al., 2014). The Fire Modeling Intercomparison Project (FireMIP) also used the satellite-based product database as a benchmark to evaluate the model simulation (Rabin et al., 2017; Li et al., 2019).

In the last few decades, several global biomass burning emission datasets based on burning area and fire radiative energy detection have been developed and used for many purposes, such as global climate and vegetation modeling, together with environmental, health, and security assessments (Ichoku et al., 2008; Mouillot et al., 2014). Although fire-related observation datasets are available and globally accessible, they have relatively large uncertainties and are poorly constrained, especially in models at the global and regional levels (Liousse et al., 2010; Petrenko et al., 2012, 2017; Bond et al., 2013; Zhang et al., 2014; Pan et al., 2015; Pereira et al., 2016).

Pan et al. (2020) reported that this uncertainty could be caused by various measurement and/or analysis processes, including the detection of fire or burned areas, retrieval of fire radiative power, emission factor information, biome type, burning stage, and fuel consumption estimation. The emission factor (EF) is considered an important factor for obtaining specific gaseous or particulate species of smoke emitted from burned dry matter in all major burned biomass (BB) emission datasets. Some EFs originate from laboratory experiments where fuel samples are burned in combustion chambers (Christian et al., 2003; Freeborn et al., 2008), whereas others originate from large-scale, open biomass burning and wildfire experiments. The combustion properties might differ greatly between these two categories; e.g., because of personnel security and other logistical considerations, some EF measurement locations are often not close enough to the biomass-burning source (Aurell et al., 2019). Another factor is the biome type, which affects the scaling factor of the emission coefficient for the FRP-based BB datasets (GFAS, FEER, and QFED). The emission factors of all BB datasets were assigned based on the type of biome, and most of the examined BB datasets had different definitions of major biome types, so uncertainty might be present at certain levels (Pan et al., 2020).

We validated the improved SEIB-DGVM fire module products by using the burned area (GFED4) and burned fraction (GFED4s) datasets, corresponding to the model's output. These datasets have higher resolutions than other burned area-based datasets, and all of the uncertainty probabilities regarding the selected database described by Pan et al. (2020) were adjusted with our model configurations. We used the emission factor (EF) from Andreae and Merlet (2001) with the latest update from Andreae (2019) and integrated the Plant Functional Types (PFTs) model with the land cover types (LCTs) used in the EF (Table 3 and Table 2).

Furthermore, fire models should be evaluated together with their associated vegetation models because the former might produce burned areas perfectly but incorrectly simulate aboveground biomass (AGB) patterns. Fire products depend on AGB availability, and fire also affects AGB availability and succession after forest fires. Thus, to ensure that the model conducted correct assessments, we evaluated the aboveground biomass variable using the ESA Biomass Climate Change Initiative dataset (Table 5). The AGB data from the ESA Biomass Climate Change Initiative (CCI) v.3 (2010,2017, and 2018) include high-quality data with a large resolution of 100 m × 100 m obtained from multiple remote sensing observations collected around the year 2010 (Santoro et al., 2021), making them suitable for validating our improved model product.

Overall, we validated the model spatially and numerically at Siberian level and in smaller regions, to determine the performance of the model in many points of view (spatial, numeric, wide and small region). We classified Siberia into three regions: west region (60^{o}-90^{o}E and 45^{o}-80^{o}N), central region (90^{o}-120^{o}E and 45^{o}-80^{o}N), and east region (120^{o}-180^{o}E and 45^{o}-80^{o}N) (Figure 7).

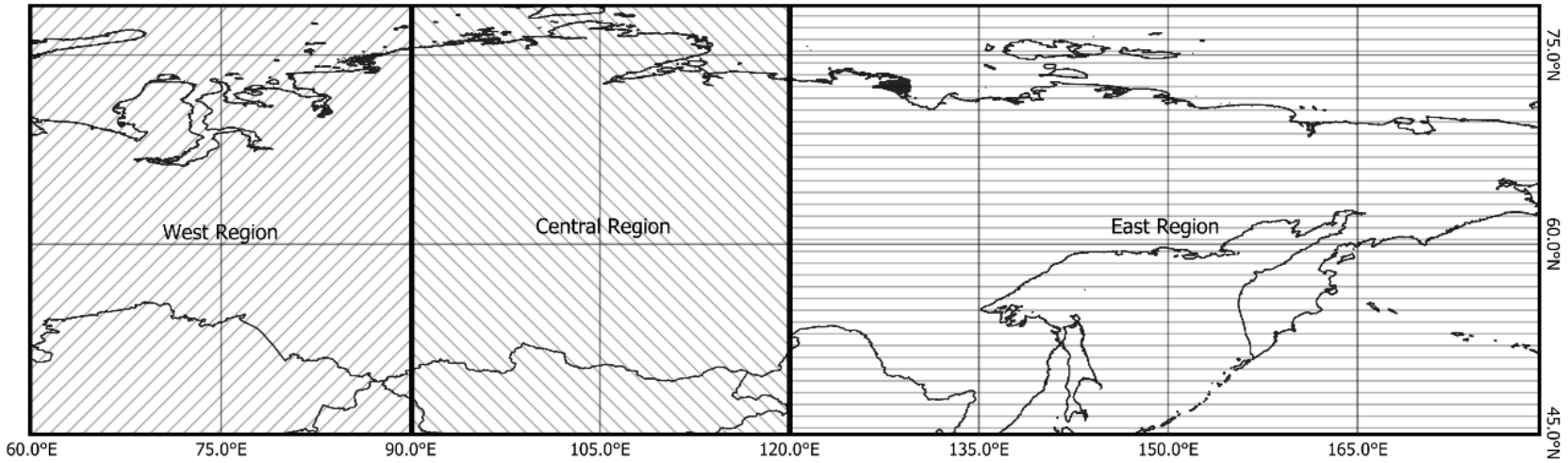

Figure 7. Division of Siberia into three regions: west region (60°-90°E and 45°-80°N), central region (90°-120°E and 45°-80°N), and east region (120°-180°E and 45°-80°N)

Table 5. Description of the observational datasets to be used for model evaluation

Type	Variable	Unit	Source	Spatial resolution	Temporal resolution	Temporal coverage	Reference
Fire	Burned area	Hectares	Global Fire Emissions Database, Version 4.0 (GFED4)	0.25 degree	Monthly, Annual	1996-2016	(Giglio et al., 2013)
	Burned fraction	-	Global Fire Emissions Database, Version 4.1	0.25 degree	Monthly, Annual	1997-2016	(Giglio et al., 2013)
	Dry matter	Kg DM^{-1} m^{-2}					

	CO_2 emissions	g CO_2 $year^{-1}$	(GFED4s)				
	CO_2 emissions	g CO_2 $year^{-1}$	Global Biomass Burning Emissions Inventory (GBEI)	1-degree	Annual	2001-2020	Shiraishi et al., (2021)
Vegetation	Above-ground biomass	Mg $hectares^{-1}$	ESA Biomass Climate Change Initiative (Biomass CCI): Global datasets of forest above-ground biomass for the years 2010, 2017 and 2018, v3	100 m	Annual	2010, 2017-2018	(Santoro and Cartus, 2021)

3. RESULTS

3.1. Improved model validation

3.1.1. Fire products

We compared the annual average distribution patterns of burned fraction variable (1997-2016) in the SEIB-DGVM SPITFIRE and GFED4s data, and most patterns differed only in eastern Siberia (Figure 8, Figure 9). Compared to the burned fraction variable, burned area GFED4 has a smaller distribution pattern because it does not consider small fires (Figure 10.a). Comparison analysis of burned fraction variables between SEIB-DGVM SPITFIRE and GFED4s showed a linear relationship with a correlation coefficient of R=0.87 (R^2=0.75) (Figure 11.a). Similar to the comparison with GFED4s, the comparison of SEIB-DGVM SPITFIRE output of burned area variables with GFED4 data (1996-2016) shows a linear relationship with a correlation coefficient of R=0.78 (R^2=0.61) (Figure 11.b). Furthermore, in the three regions (west, central and east), the partial comparison of the burned fraction variable with GFED4s showed values of R^2=0.68, R^2=0.51, and R^2=0.58 (Figure 12), while for the burned area variable showed values of R^2=0.51, R^2=0.54, and R^2=0.506 (Figure 13), respectively. The burned fraction correlated better because both the GFED4s and the model's fire module considered small fires; many scattered fire data with values less than 0.1 and approximately 0.1 were found in both the model's output and the GFED4s data.

The fire products (burned fraction and burned area) in the improved model have the same spatial distribution because they are calculated based on one core variable (fire probability) (Eq. 1). However, the spatial distributions of GFED4s (burned fraction) and GFED4 (burned area) differ for two reasons: first, because GFED4 does not consider small fires (Giglio et al., 2013) while GFED4s does, and second, because GFED4s use the modified burned fraction equation, which is able to calculate the exact fire fraction and fuel load (not uniformized) in a grid cell (Van Der Werf et al., 2017).

Although the spatial distributions and patterns of the fire products (burned fraction and burned area) in the model and benchmark datasets (GFED4s and GFED4) data slightly differed, the model was able to produce annual mean value data that were similar to both benchmark datasets. The mean average burned fraction during 1997-2016 was 0.0137 in the simulations, compared to the GFED4s, which recorded the same value of 0.0137 with an RMSE value of 7.2×10^{-4}. Furthermore, the mean average burned area of the model in 1996-

2016 was 1428.5 ha $grid^{-1}$ $year^{-1}$, compared to the GFED4 burned area data, which closely recorded value of 1425.1 ha $grid^{-1}$ $year^{-1}$ by an RMSE value of 70.2 ha $grid^{-1}$ $year^{-1}$. In summary, the model was able to produce mean average data that precisely resembled observational data.

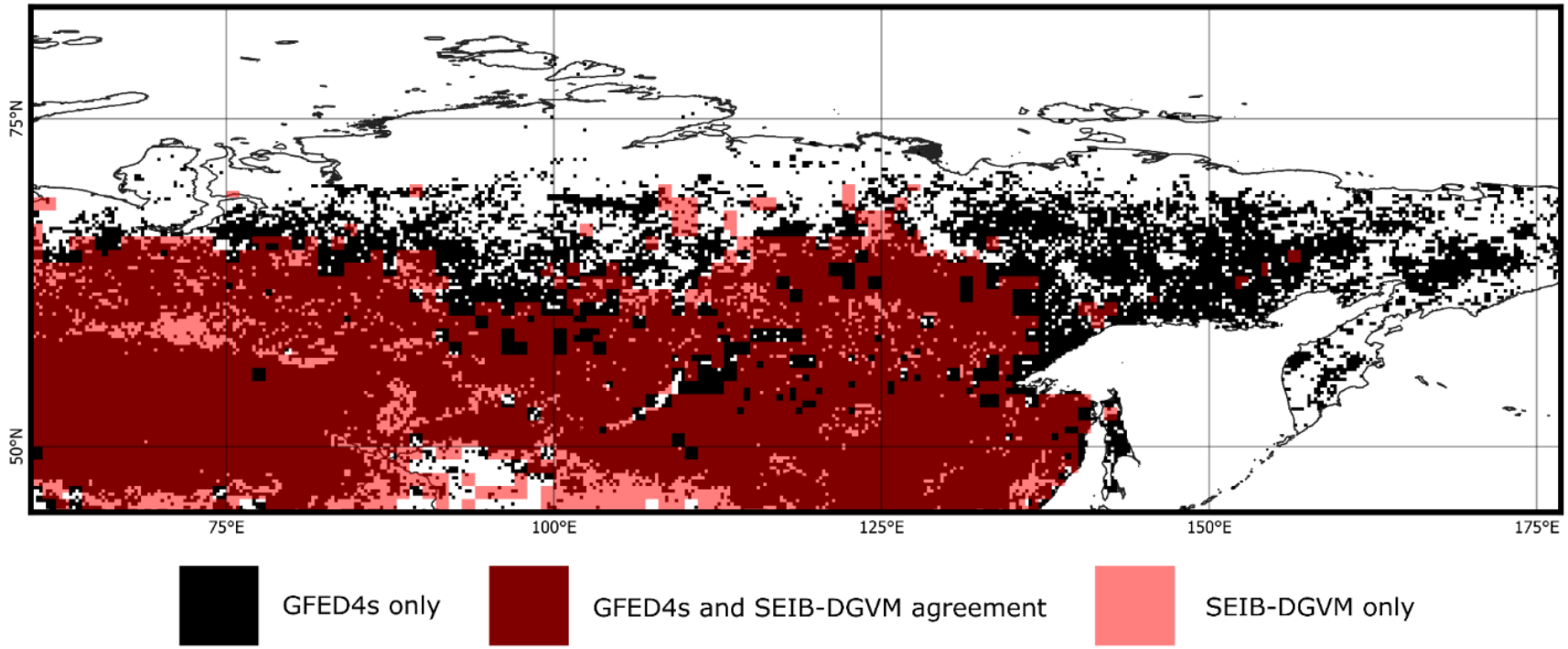

Figure 8. Spatial distribution comparison of annual averaged burned fraction variable (1997-2016) of SEIB-DGVM SPITFIRE and GFED4s

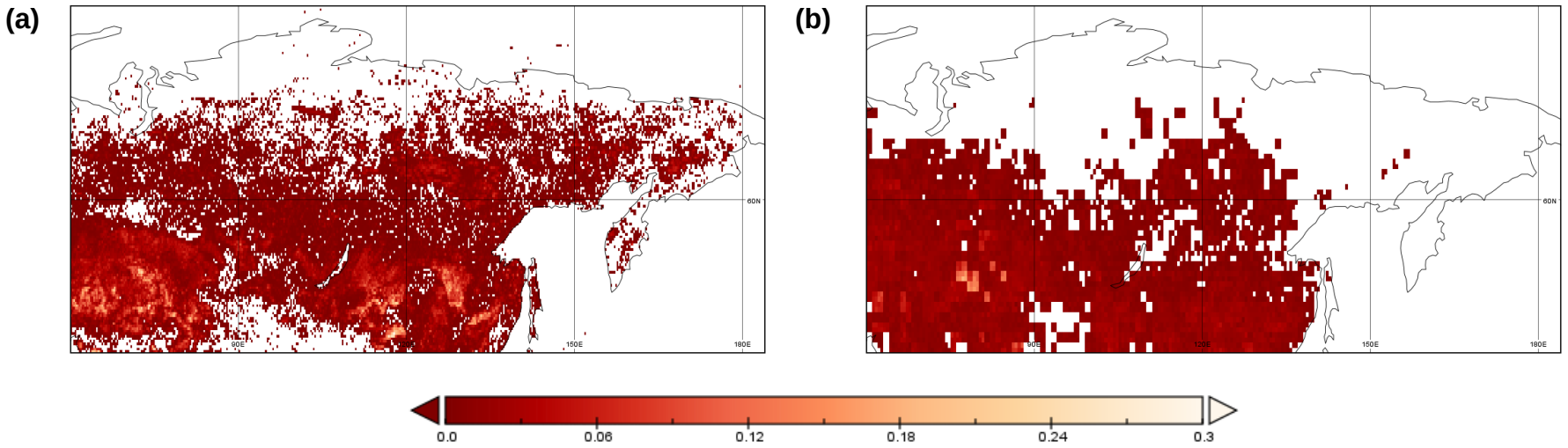

Figure 9. Spatial distribution of annual averaged (1997-2016) burned fraction variable of: **(a)** GFED4s **(b)** SEIB-DGVM SPITFIRE

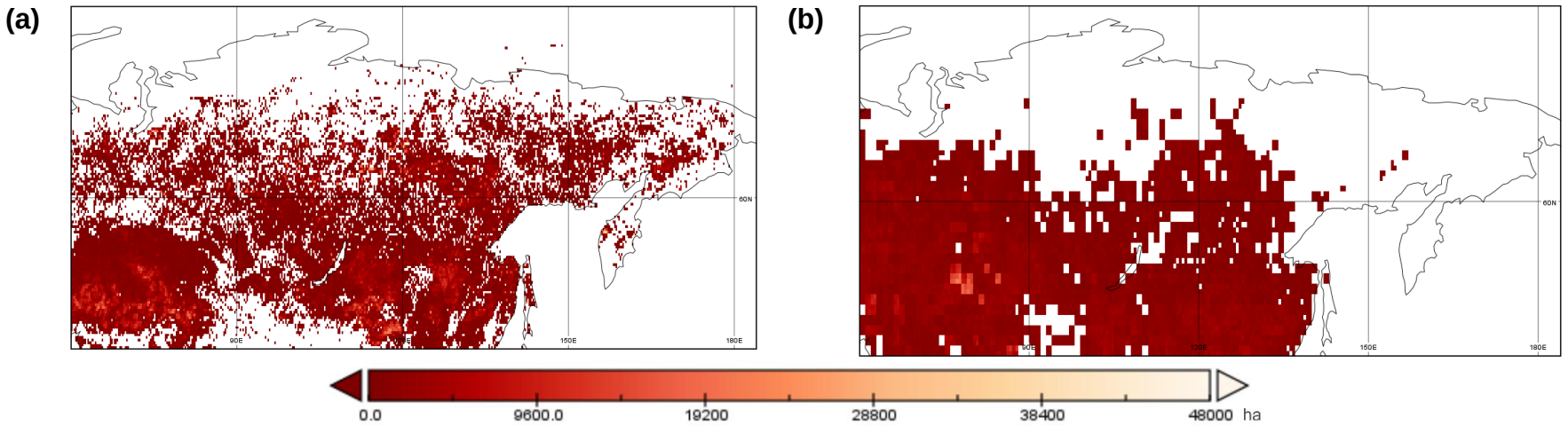

Figure 10. Spatial distribution of annual averaged (1996-2016) burned area variable of: **(a)** GFED4 **(b)** SEIB-DGVM SPITFIRE

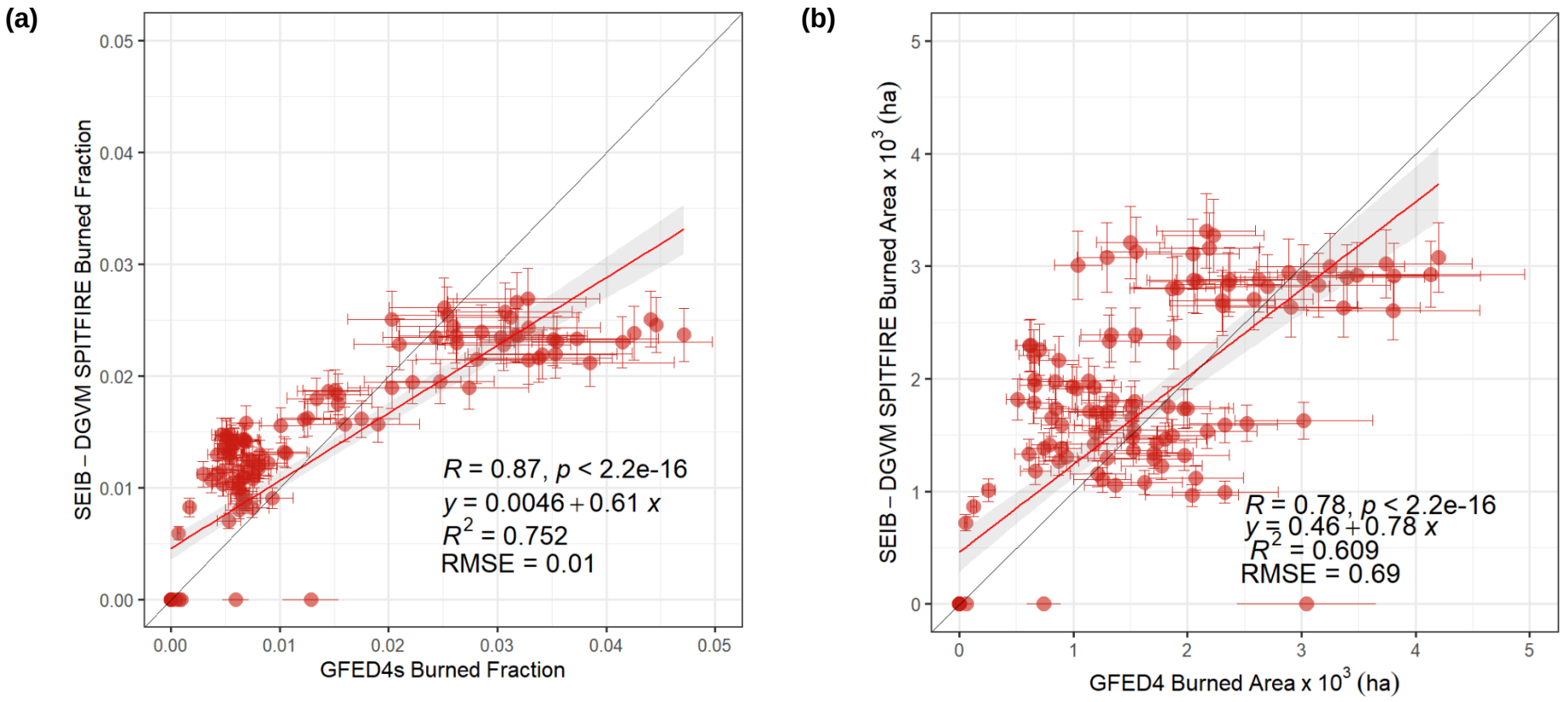

Figure 11. (a) Latitude average spatial comparison of annual averaged simulated burned fraction of SEIB-DGVM SPITFIRE and burned fraction of GFED4s from 1997 to 2016. **(b)** Latitude average spatial comparison of annual averaged simulated burned area of SEIB-DGVM SPITFIRE and burned area of GFED4 from 1996 to 2016.

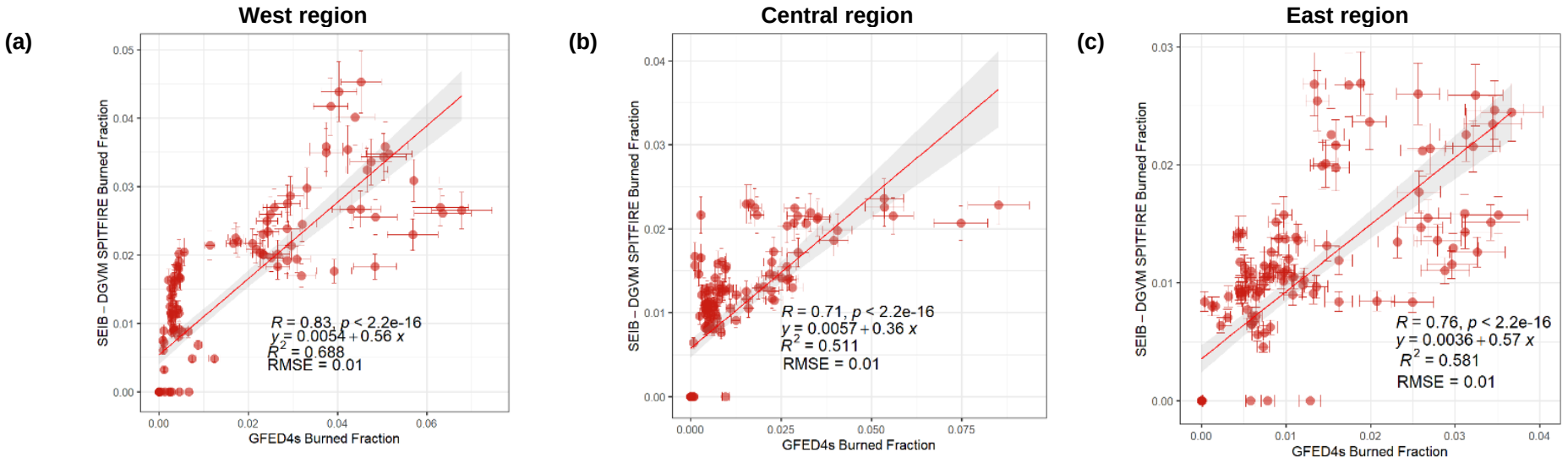

Figure 12. Latitude average spatial comparison of annual averaged (1997-2016) simulated burned fraction of SEIB-DGVM SPITFIRE and burned fraction of GFED4s in: **(a)** west region **(b)** central region, **(c)** east region

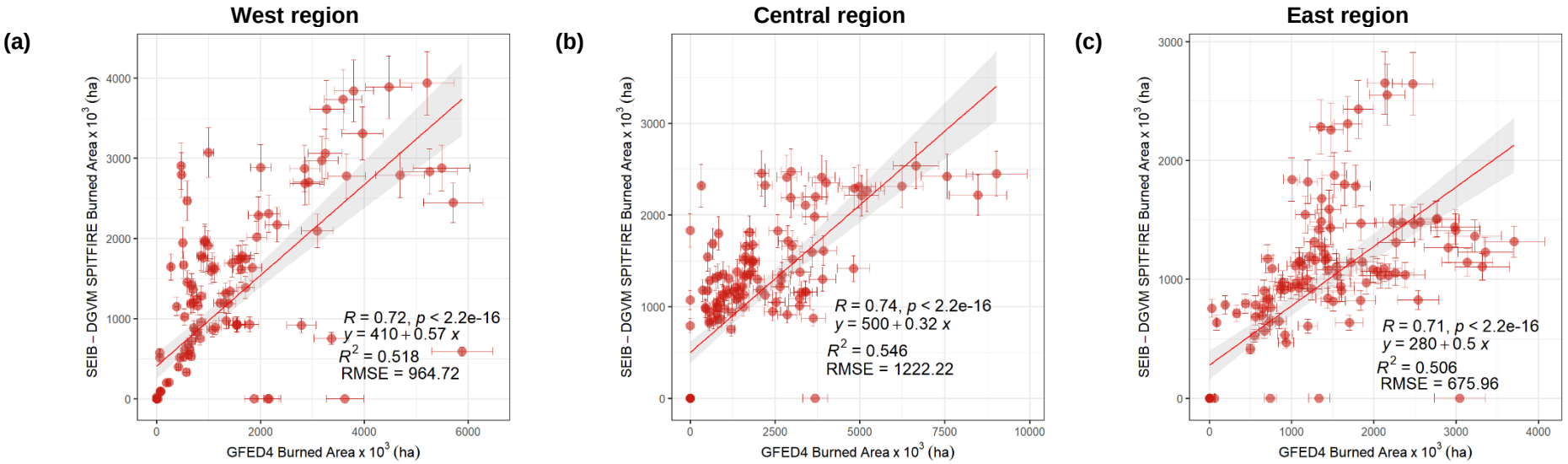

Figure 13. Latitude average spatial comparison of annual averaged (1996-2016) simulated burned area of SEIB-DGVM SPITFIRE and burned area of GFED4s in: **(a)** west region **(b)** central region, **(c)** east region

3.1.2. Aboveground biomass

The improved model simulated similar aboveground biomass values to those of the benchmark data. In 2010, 2017, and 2018, the simulations predicted 63.714 ± 64.89 Mg DM ha^{-1} $year^{-1}$, 64.141 ± 65.54 Mg DM ha^{-1} $year^{-1}$, and 64.313 ± 65.61 Mg DM ha^{-1} $year^{-1}$, respectively, while the ESA Biomass CCI data showed 64.027 ± 56.95 Mg DM ha^{-1} $year^{-1}$, 64.548 ± 54.69 Mg DM ha^{-1} $year^{-1}$, and 65.05 ± 55.78 Mg DM ha^{-1} $year^{-1}$, respectively, for the same years. The annual average AGB of the model in these years also showed the same increasing trend as that of the benchmark data, and the spatial distributions of the AGB model under CRU TS3.22 climate data and ESA Biomass CCI also agreed, with values of 83%, 85%, and 85%, respectively (Figure 14 and Figure 15 in the Supplement). Furthermore, when viewed on a smaller regional scale, the model is able to project better values in the western, central and eastern regions, with average values of R^2=0.73, R^2=0.69, and R^2=0,74, respectively (Figure 16). Although there was an annual average increase in the number of forest fires, there was a high variability trend in the model AGB values, indicating succession after forest fires and respond correctly to climate inputs variables based on each RCP scenario (Figure 38.d).

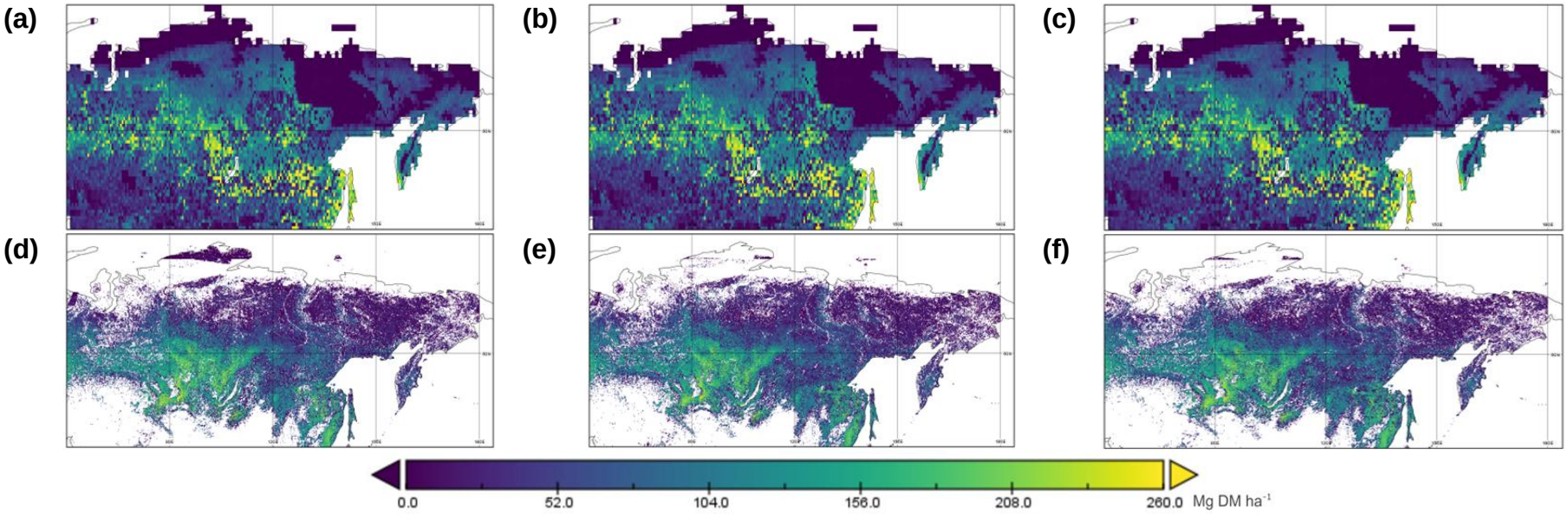

Figure 14. Spatial distribution of annual averaged aboveground biomss (AGB) of: **(a)** SEIB-DGVM SPITFIRE 2010. **(b)** SEIB-DGVM SPITFIRE 2017. **(c)** SEIB-DGVM SPITFIRE 2018. **(d)** ESA Biomass Climate Change Initative (CCI) 2010. **(e)** ESA Biomass CCI 2017. **(f)** ESA Biomass CCI 2018.

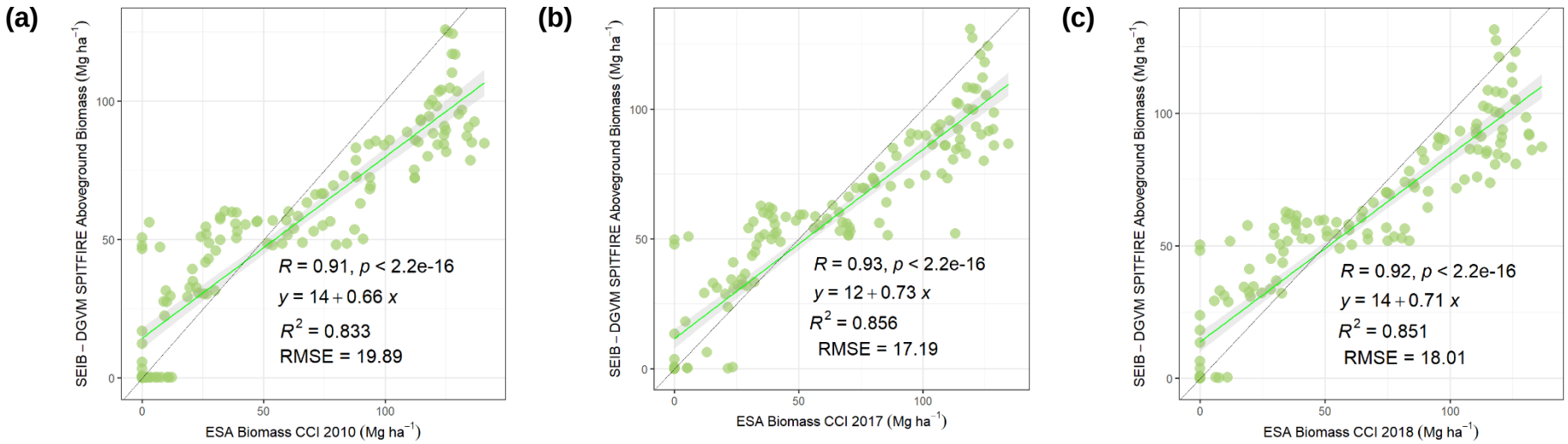

Figure 15. Latitude average spatial comparison of annual averaged simulated aboveground biomass of SEIB-DGVM SPITFIRE and aboveground biomass of ESA Biomass CCI in: **(a)** 2010. **(b)** 2017. **(c)** 2018.

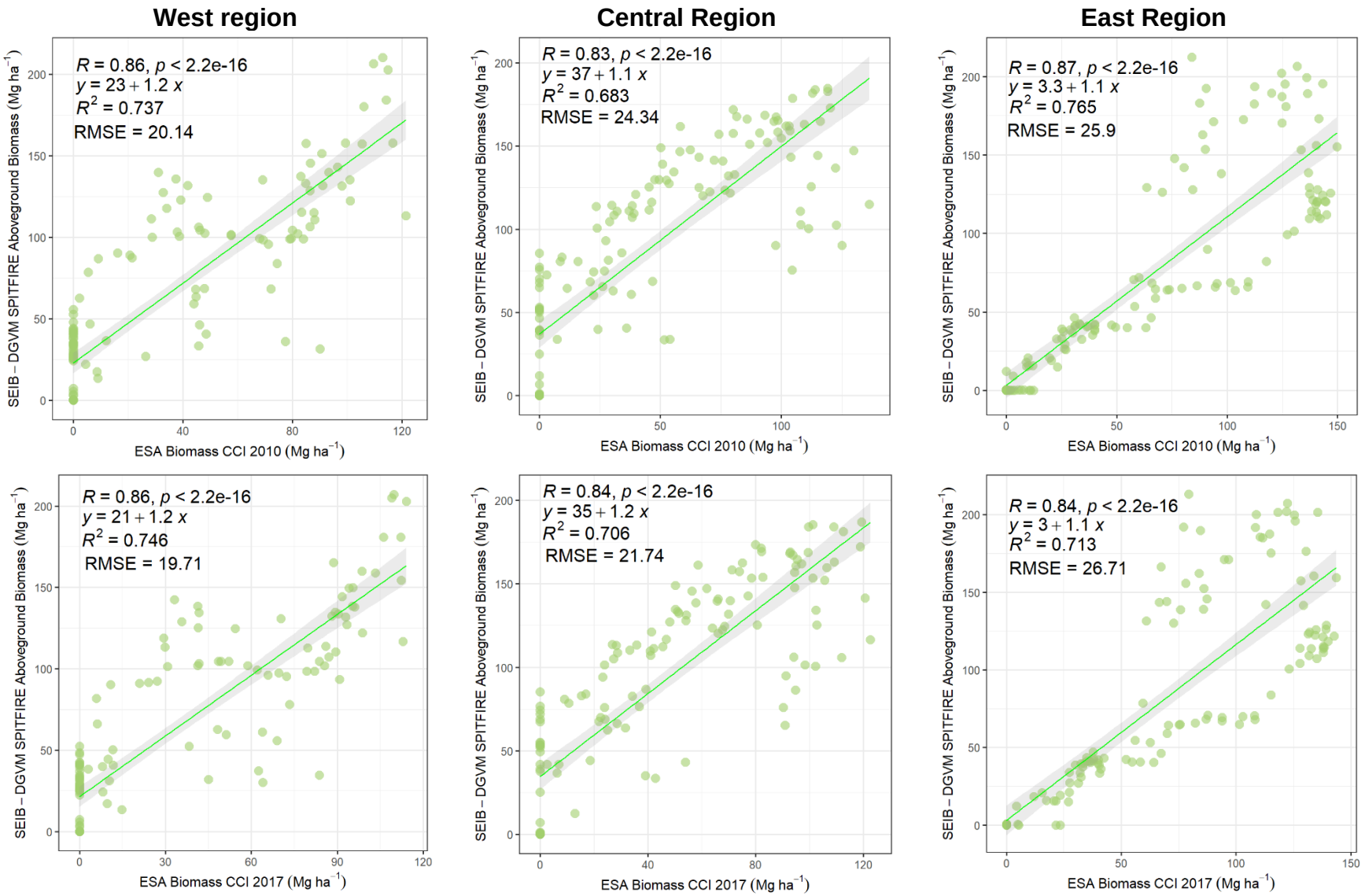
West region
Central Region
East Region
R = 0.86, p < 2.2e-16
y = 23 + 1.2 x
R² = 0.737
RMSE = 20.14
R = 0.83, p < 2.2e-16
y = 37 + 1.1 x
R² = 0.683
RMSE = 24.34
R = 0.87, p < 2.2e-16
y = 3.3 + 1.1 x
R² = 0.765
RMSE = 25.9
R = 0.86, p < 2.2e-16
y = 21 + 1.2 x
R² = 0.746
RMSE = 19.71
R = 0.84, p < 2.2e-16
y = 35 + 1.2 x
R² = 0.706
RMSE = 21.74
R = 0.84, p < 2.2e-16
y = 3 + 1.1 x
R² = 0.713
RMSE = 26.71
SEIB – DGVM SPITFIRE Aboveground Biomass (Mg ha⁻¹)
ESA Biomass CCI 2010 (Mg ha⁻¹)
ESA Biomass CCI 2017 (Mg ha⁻¹)

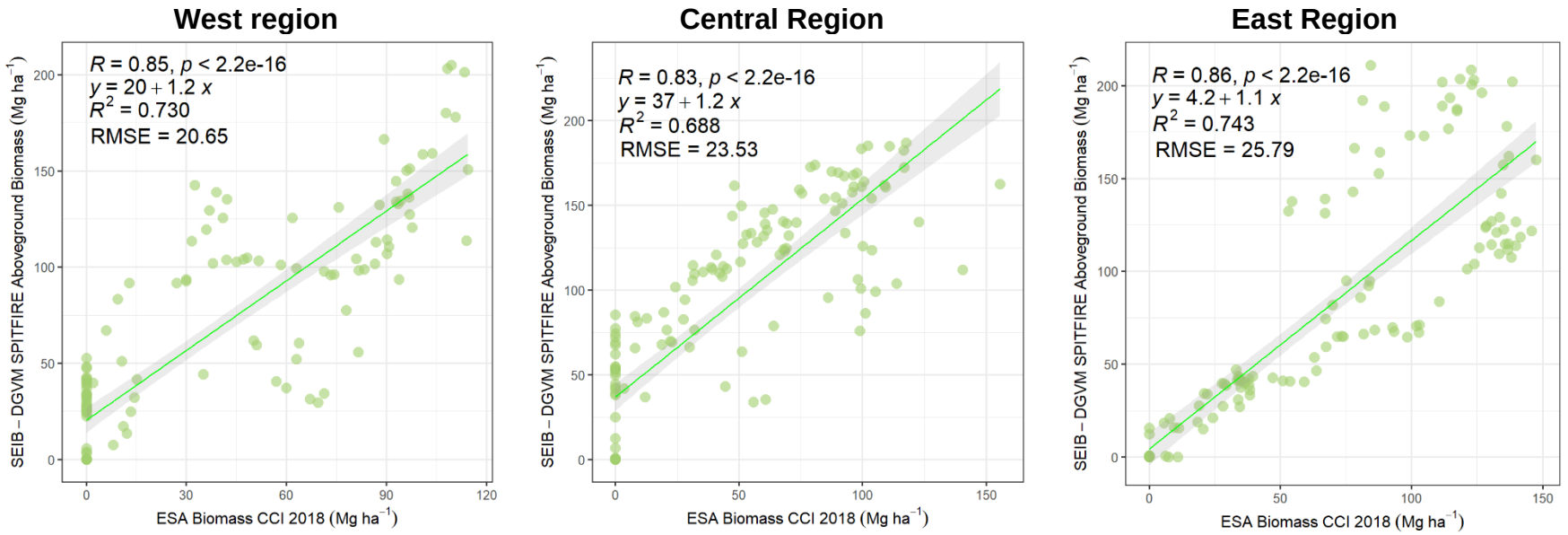

Figure 16. Latitude average spatial comparison between annual averaged (2010, 2017, 2018) simulated aboveground biomass of SEIB-DGVM SPITFIRE and aboveground biomass

3.1.3. Annual and seasonal fluctuations in burned dry matter

The model's dry matter data have a spatial distribution pattern similar to that of the model's fire products (burned fraction and burned biomass), as calculated from the available fire and fuel load data (fire product derivatives). The annual average dry matter variability from the 1997–2016 model (under the historical climate product [CRU TS.3.22]) and the GFED4s data agreed with 6.24%, similar to the agreement of the fire products (Figure 18). Spatial comparisons at the regional scale in the western, central and eastern regions of Siberia show lower values than the Siberian region as a whole, which has an agreement of 60.2%. 64.4%, and 58.8% (Figure 19).

We also compared seasonal dry matter data to ensure that the monthly outputs of the SEIB-DGVM SPITFIRE model agree with the observations, as this difference influences seasonal aerosol emissions. Between 1997 and 2016, the GFED4s data exhibited high fluctuations/dynamics depending on the month and year, while the SEIB-DGVM SPITFIRE was not able to reproduce these dynamics or accurately predict the occurrence of extreme events (Figure 17a). For example, intense forest fires were recorded in 2003, 2012, and 2016. The monthly burned dry matter data for these years peaked in 2003 in May and in 2012 and 2016 in July (Figure 17.b-d). Severe wildfires in 2003 were due to low precipitation, as total precipitation reached only 36.0 mm in the Buryatia Republic and 45.7 mm in the Chita Oblast between August 2002 and May 2003 (IFFN, 2003). While the 41-year average precipitation between August and May (1981-2022), in the Buryatia Republic was approximately 332.23 mm, and in the Chita Oblast was approximately 119.45 mm. Thus, the low precipitation in 2003 was an anomaly outside of the annual average range.

Furthermore, the improved model's monthly average burned dry matter in 2003, 2012, and 2016 was also lower compared to the GFED4s data. The burned dry matter values of the improved model were 58.64 ± 5.86 kg DM m^{-2}, 59.41 ± 5.9 kg DM m^{-2}, and 59.98 ± 5.99 kg DM m^{-2}, while the benchmark data showed values of 122.36 kg DM m^{-2}, 101.7 kg DM m^{-2}, and 69.95 kg DM m^{-2}, respectively.

However, considering the entire period from 1997 to 2016, not only during years with extreme fire events, the model was also able to reproduce similar average values for multiple years and time-series data. When comparing the monthly averages during 1997-2016, the model data yielded a value of 58.94 ± 5.89 kg DM m^{-2}, while the GFED4s data yielded 59.12 kg DM m^{-2}. The model is not yet able to reproduce the exact value at a specific time of year

or month because it runs in a long-term phase and is not yet able to predict sudden natural and anthropogenic conditions (factors). Overall, the spatial distribution comparison of the monthly dry matter variables from GFED4s and SEIB-DGVM SPITFIRE for 20 years (1997-2016) revealed a correlation of 99% (Figure 20); therefore, the model was able to approximate the monthly averages.

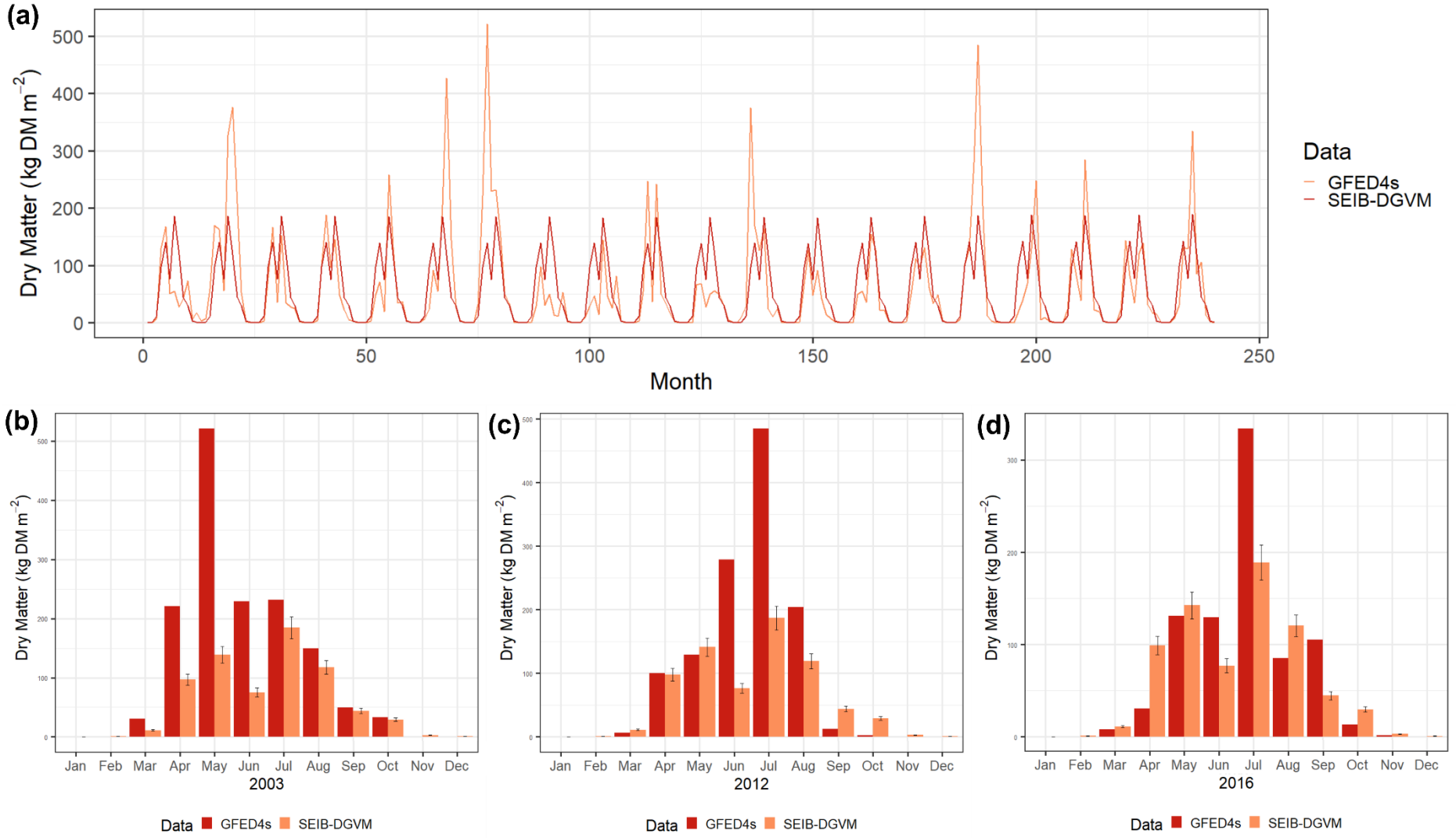

Figure 17. Temporal variation of monthly dry matter emission variable of SEIB-DGVM SPITFIRE and GFED4s. **(a)** from 1997 to 2016. **(b)** 2003. **(c)** 2012. **(d)** 2016

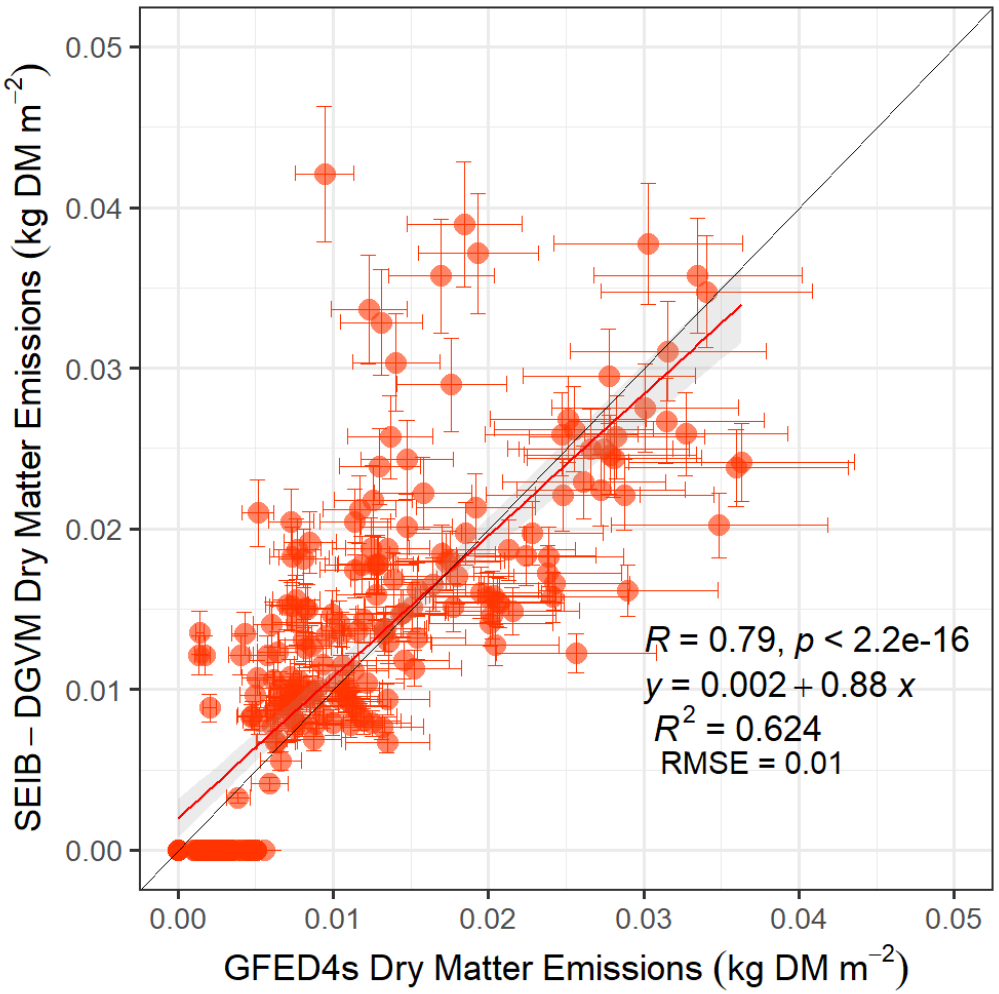

Figure 18. Latitude average spatial comparison of annual averaged simulated dry matter emission of SEIB-DGVM SPITFIRE and dry matter emission of GFED4s from 1997 to 2016.

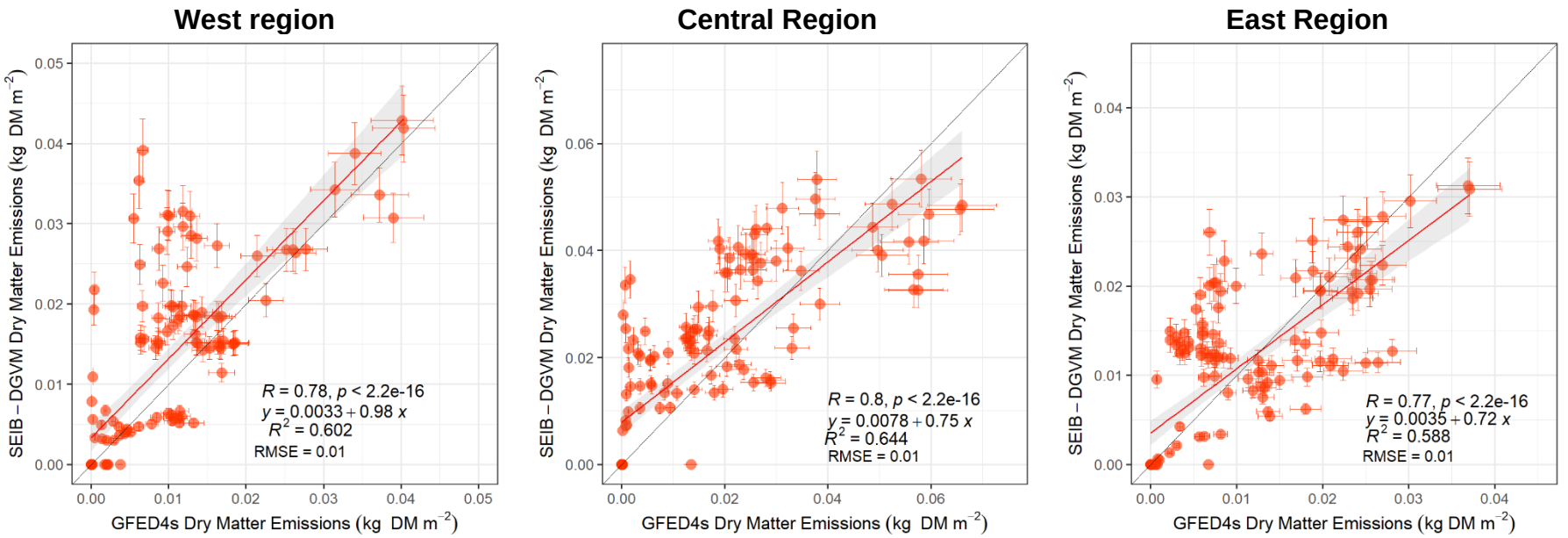

Figure 19. Latitude average spatial comparison of annual averaged (1997-2016) simulated burned fraction of SEIB-DGVM SPITFIRE and burned fraction of GFED4s in: **(a)** west region **(b)** central region, **(c)** east region

3.1.4. Carbon dioxide (CO_2) and $PM_{2.5}$ emissions

Emissions from biomass burning contribute significantly to the global budget for residual gases and aerosols that affect the climate. It's estimated that biomass burning contributed up to 50% of global CO and NO_x emissions in the troposphere (Galanter et al., 2000), and the most emitted gas during biomass burning is CO_2 (Ritchie et al., 2020). Since CO_2 emissions are the primary emissions that contribute to climate change, it is critical to assess and monitor them continuously.

In this study, out of 33 projected emissions (Table 6 and Table 7), we validated the CO_2 variable that able to represent all projected emissions because all estimated emissions are derived from the same burned dry matter variable, which differs only in the emission factor value of each gaseous emission. The highest annual average value of CO_2 emissions from 1997 to 2020 is from GFED4 data, followed by SEIB-DGVM SPITFIRE and then the GBEI product, with values of $105.64 \pm 50.69 \times 10^4$ Gg CO_2, $76.12 \pm 0.87 \times 10^4$ Gg CO_2, and $62.4 \pm 26.09 \times 10^4$ Gg CO_2, respectively (Table 8). The GFED4s and GBEI data have higher standard deviation values than does the SEIB-DGVM SPITFIRE data and appear to have a large difference.

Spatially, the annual average CO_2 emission model data were 61.3% (Figure 21.a) and 79.8% (Figure 21.b) correlated with the GFED4s and GBEI data, respectively. Furthermore, CO_2 emissions of the model compared to the GFED4s in the three regions (west, central, and east) showed lower agreement than Siberia as a whole, at 62.7%, 62.5%, and 61.6%, respectively (Figure 28). Whereas the comparison to GBEI data at the three regions, showed agreements of 74.7%, 77.6%, and 64.3%, respectively (Figure 29). In addition, spatial comparison of annual mean data over 95 years (2006-2100) from SEIB-DGVM SPITFIRE, GFED4s, and GBEI datasets reveals similar values of 141.1 ± 11.5 Gg CO_2 $year^{-1}$, 157.2 ± 14.8 Gg CO_2 $year^{-1}$, and 148.7 ± 7.12 Gg CO_2 $year^{-1}$, respectively

Our study area covers the Boreal Asia (BOAS) area and a small part of Central Asia (CEAS), differing from the GFED4 basis region classification; therefore, we extracted these areas from the GFED4s data for comparison (Figure 24). A comparison of the GFED4s CO_2 data between the BOAS area and the Siberian area showed that the two datasets had a similarity of 98.2% (Figure 25), confirming the accuracy of the GFED4s validation data.

As all emission products are derived from fire products (dry matter variables), emission factors displayed spatial and value dynamics similar to those of the fire products (Figure 23, Figure 26, Figure 27, and Figure 56). When comparing the annual average dry matter emission data and CO_2 emissions generated by the model, the results correlated perfectly (100%, Figure 30), indicating that the model runs well according to Equation (3) and the projected CO_2 and other emissions have the same distribution patterns as the dry matter variable, because all of the emissions calculation are based on the dry emission variable. However, they differ in their values because each emission species has a different emission factor.

We also compared the modelled $PM_{2.5}$ emissions and their distribution patterns with the Copernicus Atmosphere Monitoring Service (CAMS) (Romanov et al., 2022) data in seven Russian territories (Amur Region, Buryatia Republic, Irkutsk Region, Khabarovsk Territory, Krasnoyarsk Territory, Transbaikal Territory, Yakutia (Sakha Republic)) during 2010-2021. The improved model data and CAMS data both exhibited an increasing trend (Figure 22.a and Figure 2 in Romanov et al. (2022)) and a correlation of 85.8% (Figure 22.b).

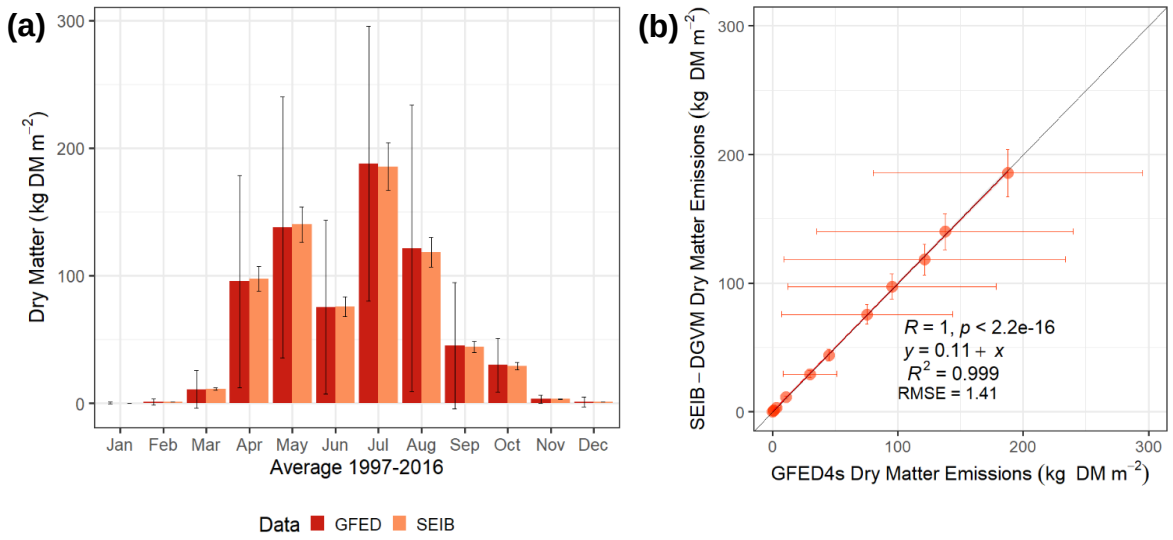

Figure 20. (a) Monthly temporal variability averaged dry matter emission of GFED4s and SEIB-DGVM from 1997 to 2016. **(b)** Comparison of monthly averaged dry matter emissions of GFED4s and SEIB-DGVM from 1997 to 2016. Standard deviation obtained from each monthly data from 1997 to 2016.

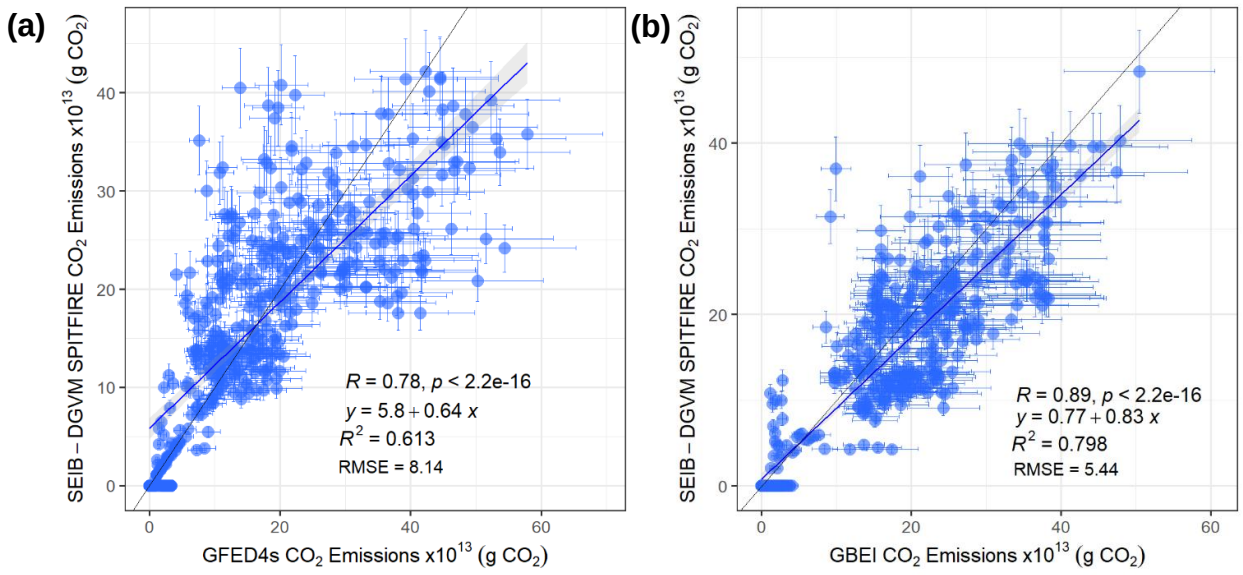

Figure 21. Latitude average spatial comparison of simulated CO_2 emissions of SEIB-DGVM SPITFIRE with GFED4s from 1997 to 2016 (**a)** and GBEI from 2001 to 2020 **(b)** dataset. Standard deviation obtained from the annual CO_2 emission data of each dataset.

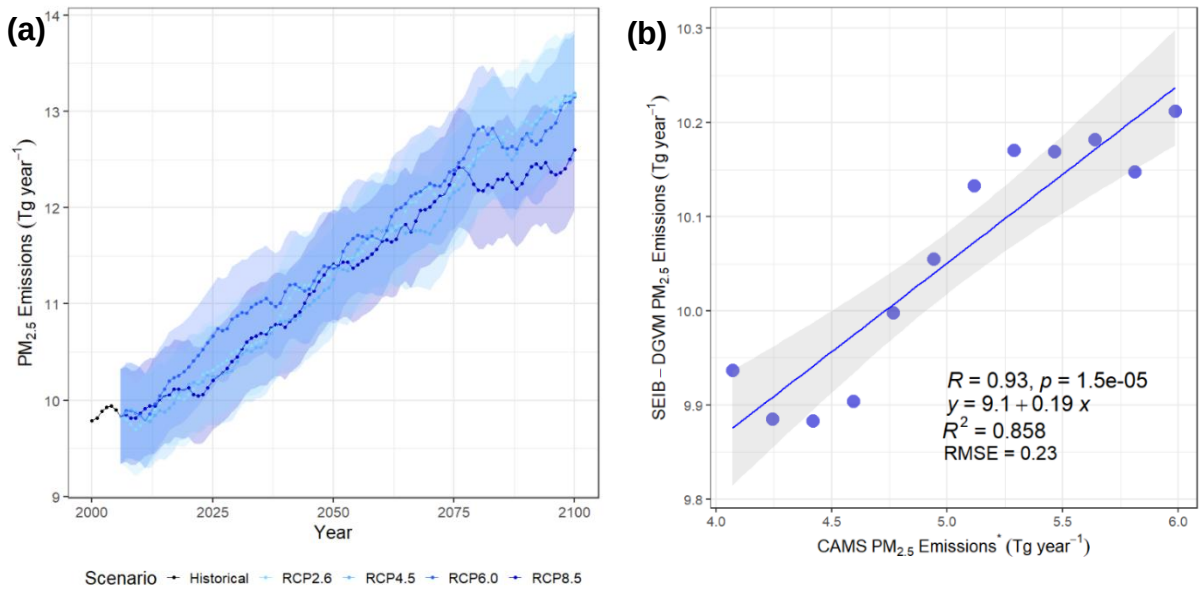

Figure 22. (a) Temporal variation of projected $PM_{2.5}$ emissions under several climate scenarios from 2000 to 2100. Standard deviation obtained from the annual $PM_{2.5}$ emission value of each climate scenarios (RCP8.5, RCP6.0, RCP4.5, and RCP2.6). **(b)** Comparison of $PM_{2.5}$ emissions from the SEIB-DGVM SPITFIRE model with the *trendline processed data from the Copernicus Atmosphere Monitoring Service in seven regions in Russia from 2004 to 2021 (Romanov et al., 2022).

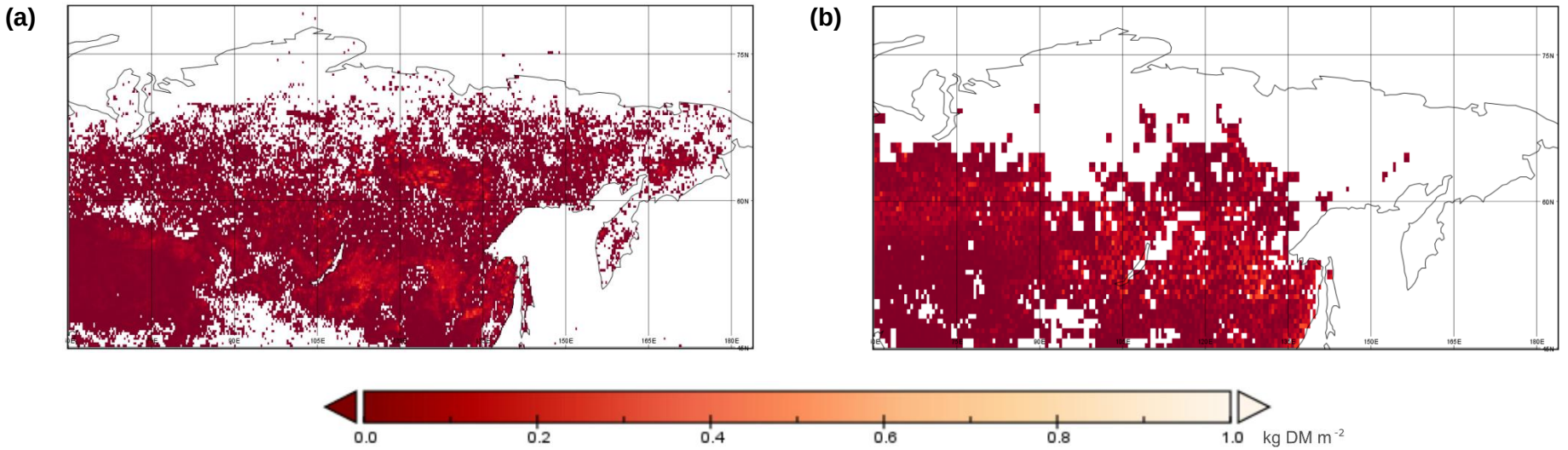

Figure 23. (a) Spatial distribution of annual averaged dry matter emissions of GFED4s from 1997-2016. **(b)** Spatial distribution of annual averaged dry matter emission of SEIB-DGVM SPITFIRE from 1997 to 2016

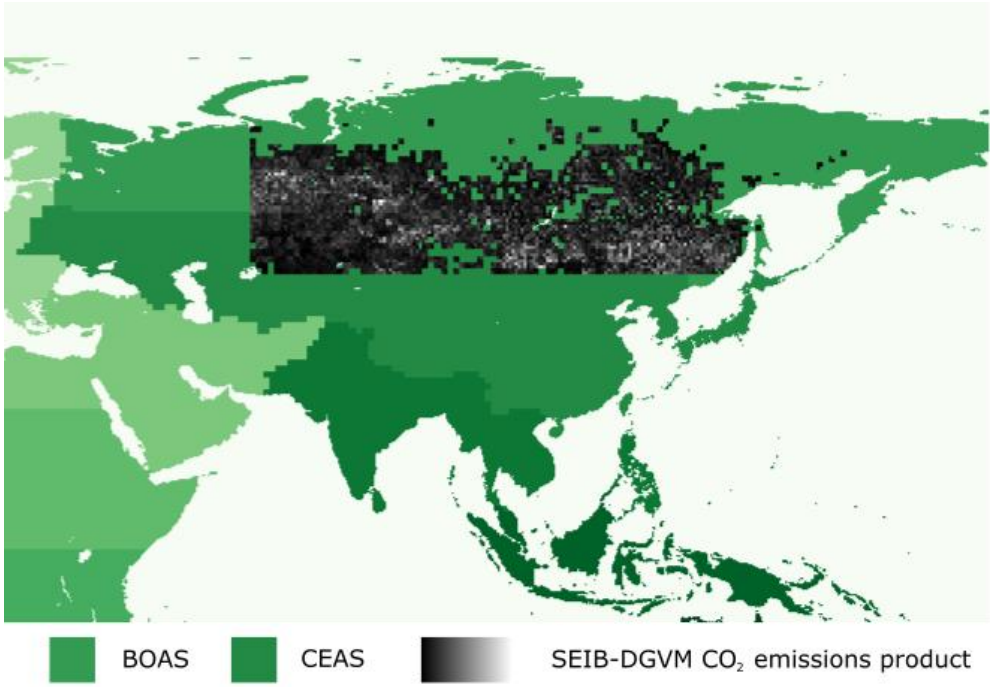

Figure 24. GFED basis region and SEIB-DGVM output area map comparison
BOAS: Boreal Asia. CEAS: Central Asia

Table 8. Annual CO_2 emissions data from GFED4s (Siberia and BOAS), GBEI, and SEIB-DGVM SPITFIRE product (1 x 10^4 Gg CO_2)

Year	Siberia			BOAS
	GFED4s	SEIB-DGVM	GBEI	GFED4s
1997	85.9423	75.06	n.a	30
1998	212.3127	75.29	n.a	89
1999	78.2312	75.05	n.a	32
2000	91.2028	75.07	n.a	35
2001	90.7241	75.27	42.49	32
2002	146.7248	75.82	58.29	51
2003	218.6563	76.12	125.1	88
2004	42.2935	76.22	43.7	14
2005	59.1899	75.90	36.37	21
2006	101.7702	75.40	64.84	43
2007	52.6425	75.57	32.62	18
2008	139.1379	75.30	89.25	57
2009	59.2727	75.28	50.47	21
2010	69.6919	75.67	41.26	28
2011	80.1802	76.04	71.73	32
2012	181.7223	76.22	126.8	67
2013	77.3021	76.24	41.23	26
2014	110.0743	76.70	71.46	41
2015	90.7468	77.08	49.86	33
2016	124.9715	77.12	70.33	46
2017	n.a	77.59	46.49	n.a
2018	n.a	77.59	55.51	n.a
2019	n.a	77.52	70.98	n.a
2020	n.a	77.67	60.8	n.a
Average	105.64 ± 50.69	76.12 ± 0.87	62.48 ± 26.09	40.2 ± 21.12

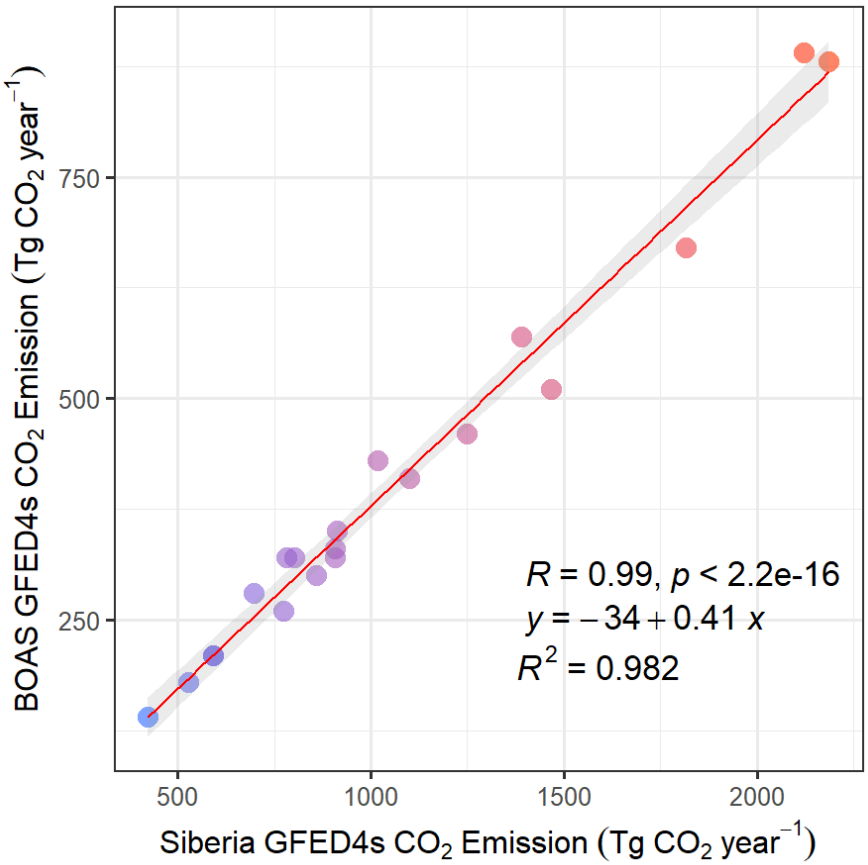

Figure 25. Comparison of annual averaged CO_2 emissions GFED4s in Siberia and Boreal Asia (BOAS) region from 1997 to 2016

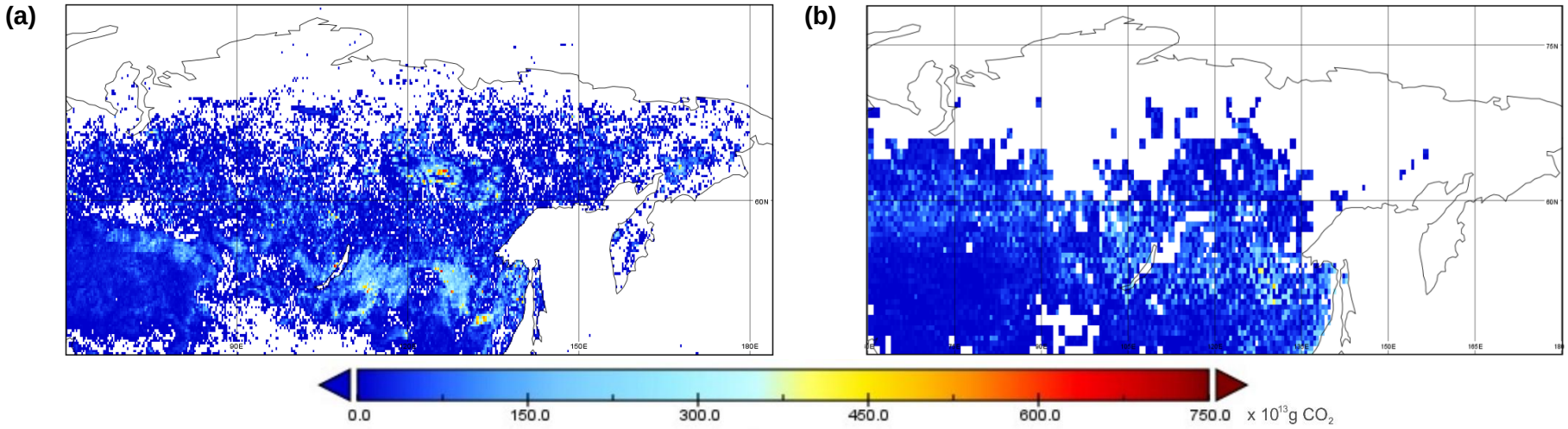

Figure 26. (a) Spatial distribution of annual averaged CO_2 emissions of GFED4s from 1997-2016. **(b)** Spatial distribution of annual averaged CO_2 emissions of SEIB-DGVM SPITFIRE from 1997-2016.

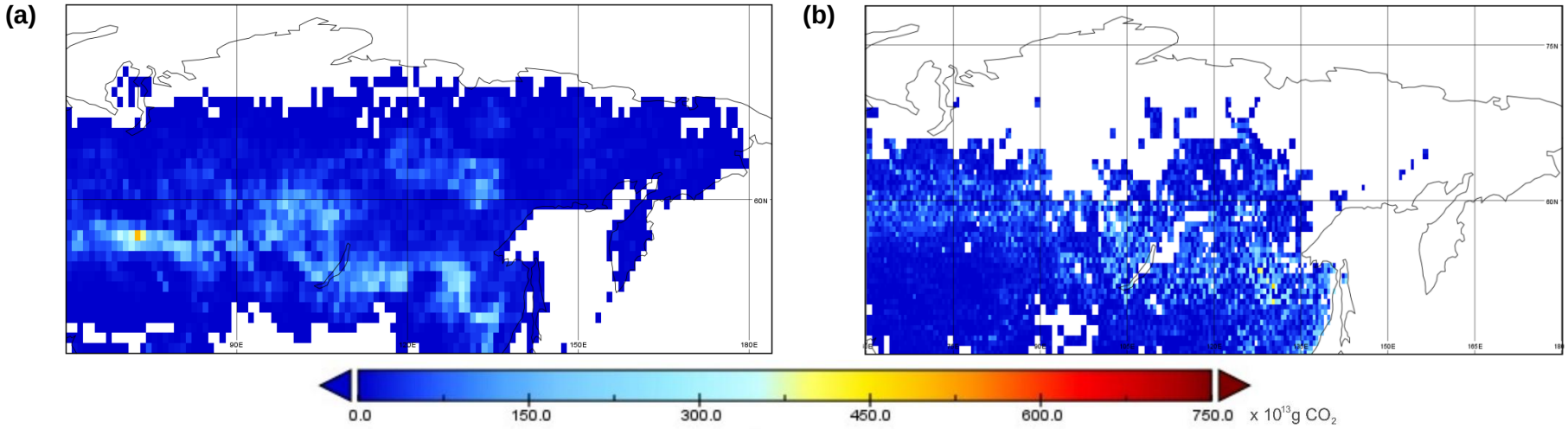

Figure 27. (a) Spatial distribution of annual averaged CO_2 emissions of GBEI from 2001 to 2020. **(b)** Spatial distribution of annual averaged CO2 emissions of SEIB-DGVM SPITFIRE from 2001 to 2020.

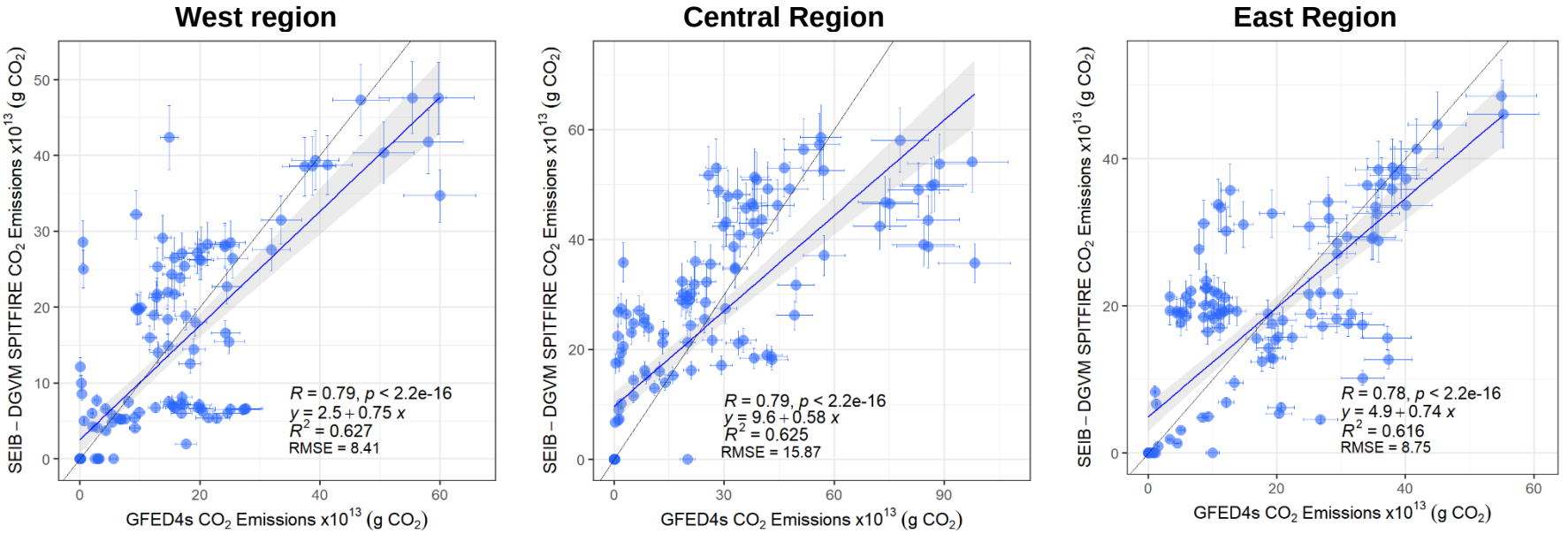

Figure 28. Latitude average spatial comparison of annual averaged (1997-2016) simulated CO_2 emissions of SEIB-DGVM SPITFIRE and CO_2 emissions of GFED4s in: **(a)** west region **(b)** central region, **(c)** east region

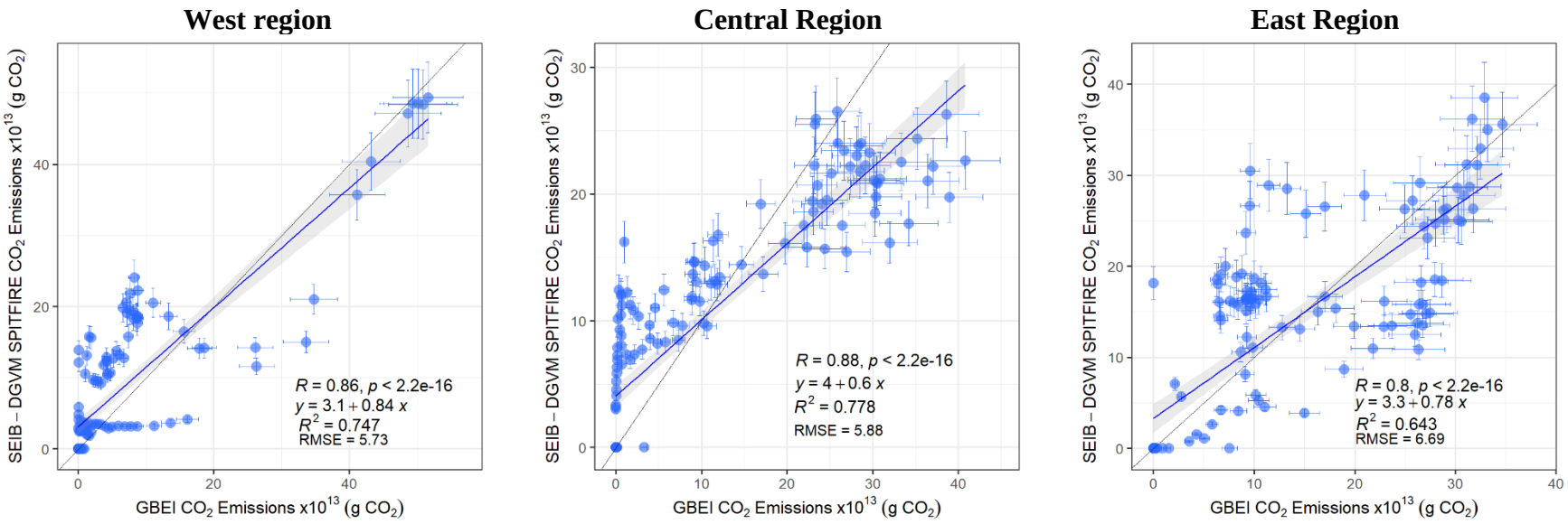

Figure 29. Latitude average spatial comparison of annual averaged (2001-2020) simulated CO_2 emissions of SEIB-DGVM SPITFIRE and CO_2 emissions of GBEI in: **(a)** west region **(b)** central region, **(c)** east region

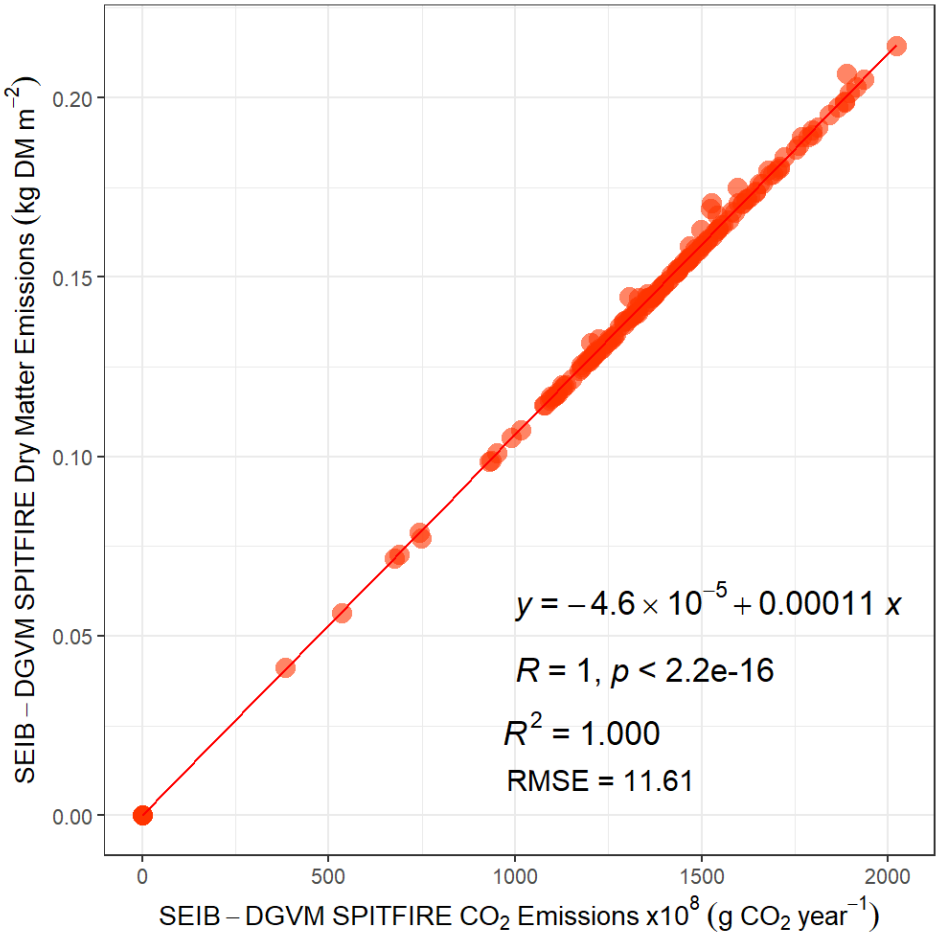

Figure 30. Comparison of annual averaged simulated dry matter and CO_2 emissions of SEIB-DGVM SPITFIRE from 1996 to 2100

3.2. Burned fraction

The improved model (SEIB-DGVM SPITFIRE) produces burned fraction variables more accurately than the default model (SEIB-DGVM GlobFIRM). A spatial comparison of the average burned fraction variables from 1997-2016 between GFED4s, SEIB-DGVM SPITFIRE, and the default SEIB-DGVM shows that SEIB-DGVM SPITFIRE achieves a 75% similarity with GFED4s data, whereas the default model achieves only 68% (Figure 32).

The burned fraction variable in the improved model exhibited a spatial distribution pattern different from that in the default model (Figure 31.a). According to the improved model, the burned fraction data were distributed in the western, central, and southern areas (Figure 31.b). We compared the burned fraction variable with the lightning flash rate and population density data to confirm that the produced variable considered the new ignition factor. The burned fraction showed a 46% correlation with the lightning flash rate and a 6% correlation with population density between 2006 and 2100 (Figure 34.a and b). In general, the burned fraction under all the RCP scenarios exhibited an increasing trend from 2006 to 2100, with the highest value occurring under the RCP4.5 scenario. Under the RCP4.5 scenario, the lowest value was 0.01371, and the highest value was 0.01427, with an average value of 0.01398 (Figure 31.d).

In contrast to the results produced from the improved model, the burned fraction data from the default model were spread throughout most of the area (Figure 31.a). From 2006 to 2100 under all RCP scenarios, the burned fraction in the default model also exhibited an increasing trend. Under the RCP4.5 scenario, the lowest value is 0.002996, and the highest value is 0.003113, with an average value of 0.00306 (Figure 31.c), which is well below the outputs of the improved model.

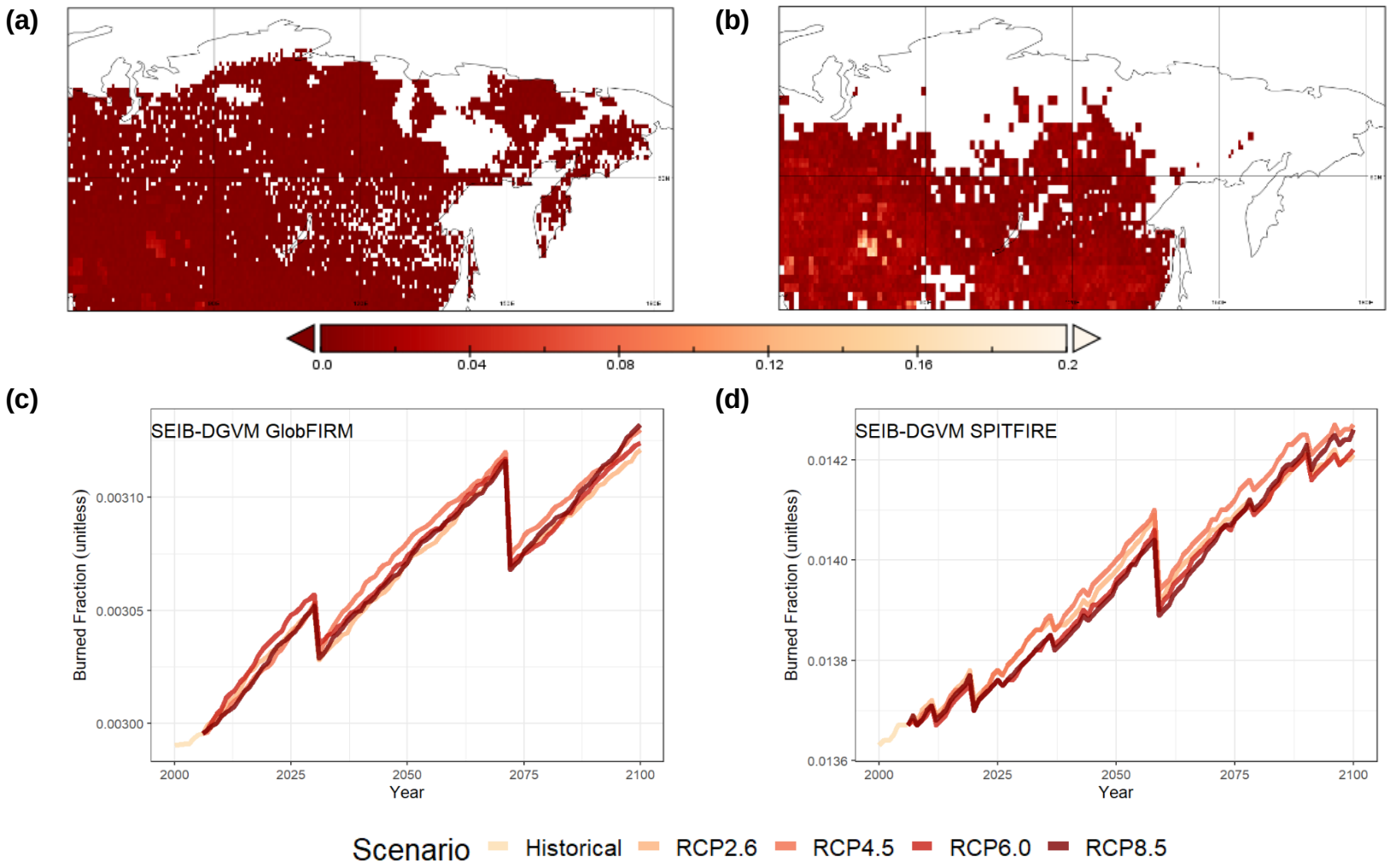

Figure 31. (a) Spatial distribution of annual averaged burned fraction of SEIB-DGVM GlobFIRM from 2006 to 2100. **(b)** Spatial distribution of annual averaged burned fraction of SEIB-DGVM SPITFIRE from 2006 to 2100. **(c)** Temporal variation of burned fraction of SEIB-DGVM GlobFIRM from 2000 to 2100. **(d)** Temporal variation of burned fraction of SEIB-DGVM SPITFIRE from 2000 to 2100.

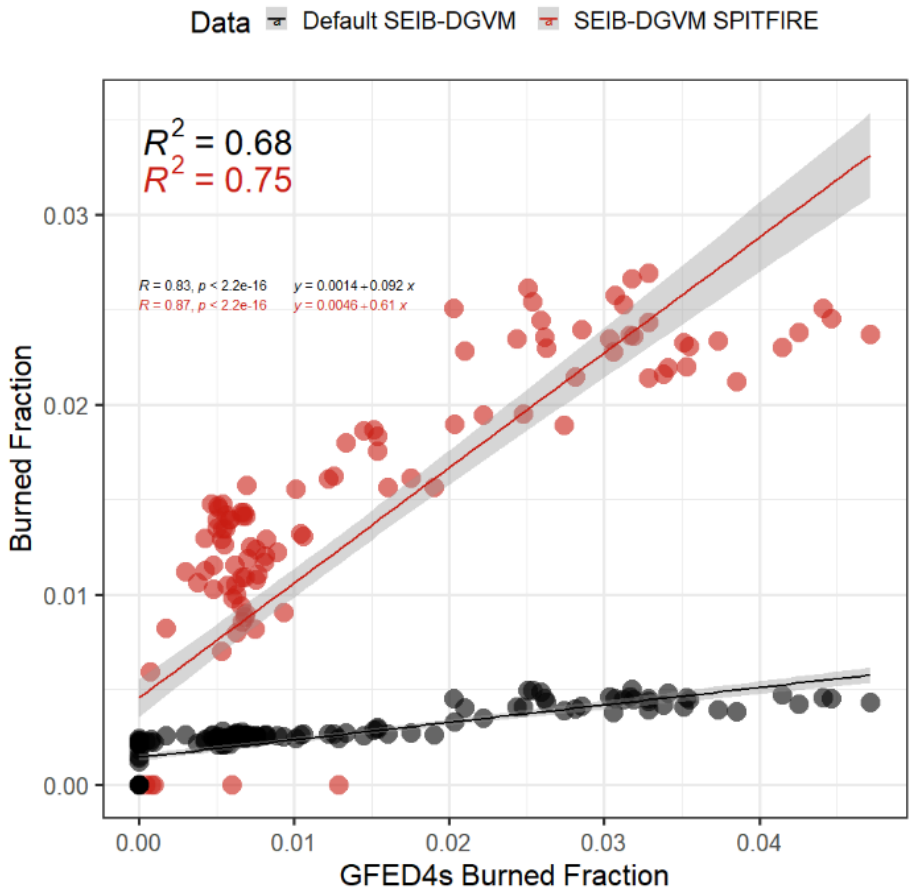

Figure 32. Comparison between annual averaged burned fraction variable of default SEIB-DGVM (GlobFIRM fire module) and SEIB-DGVM SPITFIRE with burned fraction of GFED4s from 1997 to 2016

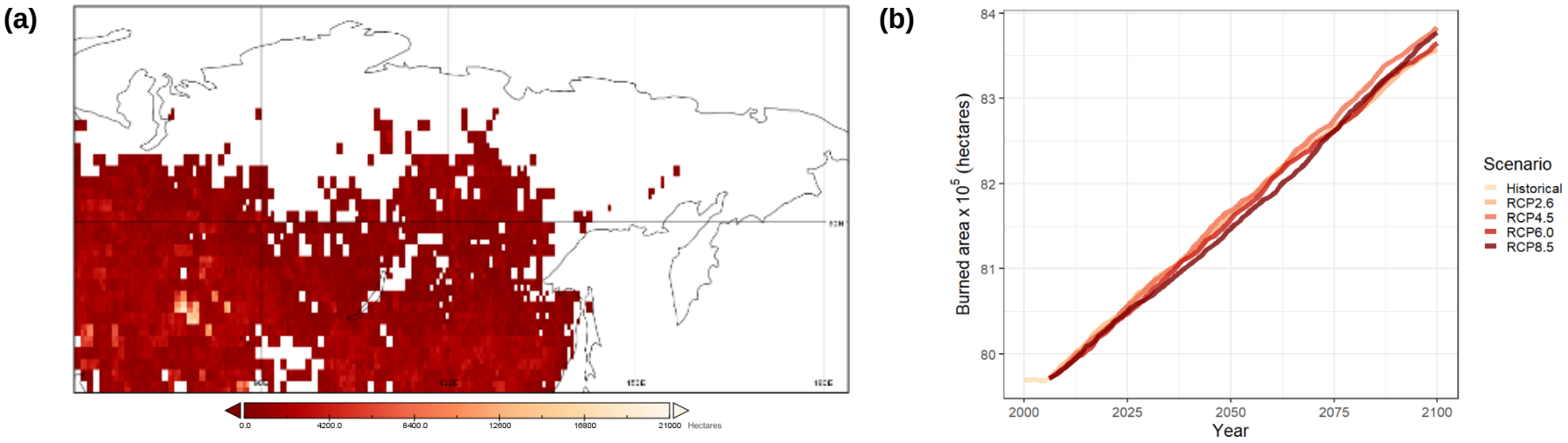

Figure 33. (a) Spatial distribution of annual averaged burned area of SEIB-DGVM SPITFIRE from 2006 to 2100. **(b)** Temporal variation of burned area of SEIB-DGVM SPITFIRE from 2000 to 2100.

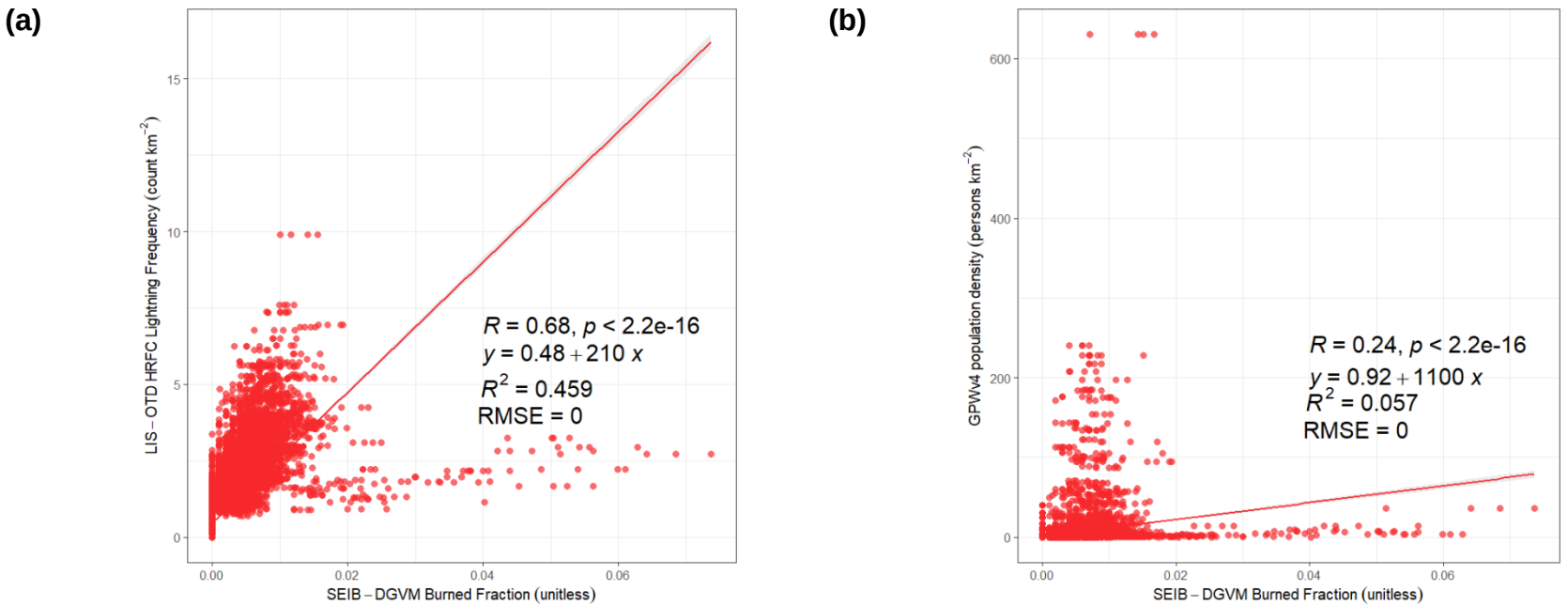

Figure 34. (a) Comparison of annual averaged LIS/OTD HRFC lightning flash rate (2000-2020) with simulated burned fraction of SEIB-DGVM SPITFIRE (1996-2005). **(b)** Comparison of annual averaged GPWv4 population density (2015) with simulated burned fraction of SEIB-DGVM SPITFIRE (1996-2005).

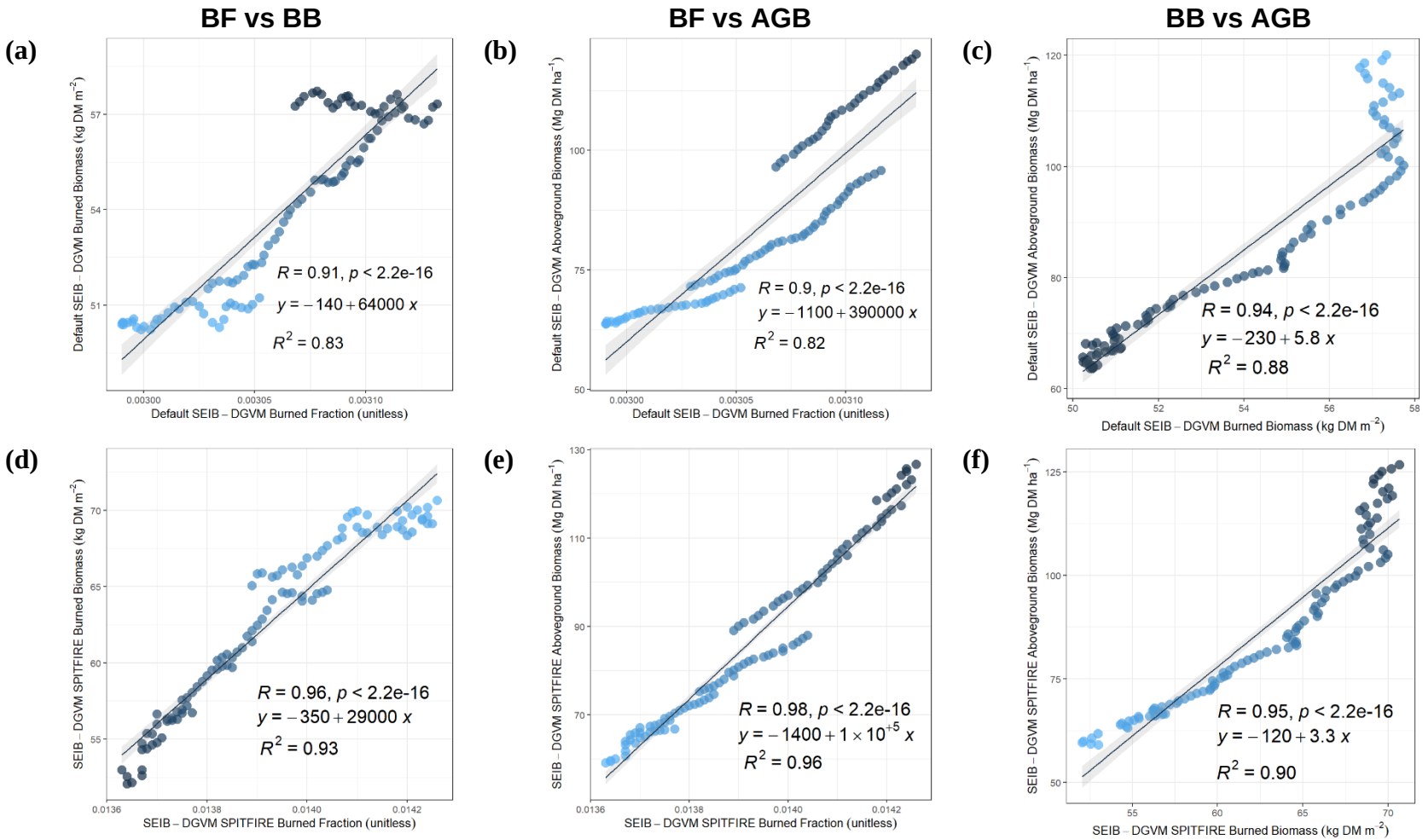

Figure 35. (a) Comparison of annual averaged burned fraction and burned biomass variables of default model (SEIB-DGVM GlobFIRM) from 2000 to 2100. **(b)** Comparison of annual averaged burned fraction and aboveground biomass variables of SEIB-DGVM GlobFIRM from 2000 to 2100. **(c)** Comparison of annual averaged burned biomass and aboveground biomass variables of SEIB-DGVM GlobFIRM from 2000 to 2100. **(d)** Comparison of annual averaged burned fraction and burned biomass variables of improved model (SEIB-DGVM SPITFIRE) from 2000 to 2100. **(e)** Comparison of annual averaged burned fraction and aboveground biomass variables of SEIB-DGVM SPITFIRE from 2000 to 2100. **(f)** Comparison of annual averaged burned biomass and aboveground biomass variables of SEIB-DGVM SPITFIRE from 2000 to 2100.

3.3. Burned area

The burned area of the improved model showed a similar spatial distribution pattern under all the RCP scenarios (Figure 33.a). The distribution pattern of the burned area variable was also similar to that of the burned fraction variable, as the burned area and burned fraction calculation processes are both based on fire probability (Eq. 1). Overall, under all the scenarios, the burned area exhibited the same increasing trend, with the RCP4.5 scenario reaching the highest value. Under the RCP4.5 scenario from 2006 to 2100, the burned area has an average value of 1945.9 ha $grid^{-1}$ $year^{-1}$ and is projected to increase with values of 79.7 to 83.8 x 10^5 hectares (Figure 33.b). Since the default model does not compute burned area, this variable could not be compared between the improved model and the default model.

3.4. Burned biomass

The improved model confirmed uniform spatial distribution patterns for the fire variables: burned fraction (Figure 31.b), burned area (Figure 33.a), and burned biomass (Figure 36.b). All of the improved module fire variables confirmed to be mutually integrated because the calculation process comes from the first fire variable (burned fraction). Compared to the improved model, the spatial distribution pattern of the burned biomass variable from the default model was wider and spread across the entire Siberia region (Figure 36.a). The spatial distribution pattern of burned fraction (S4.a-d) and burned biomass (Figure 36.a) in the default model is different and exhibited a box-like pattern in the center of the map. The internal model calculation flow relationship between the burned fraction and burned biomass variables in both the default and improved models shows a positive linear correlation, indicating harmony between these variables. A higher burned fraction corresponds to a higher burned biomass. The default model (SEIB-DGVM GlobFIRM) has an R^2 value of 0.83, while the improved model (SEIB-DGVM SPITFIRE) demonstrates better integration, with an R^2 value of 0.93 (Figure 35.a and d).

Under all RCP scenarios from 2006 to 2100, the burned biomass variable in both the default and improved models exhibited an increasing trend (Figure 36.c and d). This indicates correct integration between the burned fraction and burned area variables, and an appropriate response to the climate input data. Furthermore, under the RCP6.0 climate scenario from 2000 to 2100, the burned biomass value in the default model increases from 50.4 to 60.6 kg DM m^{-2} (Figure 36.dc), while in the improved model it increases from 53 to 73.98 kg DM m^{-2} (Figure 36.d). The twenty-year variations and their trends of dry matter emissions up to 2100

in the improved model (SEIB-DGVM SPITFIRE) are 55.90 ± 1.31 (10.5 %), 60.52 ± 1.12 (11.4 %), 64.43 ± 1.36 (12.1 %), 69.23 ± 1.37 (13 %), 71.81 ± 0.94 (13.5 %) (Figure 37).

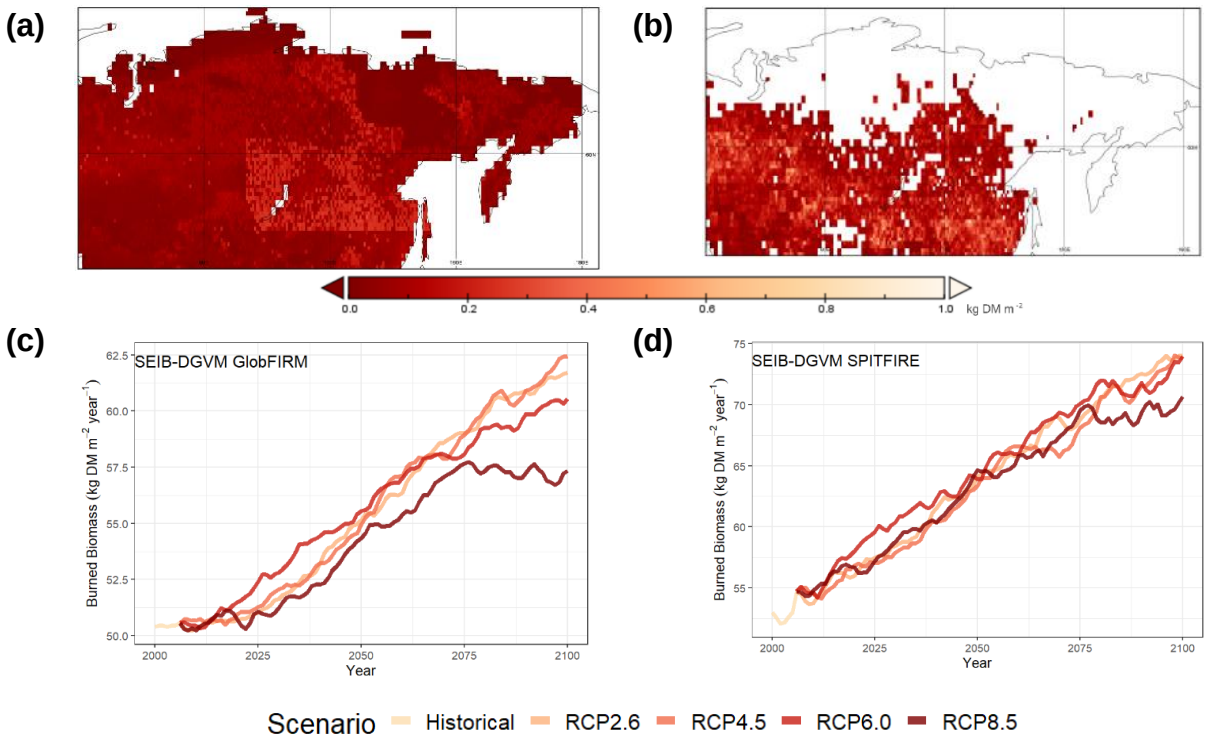

Figure 36. (a) Spatial distribution of annual averaged burned biomass of SEIB-DGVM GlobFIRM from 2006 to 2100. **(b)** Spatial distribution of annual averaged burned biomass of SEIB-DGVM SPITFIRE from 2006 to 2100. **(c)** Temporal variation of burned biomass of SEIB-DGVM GlobFIRM from 2006 to 2100. **(d)** Temporal variation of burned biomass of SEIB-DGVM SPITFIRE from 2006 to 2100.

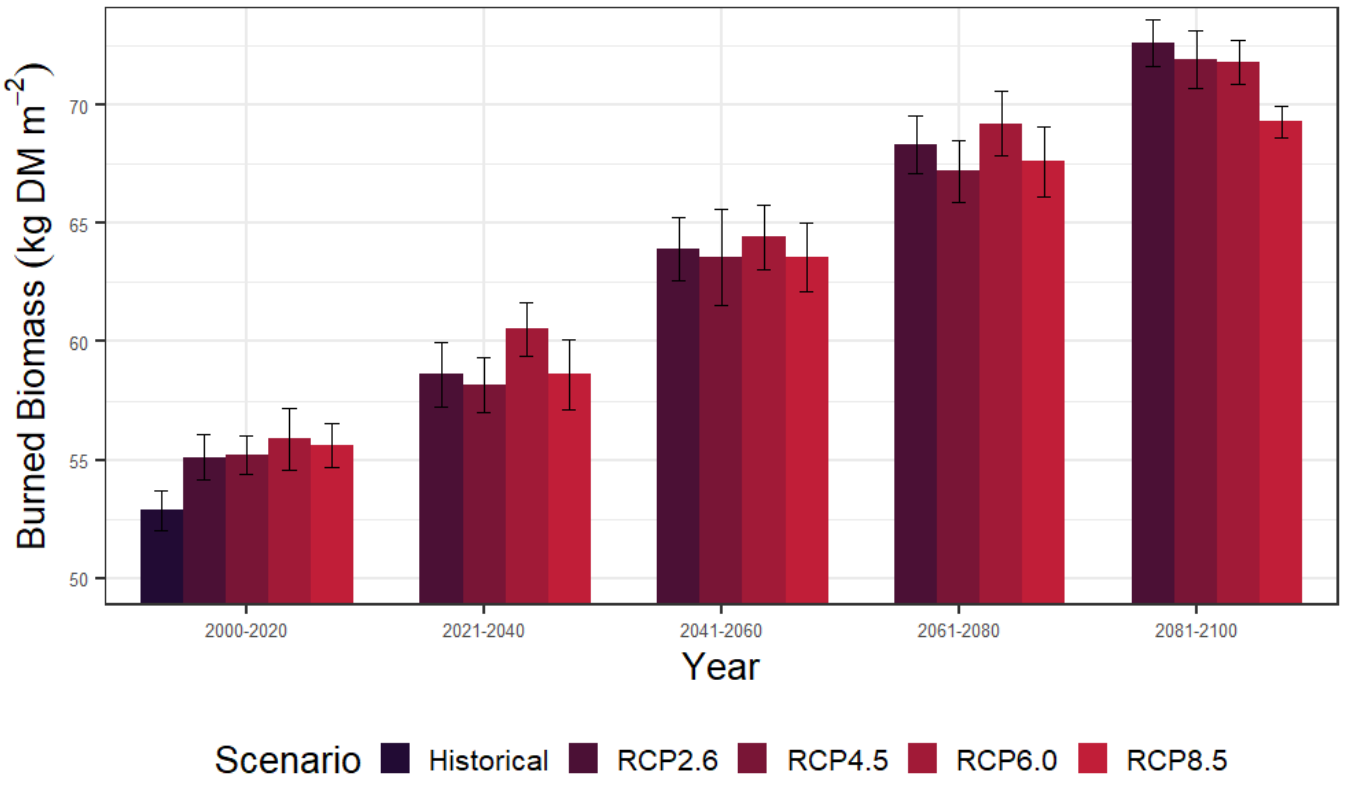

Figure 37. Temporal variation of projected burned biomass from 2000 to 2100 under different RCPs scenarios.

3.5. Aboveground biomass

The aboveground biomass calculations in the default model and improved model used the same estimation process because the trunk biomass in the SEIB-DGVM included coarse root biomass; therefore, only approximately 2/3 of the trunk biomass was classified as aboveground biomass (Sato et al., 2007). However, during the calibration of the aboveground biomass variable with the ESA Biomass CCI benchmark dataset, we adjusted the calculation impact of fire and its distribution pattern (based on natural and anthropogenic ignition factors) on the availability of aboveground biomass.

According to the default model, the AGB distribution pattern appears to be the same as that of the fire variable, a box-like pattern still occurs on the map (Figure 38.a). Under the RCP8.5 scenario, from 2000 to 2100, the AGB increased from 63.72 to 120.1 Mg DM ha^{-1}, and the average value was 86.3 Mg DM ha^{-1} (Figure 38.c). The aboveground biomass (AGB) variables in both the default and improved models exhibit an increasing trend and vary across RCP scenarios, with the highest values observed under RCP8.5 and the lowest under RCP2.6. This indicates that the models effectively read and process the RCP input climate data.

Compared to the default model, the improved AGB model has a bit difference in distribution patterns (Figure 38.b). In the central Siberian region, in some locations that have high AGB has been reduced due to the impact of forest fires, so that the box-like pattern is no longer visible (Figure 38.b). The temporal variation of aboveground biomass in the improved model also shows an increasing trend due to the warming scenario of each RCP climate data input. The AGB under the RCP8.5 scenario from 2000 to 2100 increased from 59.08 to 126.7 Mg DM ha^{-1} (Figure 38.d), and the mean was 88.68 Mg DM ha^{-1}. The twenty-year variations and their trends of aboveground biomass up to 2100 are 65.45 ± 1.19 (10.8 %), 71.69 ± 2.90 (11.8 %), 83.38 ± 3.61 (13.7 %), 99.17 ± 5.06 (16.3 %), 117.92 ± 5.41 (19.4 %) (Figure 39).

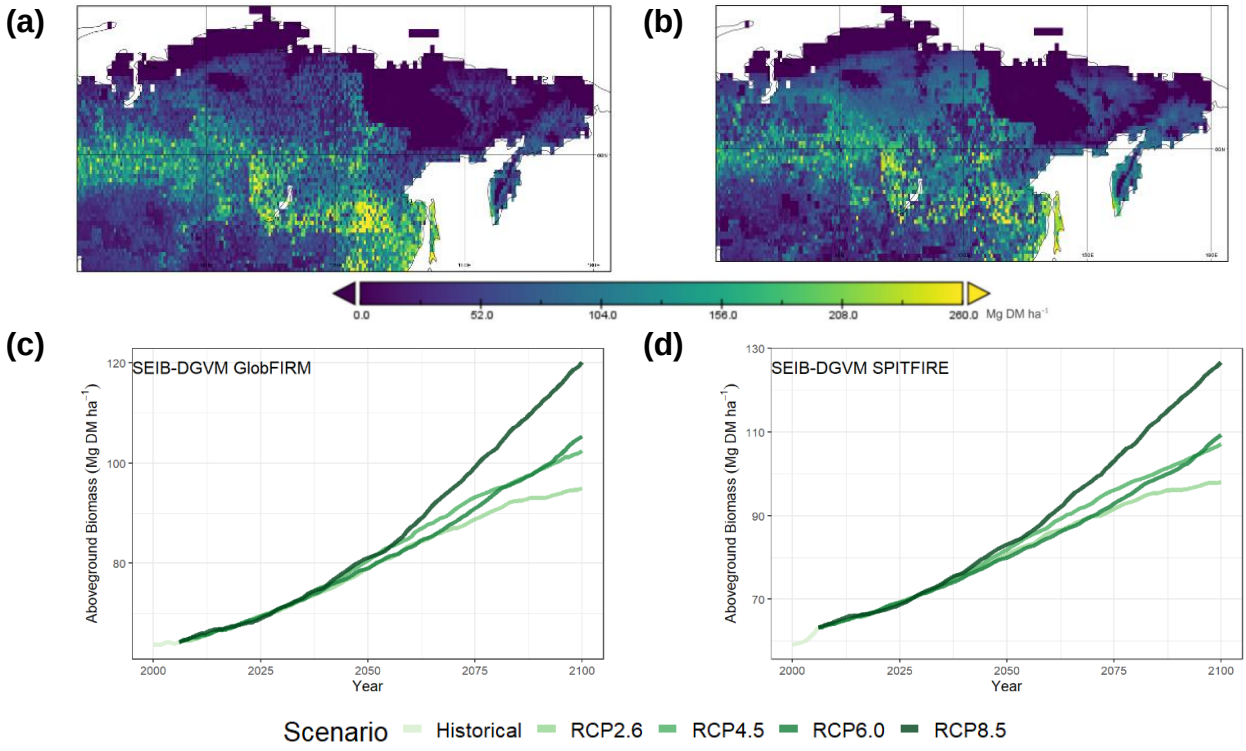

Figure 38. (a) Spatial distribution of annual averaged aboveground biomass of SEIB-DGVM GlobFIRM from 2006 to 2100. **(b)** Spatial distribution of annual averaged aboveground biomass of SEIB-DGVM SPITFIRE from 2006 to 2100. **(c)** Temporal variation of aboveground biomass of SEIB-DGVM GlobFIRM from 2006 to 2100. **(d)** Temporal variation of aboveground biomass of SEIB-DGVM SPITFIRE from 2006 to 2100.

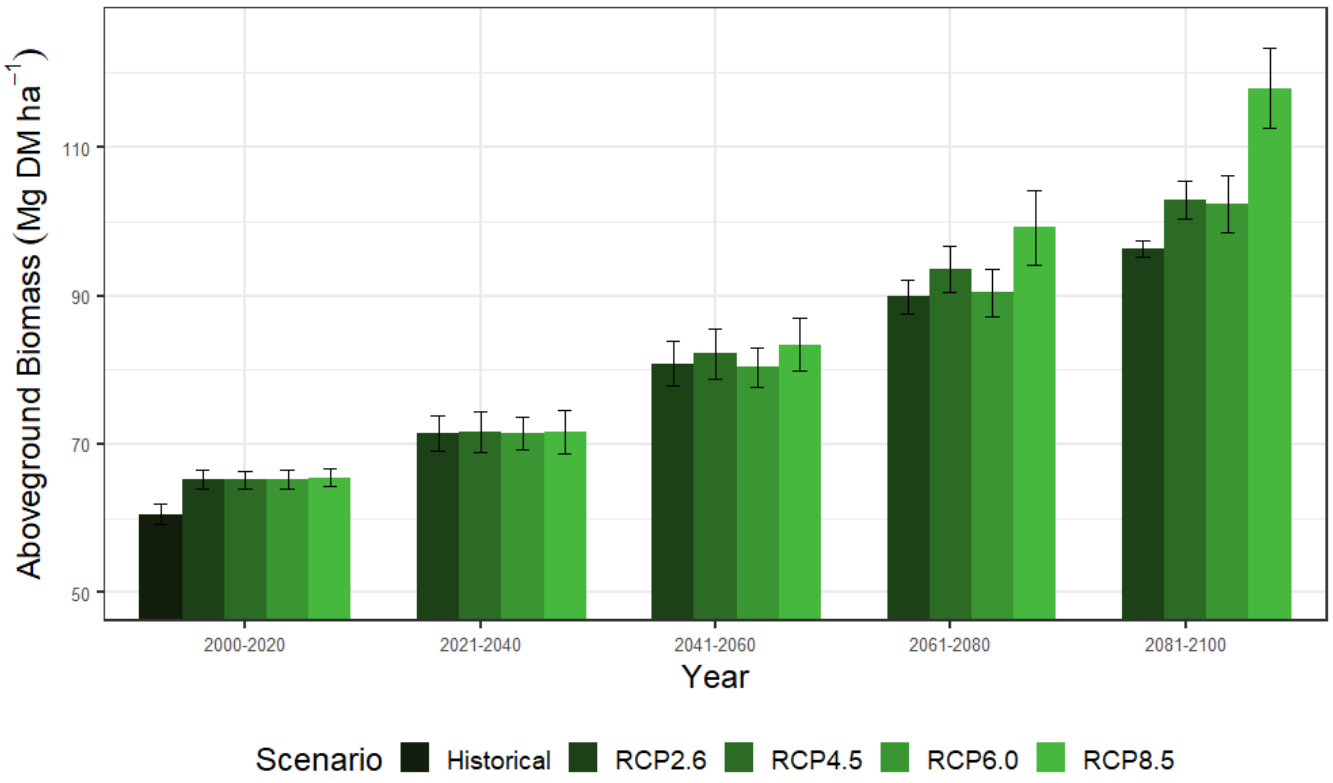

Figure 39. Temporal variation of projected aboveground biomass from 2000 to 2100 under different RCPs scenarios.

3.6. Forest ecological variables under fire-on and fire-off simulation

We conducted complete simulations under fire-on and fire-off modes to compare and assess vegetation dynamics during forest fires. Assessing vegetation dynamics can be done by understanding the carbon pools in the certain region or globally, where carbon pools are easier to measure than carbon fluxes. In this study, the net primary production (NPP) is used as a reference variable because it is an important metric of the global carbon cycle (Running, 2022) and measures the rate of global plant growth. We obtained the NPP lost variable due to wildfire from fire-on and fire-off simulations. The NPP lost variable under all RCP scenarios shows a increasing trend. Under the RCP8.5 scenario, an average NPP loss of 385.19 ± 40.4 g C m^{-2} $year^{-1}$ occurred during 2000–2100 (Figure 42.a). In addition to the NPP variable, the improved model (SEIB-DGVM SPITFIRE) can also simulate Net Biome Production (NBP). Under the same RCP8.5 scenario, the annual average NBP from 2000-2100 shows a positive value of 307.7 ± 43 Tg C $year^{-1}$ (Figure 42.b), with a continuous increasing trend.

In relation to wildfires, assessing pre- and postfire tree density variables is critical for measuring the impact of fires. Under the RCP8.5 scenario, in the fire-on simulation from 1997 to 2100, it is projected that the tree density in Siberia was 2,181 tree ha^{-1}. However, under the same RCP and time range in the fire-off simulation, the tree density was 2,363 tree ha^{-1}. We also compared the tree density between the fire-on and fire-off simulations under all the RCP scenarios and found that the tree density increased in the fire-off simulations compared to that in the fire-on simulations. Under the RCP8.5 scenario, on average, 174 trees ha^{-1} $year^{-1}$ died due to the fire (Figure 42.c).

We also conducted a more detailed assessment of several forest structure variables, such as tree DBH, crown area, and tree height, from 2006 to 2100 under all the RCP scenarios. Under the RCP8.5 scenario, in the fire-on simulation, the results showed that tree DBH values varied from 0 to 4.7 m (average 0.9 m), tree height from 0 to 75.4 m (average 24.2 m), and crown area from 0 to 15.1 m^2 (average 5.7 m^2). The average tree structure in the fire-off simulation was greater than that in the fire-on simulation, with average tree DBH, tree height, and crown area of 0.97 m, 24.1 m, and 6.5 m^2, respectively. The correlations between the tree structure variables under fire-on and fire-off simulation conditions were similar and highly correlated; the overall average correlation among the tree DBH, tree height, and crown area variables was 97 % (Figure 40). Specifically, according to region classification, highest to the lowest value of tree height, tree DBH, and crown area value is in the west region, then central

region, and east region. On average for 2081-2100 under RCP8.5 in each region, the tree height, tree DBH, and crown area variables show values of 28.43 ± 0.8 m, 1.1 ± 0.004 m, 5.7 ± 0.01 m^2 (west region), 28.3 ± 0.9 m, 1.2 ± 0.04 m, 7.8 ± 0.08 m^2 (central region), and 30.2 ± 1.0 m, 1.2 ± 0.06 m, 8.5 ± 0.2 m^2 (east region) (Figure 43, Figure 44, and Figure 45). Furthermore, we found an interesting pattern, the simulated tree allometry variables (tree height, tree DBH, and crown area) in eastern Siberia exhibit a greater range of values compared to those in central and western Siberia (Figure 43, Figure 44, and Figure 45). Overall, all tree allometry variables in Siberia exhibit an increasing trend, and the differences between fire-on and fire-off simulations for all tree allometry variables are most pronounced in eastern Siberia.

In addition, the relationship between the three variables (tree height, tree DBH, and crown area) in the west region and central region shows a linear trend where the higher the tree height, the greater the tree DBH and the wider the crown area (Figure 41). The east region shows an interesting pattern, different from other regions, where there is low tree (Figure 41.c). The western and central Siberia exhibit a greater range of tree height values compared to eastern Siberia (Figure 41.a and b). An interesting pattern was observed in western Siberia, where trees with high tree height and large DBH but low crown area were detected in some locations (Figure 41.a).

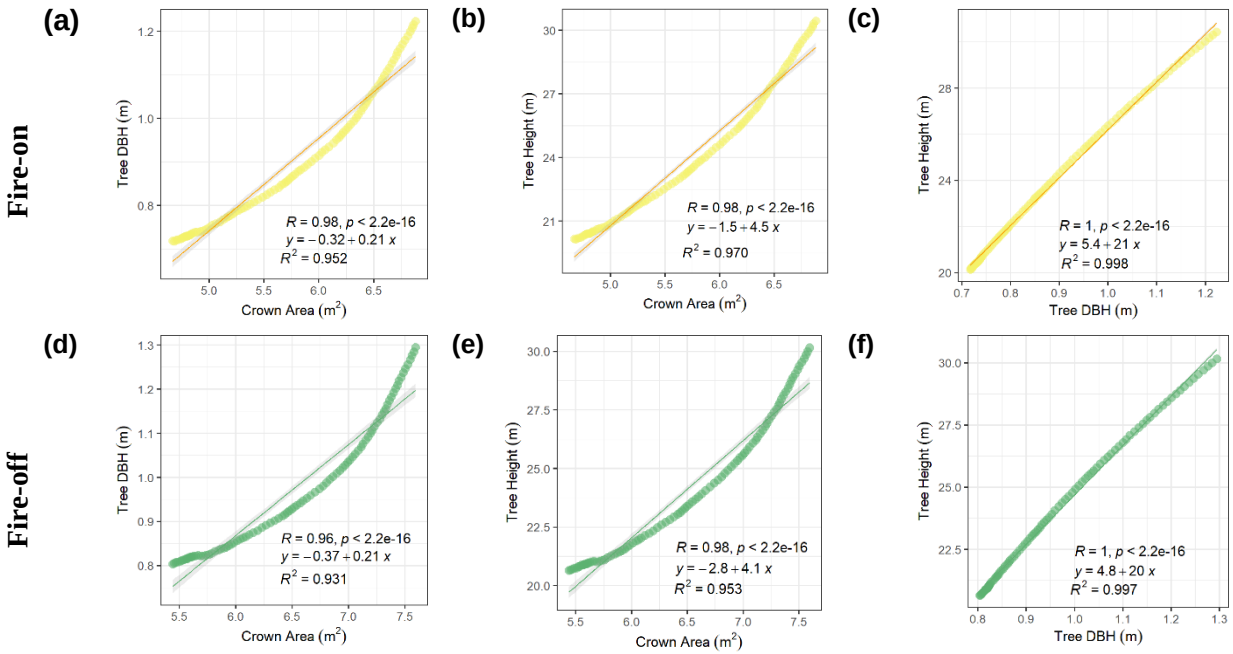

Figure 40. Annual average comparison of tree DBH, tree height and crown area variables in **(a-c)** fire-on and **(d-f)** fire-off simulations (1996-2100). Each point represents one grid latitude average of each variable.

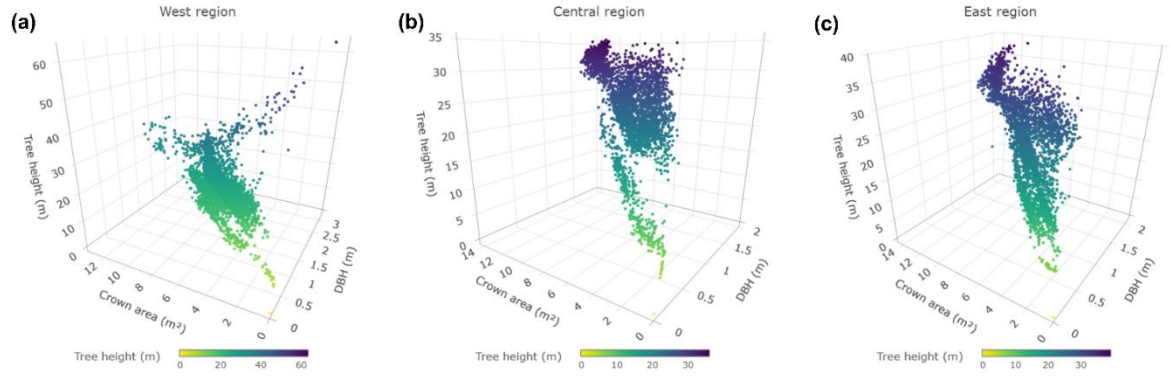

Figure 41. Relationships between simulated tree height, tree DBH, and crown area under fire-on simulation and RCP8.5 scenario from 2000 to 2100 in: **(a)** West region, **(b)** Central region, and **(c)** East region of Siberia.

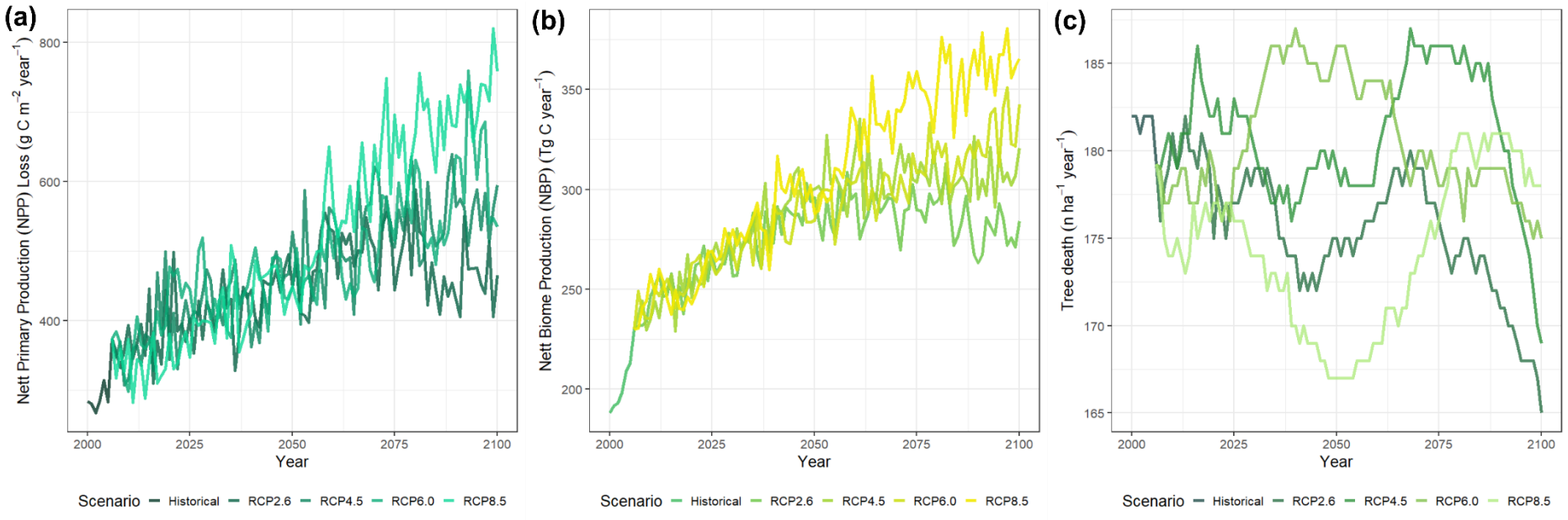

Figure 42. Temporal variation of simulated variables of SEIB-DGVM SPITFIRE in Siberia from 2000 to 2100: **(a)** NPP loss. **(b)** NBP. **(c)** Killed tree due to wildfire

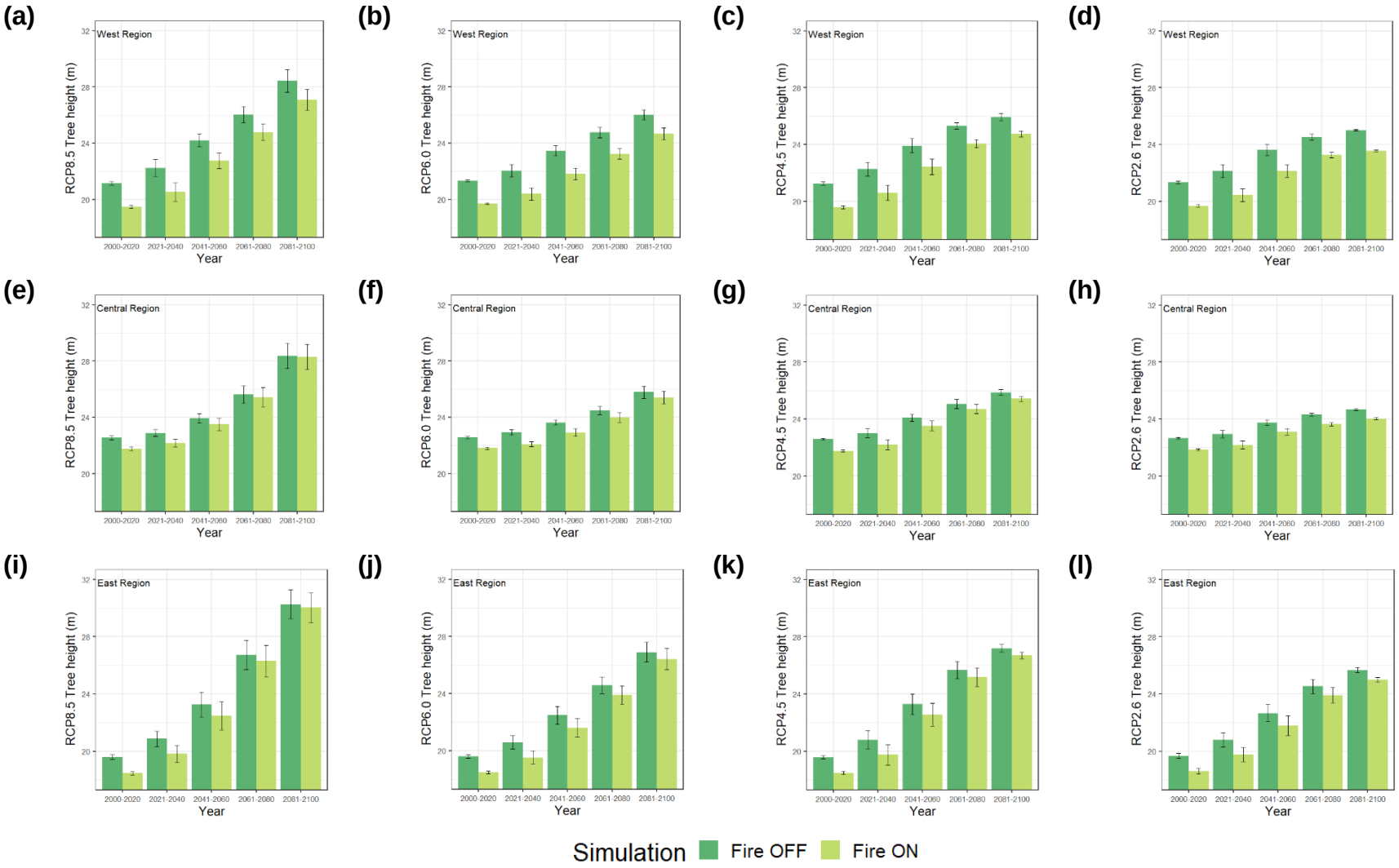

Figure 43. Twenty-year average of tree height variables under fire on and fire off simulation and under RCPs climate scenarios from 2000-2100: **(a-d)** West region, **(e-h)** Central region, dan **(i-l)** East region of Siberia

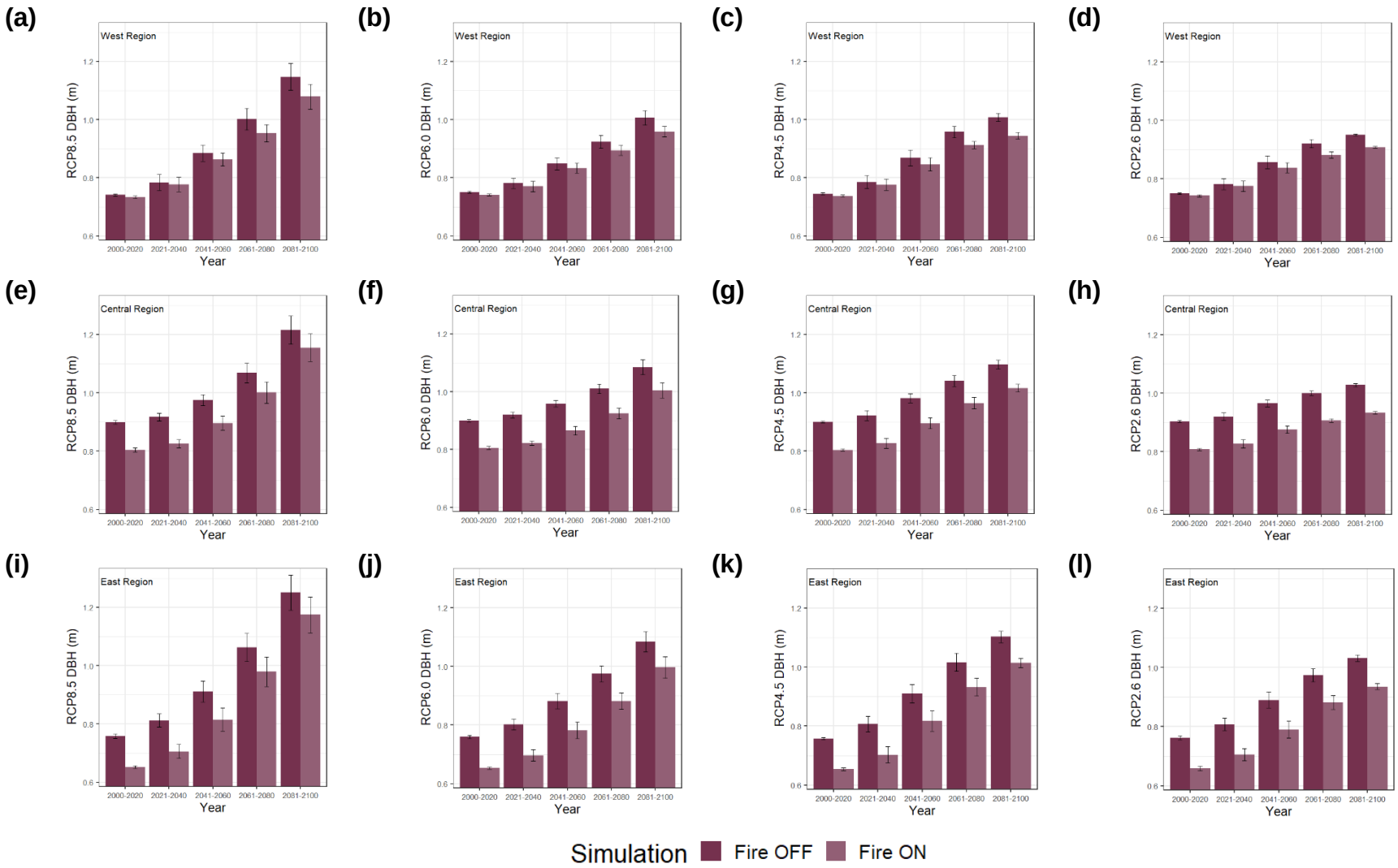

Figure 44. Twenty-year average of DBH variables under fire on and fire off simulation and under RCPs climate scenarios from 2000-2100: **(a-d)** West region, **(e-h)** Central region, dan **(i-l)** East region of Siberia

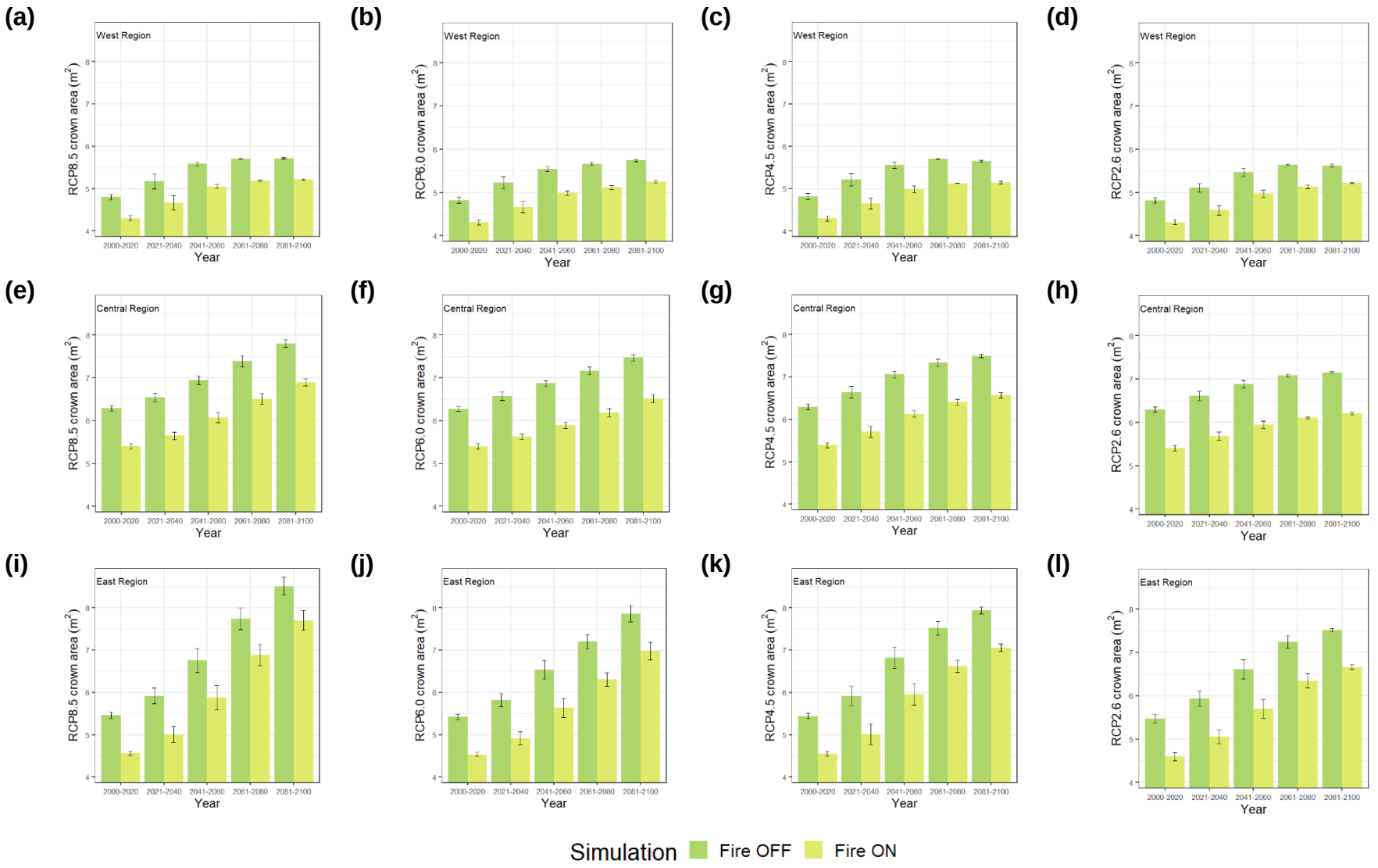

Figure 45. Twenty-year average of crown area variables under fire on and fire off simulation and under RCPs climate scenarios from 2000-2100: **(a-d)** West region, **(e-h)** Central region, dan **(i-l)** East region of Siberia

3.7. Fire and AGB variable comparison

We performed internal comparisons of fire and AGB variables within the improved model to ensure that the model worked properly and that the variable calculation processes were interrelated. Eastern Siberia had low fire patterns (Figure 46), and when compared with the AGB, this area also had very low AGB. We extracted the AGB data in the marked area with coordinates of 130-142°E and 65-80°N and discovered that the average simulated aboveground biomass in the area was 65.59 g C m^{-2} from 1997 to 2023, compared to 416.4 g C m^{-2} in the one-grid high-AGB areas. Furthermore, we assessed the fire danger index (FDI) variable in these low AGB areas and found that the mentioned region had a value of 0, indicating that it had a very low fire potential (Figure 49.a).

We also compared the fire variables (burned fraction, burned biomass) and AGB variables between the improved model and the default model. According to the default model, the correlation between the burned fraction and burned biomass was 0.83, the correlation between burned fraction and AGB was 0.82, and the correlation between burned biomass and the AGB was 0.88 (Figure 35.a-c). According to the improved model, the correlation between the burned fraction and burned biomass was 0.93, the correlation between burned fraction and AGB was 0.96, and the correlation between burned biomass and the AGB was 0.9 (Figure 35.d-f). Overall, both the default and improved models are well integrated, with the improved model demonstrating superior integration compared to the default model.

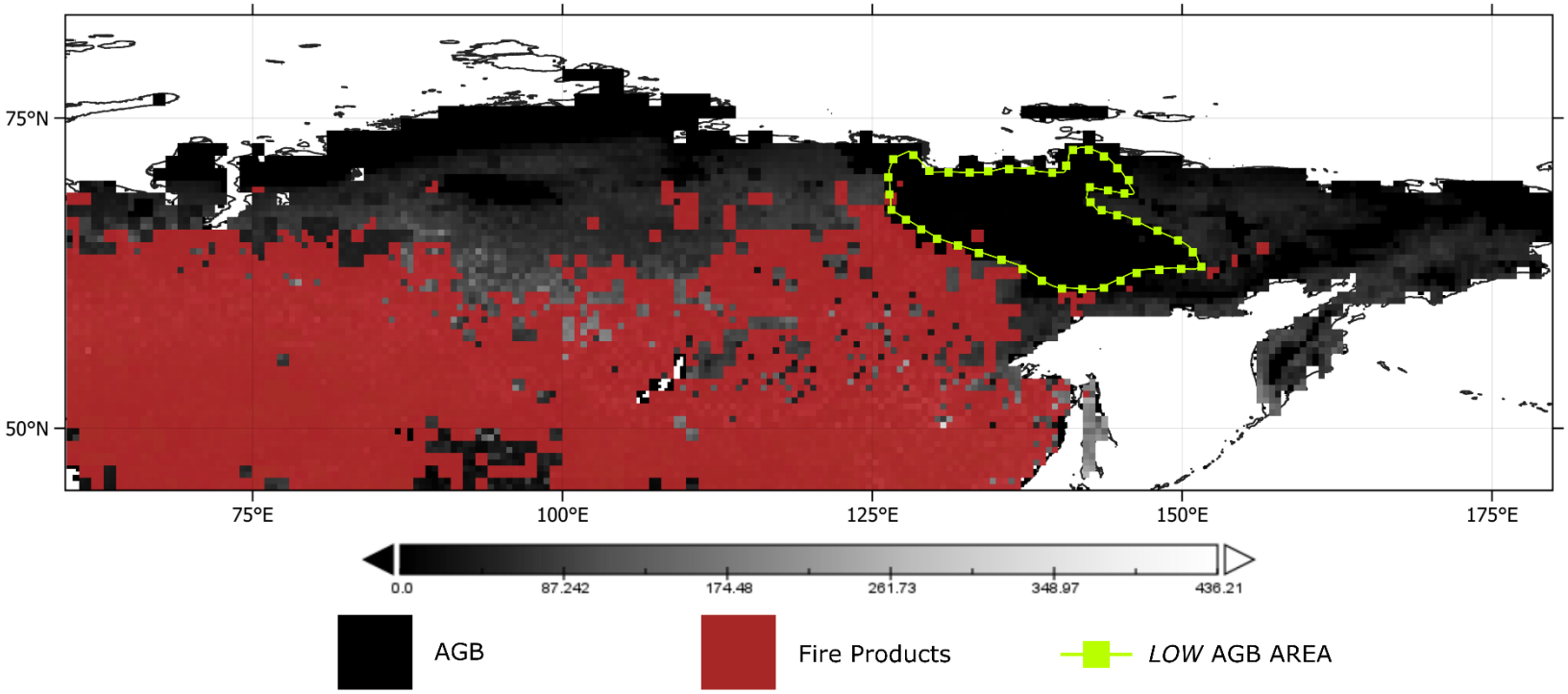

Figure 46. Spatial distribution comparison between annual averaged (1997-2016) of fire products (burned fraction, burned area, burned biomass) and aboveground biomass variable of SEIB-DGVM SPITFIRE

3.8. Future projection of burned biomass emissions

Our model projects that from 2000 to 2100, Siberia will produce CO_2 emissions ranging from 10 to 11,000 $x10^8$ g CO_2 $year^{-1}$ (Figure 47). The distribution patterns of CO_2 and other emissions are similar because all emissions are calculated based on the same variable dry matter emissions. Over the twenty-year period, we projected an increasing trend in CO_2 emissions across the various RCP scenarios, which aligns with the projected increase in forest fires through 2100.

The average from 2000 to 2100 shows that CO_2 emissions are highest under the RCP6.0, RCP2.6, RCP4.5, and RCP8.5 scenarios, with values of 885.8 ± 75.4, 877.82 ± 82.6, 871.4 ± 80.6, and 865.5 ± 69.6 Tg CO_2, respectively. Specifically under the RCP6.0 scenario, the highest projected emissions are expected in the periods 2021-2040, 2041-2060, 2061-2080, and 2081-2100, with Siberia producing CO_2 emissions of 769.24 ± 14.37, 830.52 ± 15.61, 877.93 ± 16.34, 940.46 ± 20.59, and 981.73 ± 12.61 Tg CO_2, respectively (Figure 48).

The highest gaseous species emissions were CO_2, CO, $PM_{2.5}$, TPM, and TPC, and all of them exhibited similar increasing trends from 2000 to 2100 under all RCP scenarios. Under the RCP6.0 scenario, these emissions are expected to increase by 2.58 ± 0.75, 0.21 ± 0.06, 0.03 ± 0.01, 0.02 ± 0.01, and 0.014 ± 0.006 Tg species $year^{-1}$, respectively. The increasing trend of emissions production until 2100 is also in line with the FDI variable, which shows the same increasing trend (Figure 49.b). Overall, by 2100, under the RCP6.0 scenario, the production of CO_2, CO, $PM_{2.5}$, TPM, and TPC emissions from forest biomass burning combustion are projected to reach 1,009.00 ± 75.44, 80.74 ± 6.04, 12.60 ± 0.91, 9.54 ± 0.69, and 6.61 ± 0.48 Tg, respectively. The twenty-year averages of the CO_2, CO, $PM_{2.5}$, TPM, and TPC emission data under all the RCP scenarios are provided in Table 6, and the other twenty-eight emissions are provided in Table 7.

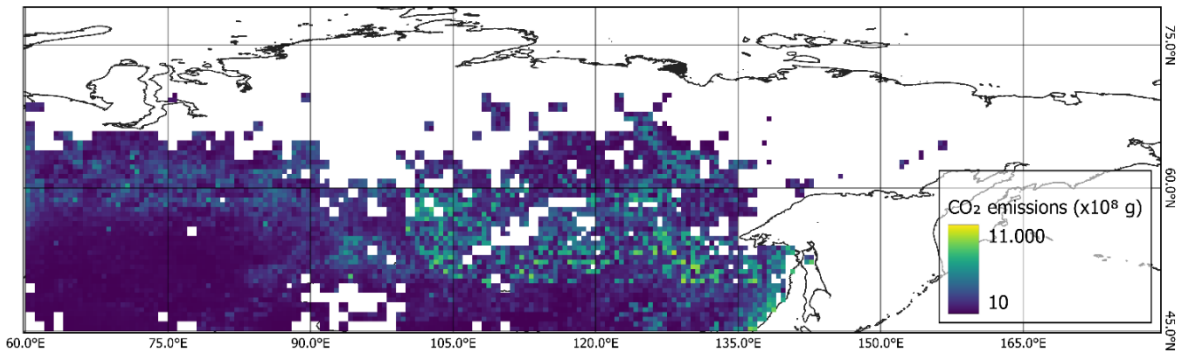

Figure 47. Spatial distribution of annual average projected CO_2 emissions (1996-2100) under RCP8.5 scenario.

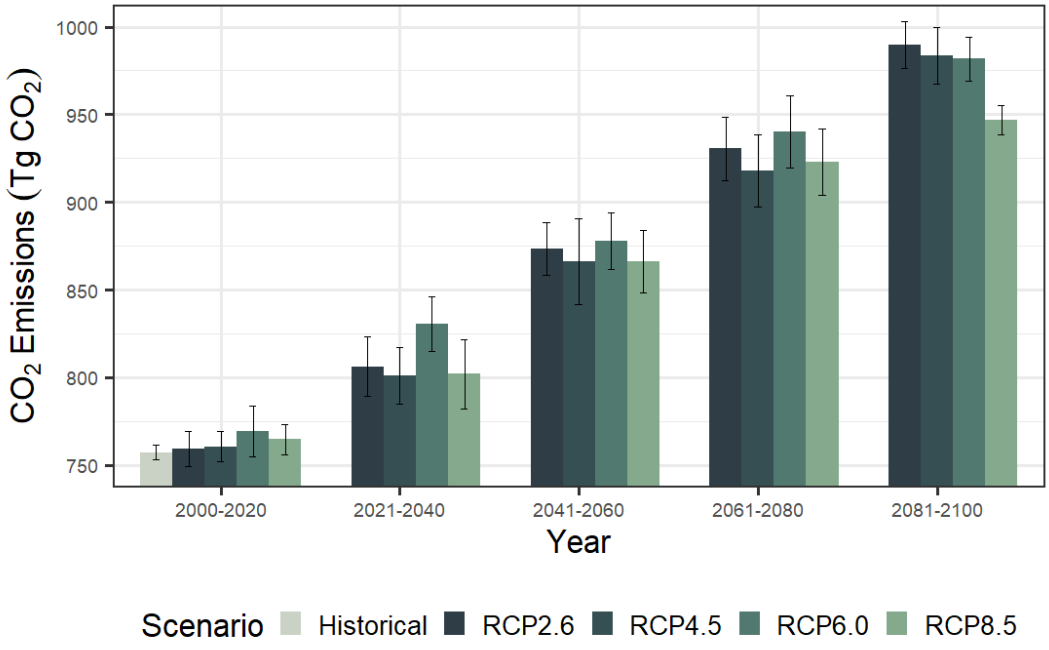

Figure 48. Temporal variation of projected CO_2 emissions from 2000 to 2100 under different RCPs scenarios.

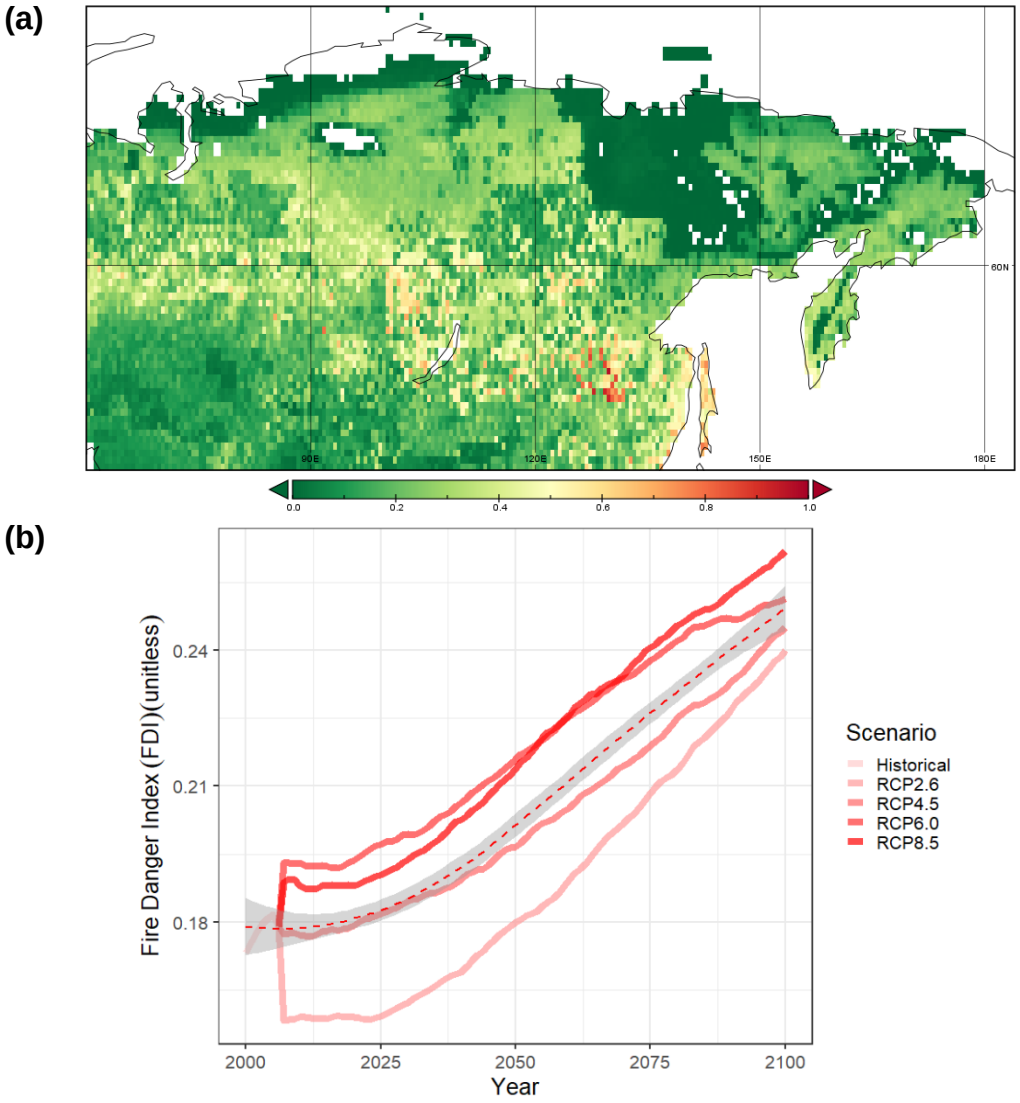

Figure 49. (a) Spatial distribution of annual averaged Fire Danger Index (FDI) of SEIB-DGVM SPITFIRE from 2000 to 2100. **(b)** Temporal variation of annual averaged Fire Danger Index (FDI) of SEIB-DGVM SPITFIRE from 2000 to 2100

Table 6. Projected emissions of CO_2, CO, $PM_{2.5}$, TPM, and TPC species from forest fires in Siberia (2023-2100). The rest of the 28 species emissions are in Table 7 in the Supplement.

Emissions	**Year**	**2000 - 2020**	**2021 - 2040**	**2041 - 2060**	**2061 - 2080**	**2081 - 2100**
Tg CO_2 year^{-1}	Baseline	757.33 ± 4.64	n.a	n.a	n.a	n.a
	RCP85	764.70 ± 9.04	801.94 ± 20.50	866.21 ± 18.29	922.85 ± 19.59	946.99 ± 8.47
	RCP60	769.24 ± 14.87	830.52 ± 16.01	877.93 ± 16.77	940.46 ± 21.12	981.73 ± 12.93
	RCP45	760.56 ± 8.82	800.86 ± 16.51	866.33 ± 25.06	918.01 ± 20.92	983.71 ± 16.74
	RCP26	759.38 ± 10.19	806.32 ± 17.42	873.30 ± 15.29	930.61 ± 18.45	989.93 ± 13.72
Tg CO year^{-1}	Baseline	60.63 ± 0.37	n.a	n.a	n.a	n.a
	RCP85	61.22 ± 0.72	64.20 ± 1.64	69.34 ± 1.46	73.88 ± 1.57	75.81 ± 0.68
	RCP60	61.58 ± 1.19	66.48 ± 1.28	70.28 ± 1.34	75.28 ± 1.69	78.59 ± 1.04
	RCP45	60.88 ± 0.71	64.11 ± 1.32	69.35 ± 2.01	73.49 ± 1.68	78.75 ± 1.34
	RCP26	60.79 ± 0.82	64.55 ± 1.39	69.91 ± 1.22	74.50 ± 1.48	79.24 ± 1.10
Tg $PM_{2.5}$ year^{-1}	Baseline	9.88 ± 0.06	n.a	n.a	n.a	n.a
	RCP85	9.97 ± 0.12	10.46 ± 0.27	11.30 ± 0.24	12.03 ± 0.26	12.35 ± 0.11
	RCP60	10.03 ± 0.19	10.83 ± 0.21	11.45 ± 0.22	12.26 ± 0.28	12.80 ± 0.17
	RCP45	9.92 ± 0.11	10.44 ± 0.22	11.30 ± 0.33	11.97 ± 0.27	12.83 ± 0.22
	RCP26	9.90 ± 0.13	10.51 ± 0.23	11.39 ± 0.20	12.14 ± 0.24	12.91 ± 0.18
Tg TPM year^{-1}	Baseline	7.48 ± 0.05	n.a	n.a	n.a	n.a

Emissions	Year	2000 - 2020	2021 - 2040	2041 - 2060	2061 - 2080	2081 - 2100
	RCP85	7.55 ± 0.09	7.92 ± 0.20	8.56 ± 0.18	9.12 ± 0.19	9.35 ± 0.08
	RCP60	7.60 ± 0.15	8.20 ± 0.16	8.67 ± 0.17	9.29 ± 0.21	9.70 ± 0.13
	RCP45	7.51 ± 0.09	7.91 ± 0.16	8.56 ± 0.25	9.07 ± 0.21	9.72 ± 0.17
	RCP26	7.50 ± 0.10	7.96 ± 0.17	8.63 ± 0.15	9.19 ± 0.18	9.78 ± 0.14
Tg TPC year^{-1}	Baseline	5.18 ± 0.03	n.a	n.a	n.a	n.a
	RCP85	5.23 ± 0.06	5.49 ± 0.14	5.93 ± 0.13	6.32 ± 0.13	6.48 ± 0.06
	RCP60	5.26 ± 0.10	5.68 ± 0.11	6.01 ± 0.11	6.44 ± 0.14	6.72 ± 0.09
	RCP45	5.20 ± 0.06	5.48 ± 0.11	5.93 ± 0.17	6.28 ± 0.14	6.73 ± 0.11
	RCP26	5.20 ± 0.07	5.52 ± 0.12	5.98 ± 0.10	6.37 ± 0.13	6.77 ± 0.09

Table 7. Projected emissions of 28 gaseous species from forest fires in Siberia from 2000 to 2100 ± 2 standard deviation.

sp.	Year	2000 - 2020	2021 - 2040	2041 - 2060	2061 - 2080	2081 - 2100
Gg CH_4 year^{-1}	**Historical**	2493.47 ± 15.23	n.a	n.a	n.a	n.a
	RCP8.5	2517.75 ± 29.76	2640.33 ± 67.50	2851.95 ± 60.22	3038.45 ± 64.50	3117.90 ± 27.88
	RCP6.0	2532.65 ± 48.92	2734.43 ± 52.75	2890.50 ± 55.16	3096.40 ± 69.57	3232.36 ± 42.66
	RCP4.5	2504.09 ± 29.04	2636.79 ± 54.37	2852.33 ± 82.49	3022.48 ± 68.91	3238.76 ± 55.07
	RCP2.6	2500.19 ± 33.52	2654.75 ± 57.36	2875.34 ± 50.33	3063.99 ± 60.75	3259.20 ± 45.08

sp.	Year	2000 - 2020	2021 - 2040	2041 - 2060	2061 - 2080	2081 - 2100
Gg NMHC $year^{-1}$	**Historical**	2591.25 ± 15.83	n.a	n.a	n.a	n.a
	RCP8.5	2616.47 ± 30.93	2743.87 ± 70.16	2963.81 ± 62.60	3157.60 ± 67.03	3240.17 ± 28.99
	RCP6.0	2631.97 ± 50.86	2841.67 ± 54.82	3003.87 ± 57.35	3217.82 ± 72.30	3359.12 ± 44.34
	RCP4.5	2602.31 ± 30.18	2740.20 ± 56.50	2964.18 ± 85.73	3141.01 ± 71.61	3365.78 ± 57.25
	RCP2.6	2598.25 ± 34.84	2758.86 ± 59.59	2988.11 ± 52.29	3184.15 ± 63.12	3387.01 ± 46.84
Gg H_2 $year^{-1}$	**Historical**	811.60 ± 4.98	n.a	n.a	n.a	n.a
	RCP8.5	819.49 ± 9.69	859.41 ± 21.97	928.27 ± 19.59	988.98 ± 21.00	1014.85 ± 9.07
	RCP6.0	824.33 ± 15.93	890.04 ± 17.16	940.83 ± 17.94	1007.85 ± 22.65	1052.10 ± 13.88
	RCP4.5	815.04 ± 9.45	858.25 ± 17.69	928.39 ± 26.84	983.78 ± 22.44	1054.18 ± 17.92
	RCP2.6	813.77 ± 10.91	864.08 ± 18.67	935.89 ± 16.38	997.29 ± 19.78	1060.82 ± 14.66
Gg NO_X $year^{-1}$	**Historical**	826.23 ± 5.06	n.a	n.a	n.a	n.a
	RCP8.5	834.29 ± 9.86	874.93 ± 22.39	945.06 ± 19.97	1006.86 ± 21.39	1033.19 ± 9.22
	RCP6.0	839.24 ± 16.22	906.12 ± 17.48	957.83 ± 18.28	1026.06 ± 23.05	1071.11 ± 14.15
	RCP4.5	829.77 ± 9.63	873.76 ± 18.01	945.18 ± 27.34	1001.56 ± 22.84	1073.24 ± 18.26
	RCP2.6	828.49 ± 11.11	879.71 ± 19.01	952.81 ± 16.68	1015.31 ± 20.14	1080.00 ± 14.95
Gg N_2O $year^{-1}$	**Historical**	122.17 ± 0.76	n.a	n.a	n.a	n.a
	RCP8.5	123.38 ± 1.45	129.38 ± 3.32	139.77 ± 2.96	148.94 ± 3.17	152.81 ± 1.36
	RCP6.0	124.11 ± 2.39	134.01 ± 2.61	141.66 ± 2.71	151.77 ± 3.41	158.43 ± 2.10
	RCP4.5	122.71 ± 1.43	129.23 ± 2.67	139.79 ± 4.05	148.14 ± 3.38	158.72 ± 2.69
	RCP2.6	122.52 ± 1.65	130.09 ± 2.80	140.93 ± 2.48	150.18 ± 2.97	159.74 ± 2.22
Gg OC $year^{-1}$	**Historical**	4938.03 ± 30.25	n.a	n.a	n.a	n.a
	RCP8.5	4986.12 ± 58.95	5228.90 ± 133.69	5647.99 ± 119.28	6017.33 ± 127.76	6174.67 ± 55.21
	RCP6.0	5015.62 ± 96.91	5415.27 ± 104.47	5724.37 ± 109.25	6132.08 ± 137.76	6401.33 ± 84.51
	RCP4.5	4959.11 ± 57.49	5221.89 ± 107.65	5648.72 ± 163.36	5985.69 ± 136.45	6414.01 ± 109.07
	RCP2.6	4951.38 ± 66.41	5257.44 ± 113.59	5694.32 ± 99.65	6067.91 ± 120.32	6454.48 ± 89.26
Gg BC $year^{-1}$	**Historical**	244.45 ± 1.49	n.a	n.a	n.a	n.a
	RCP8.5	246.82 ± 2.91	258.84 ± 6.61	279.61 ± 5.90	297.87 ± 6.31	305.67 ± 2.73

sp.	Year	2000 - 2020	2021 - 2040	2041 - 2060	2061 - 2080	2081 - 2100
	RCP6.0	248.27 ± 4.79	268.06 ± 5.17	283.39 ± 5.40	303.57 ± 6.82	316.89 ± 4.19
	RCP4.5	249.83 ± 3.90	261.82 ± 7.74	282.74 ± 11.37	293.47 ± 19.22	310.66 ± 23.28
	RCP2.6	245.09 ± 3.27	260.25 ± 5.62	281.87 ± 4.93	300.39 ± 5.97	319.51 ± 4.42
Gg SO_2 $year^{-1}$	**Historical**	366.68 ± 2.25	n.a	n.a	n.a	n.a
	RCP8.5	370.23 ± 4.38	388.26 ± 9.93	419.42 ± 8.86	446.82 ± 9.49	458.52 ± 4.11
	RCP6.0	372.43 ± 7.20	402.12 ± 7.75	425.06 ± 8.12	455.35 ± 10.23	475.33 ± 6.27
	RCP4.5	368.23 ± 4.27	387.77 ± 8.00	419.45 ± 12.13	444.48 ± 10.13	476.28 ± 8.09
	RCP2.6	367.67 ± 4.94	390.40 ± 8.44	422.82 ± 7.39	450.57 ± 8.94	479.29 ± 6.64
Gg C_2H_6 $year^{-1}$	**Historical**	440.02 ± 2.69	n.a	n.a	n.a	n.a
	RCP8.5	444.30 ± 5.26	465.93 ± 11.91	503.28 ± 10.62	536.19 ± 11.38	550.21 ± 4.92
	RCP6.0	446.91 ± 8.64	482.53 ± 9.30	510.09 ± 9.74	546.42 ± 12.27	570.40 ± 7.53
	RCP4.5	441.89 ± 5.13	465.31 ± 9.60	503.34 ± 14.56	533.37 ± 12.16	571.54 ± 9.73
	RCP2.6	441.19 ± 5.93	468.47 ± 10.13	507.41 ± 8.90	540.68 ± 10.74	575.14 ± 7.95
Gg CH_3OH $year^{-1}$	**Historical**	748.03 ± 4.57	n.a	n.a	n.a	n.a
	RCP8.5	755.32 ± 8.93	792.10 ± 20.25	855.59 ± 18.08	911.53 ± 19.36	935.37 ± 8.38
	RCP6.0	759.79 ± 14.67	820.33 ± 15.83	867.15 ± 16.55	928.92 ± 20.88	969.70 ± 12.81
	RCP4.5	751.21 ± 8.72	791.03 ± 16.31	855.70 ± 24.75	906.75 ± 20.66	971.62 ± 16.52
	RCP2.6	750.05 ± 10.07	796.42 ± 17.21	862.59 ± 15.10	919.19 ± 18.22	977.75 ± 13.53
Gg C_3H_8 $year^{-1}$	**Historical**	136.85 ± 0.83	n.a	n.a	n.a	n.a
	RCP8.5	138.18 ± 1.65	144.92 ± 3.71	156.54 ± 3.31	166.80 ± 3.54	171.15 ± 1.55
	RCP6.0	139.01 ± 2.68	150.10 ± 2.89	158.67 ± 3.03	169.98 ± 3.82	177.44 ± 2.34
	RCP4.5	137.45 ± 1.60	144.74 ± 2.97	156.58 ± 4.53	165.93 ± 3.79	177.79 ± 3.03
	RCP2.6	137.22 ± 1.84	145.71 ± 3.15	157.85 ± 2.77	168.21 ± 3.33	178.91 ± 2.47
Gg C_2H_2 $year^{-1}$	**Historical**	131.97 ± 0.81	n.a	n.a	n.a	n.a
	RCP8.5	133.24 ± 1.58	139.76 ± 3.59	150.95 ± 3.19	160.84 ± 3.40	165.03 ± 1.47

sp.	Year	2000 - 2020	2021 - 2040	2041 - 2060	2061 - 2080	2081 - 2100
	RCP6.0	134.04 ± 2.60	144.74 ± 2.79	153.00 ± 2.92	163.90 ± 3.67	171.10 ± 2.25
	RCP4.5	132.53 ± 1.52	139.56 ± 2.87	150.99 ± 4.36	160.00 ± 3.64	171.45 ± 2.91
	RCP2.6	132.32 ± 1.78	140.52 ± 3.03	152.20 ± 2.66	162.19 ± 3.23	172.52 ± 2.40
Gg C_2H_4 $year^{-1}$	**Historical**	728.47 ± 4.46	n.a	n.a	n.a	n.a
	RCP8.5	735.55 ± 8.68	771.39 ± 19.72	833.22 ± 17.59	887.70 ± 18.83	910.92 ± 8.14
	RCP6.0	739.90 ± 14.28	798.88 ± 15.42	844.48 ± 16.13	904.63 ± 20.33	944.34 ± 12.47
	RCP4.5	731.57 ± 8.47	770.35 ± 15.88	833.33 ± 24.11	883.04 ± 20.14	946.23 ± 16.09
	RCP2.6	730.45 ± 9.78	775.60 ± 16.76	840.04 ± 14.69	895.17 ± 17.75	952.18 ± 13.17
Gg C_3H_6 $year^{-1}$	**Historical**	322.65 ± 1.98	n.a	n.a	n.a	n.a
	RCP8.5	325.79 ± 3.86	341.68 ± 8.73	369.07 ± 7.80	393.21 ± 8.34	403.48 ± 3.61
	RCP6.0	327.72 ± 6.34	353.84 ± 6.83	374.04 ± 7.14	400.70 ± 9.02	418.29 ± 5.53
	RCP4.5	324.03 ± 3.76	341.22 ± 7.04	369.13 ± 10.67	391.15 ± 8.91	419.12 ± 7.12
	RCP2.6	323.53 ± 4.35	343.54 ± 7.42	372.11 ± 6.51	396.51 ± 7.85	421.77 ± 5.83
Gg C_5H_8 $year^{-1}$	**Historical**	34.15 ± 0.21	n.a	n.a	n.a	n.a
	RCP8.5	34.45 ± 0.41	36.14 ± 0.94	39.04 ± 0.82	41.62 ± 0.89	42.68 ± 0.38
	RCP6.0	34.65 ± 0.68	37.44 ± 0.71	39.60 ± 0.76	42.42 ± 0.96	44.28 ± 0.59
	RCP4.5	34.27 ± 0.41	36.10 ± 0.76	39.06 ± 1.12	41.40 ± 0.96	44.38 ± 0.75
	RCP2.6	34.21 ± 0.48	36.34 ± 0.78	39.38 ± 0.71	41.98 ± 0.84	44.69 ± 0.62
Gg $C_{10}H_{16}$ $year^{-1}$	**Historical**	748.03 ± 4.57	n.a	n.a	n.a	n.a
	RCP8.5	755.32 ± 8.93	792.10 ± 20.25	855.59 ± 18.08	911.53 ± 19.36	935.37 ± 8.38
	RCP6.0	759.79 ± 14.67	820.33 ± 15.83	867.15 ± 16.55	928.92 ± 20.88	969.70 ± 12.81
	RCP4.5	751.21 ± 8.72	791.03 ± 16.31	855.70 ± 24.75	906.75 ± 20.66	971.62 ± 16.52
	RCP2.6	750.05 ± 10.07	796.42 ± 17.21	862.59 ± 15.10	919.19 ± 18.22	977.75 ± 13.53
Gg C_7H_8 ye ar-	**Historical**	156.42 ± 0.96	n.a	n.a	n.a	n.a

sp.	Year	2000 - 2020	2021 - 2040	2041 - 2060	2061 - 2080	2081 - 2100
	RCP8.5	157.94 ± 1.86	165.64 ± 4.25	178.92 ± 3.80	190.63 ± 4.06	195.63 ± 1.75
	RCP6.0	158.87 ± 3.08	171.55 ± 3.31	181.33 ± 3.46	194.25 ± 4.37	202.80 ± 2.67
	RCP4.5	157.09 ± 1.81	165.43 ± 3.42	178.95 ± 5.18	189.63 ± 4.33	203.20 ± 3.47
	RCP2.6	156.83 ± 2.11	166.55 ± 3.60	180.39 ± 3.17	192.25 ± 3.80	204.48 ± 2.83
Gg C_6H_6 $year^{-1}$	**Historical**	254.23 ± 1.56	n.a	n.a	n.a	n.a
	RCP8.5	256.68 ± 3.03	269.19 ± 6.88	290.77 ± 6.14	309.78 ± 6.57	317.90 ± 2.85
	RCP6.0	258.21 ± 5.01	278.79 ± 5.37	294.71 ± 5.63	315.69 ± 7.10	329.57 ± 4.36
	RCP4.5	255.30 ± 2.97	268.82 ± 5.55	290.82 ± 8.42	308.16 ± 7.03	330.22 ± 5.61
	RCP2.6	254.89 ± 3.42	270.66 ± 5.86	293.15 ± 5.13	312.40 ± 6.19	332.31 ± 4.59
Gg C_8H_{10} $year^{-1}$	**Historical**	48.81 ± 0.30	n.a	n.a	n.a	n.a
	RCP8.5	49.30 ± 0.59	51.70 ± 1.33	55.85 ± 1.19	59.52 ± 1.27	61.07 ± 0.54
	RCP6.0	49.59 ± 0.97	53.56 ± 1.04	56.63 ± 1.08	60.67 ± 1.36	63.33 ± 0.84
	RCP4.5	49.04 ± 0.57	51.64 ± 1.07	55.88 ± 1.63	59.22 ± 1.35	63.46 ± 1.08
	RCP2.6	48.96 ± 0.65	51.99 ± 1.13	56.33 ± 0.99	60.03 ± 1.19	63.85 ± 0.89
Gg CH_2O $year^{-1}$	**Historical**	860.47 ± 5.29	n.a	n.a	n.a	n.a
	RCP8.5	868.86 ± 10.27	911.17 ± 23.31	984.20 ± 20.79	1048.56 ± 22.26	1075.97 ± 9.62
	RCP6.0	873.99 ± 16.87	943.63 ± 18.19	997.50 ± 19.03	1068.56 ± 24.00	1115.47 ± 14.74
	RCP4.5	864.15 ± 10.01	909.94 ± 18.77	984.32 ± 28.47	1043.05 ± 23.77	1117.69 ± 19.01
	RCP2.6	862.80 ± 11.55	916.15 ± 19.79	992.27 ± 17.37	1057.38 ± 20.96	1124.73 ± 15.55
Gg C_2H_4O $year^{-1}$	**Historical**	381.33 ± 2.34	n.a	n.a	n.a	n.a
	RCP8.5	385.05 ± 4.54	403.81 ± 10.33	436.19 ± 9.20	464.70 ± 9.85	476.84 ± 4.28
	RCP6.0	387.33 ± 7.47	418.18 ± 8.07	442.07 ± 8.46	473.57 ± 10.65	494.35 ± 6.54
	RCP4.5	382.96 ± 4.43	403.27 ± 8.31	436.23 ± 12.61	462.26 ± 10.55	495.33 ± 8.42
	RCP2.6	382.37 ± 5.12	406.01 ± 8.77	439.76 ± 7.70	468.60 ± 9.28	498.47 ± 6.90

sp.	Year	2000 - 2020	2021 - 2040	2041 - 2060	2061 - 2080	2081 - 2100
Gg C_3H_6O $year^{-1}$	**Historical**	728.47 ± 4.46	n.a	n.a	n.a	n.a
	RCP8.5	735.55 ± 8.68	771.39 ± 19.72	833.22 ± 17.59	887.70 ± 18.83	910.92 ± 8.14
	RCP6.0	739.90 ± 14.28	798.88 ± 15.42	844.48 ± 16.13	904.63 ± 20.33	944.34 ± 12.47
	RCP4.5	731.57 ± 8.47	770.35 ± 15.88	833.33 ± 24.11	883.04 ± 20.14	946.23 ± 16.09
	RCP2.6	730.45 ± 9.78	775.60 ± 16.76	840.04 ± 14.69	895.17 ± 17.75	952.18 ± 13.17
Gg $C_3H_6O_2$ $year^{-1}$	**Historical**	723.58 ± 4.44	n.a	n.a	n.a	n.a
	RCP8.5	730.63 ± 8.62	766.22 ± 19.60	827.62 ± 17.48	881.74 ± 18.72	904.80 ± 8.08
	RCP6.0	734.96 ± 14.19	793.51 ± 15.31	838.81 ± 16.01	898.56 ± 20.19	938.02 ± 12.38
	RCP4.5	726.66 ± 8.42	765.16 ± 15.79	827.72 ± 23.93	877.11 ± 19.99	939.87 ± 15.97
	RCP2.6	725.55 ± 9.74	770.38 ± 16.64	834.41 ± 14.61	889.16 ± 17.63	945.79 ± 13.09
Gg C_6H_5OH $year^{-1}$	**Historical**	1447.18 ± 8.86	n.a	n.a	n.a	n.a
	RCP8.5	1043.78 ± 676.60	1532.42 ± 39.17	1655.24 ± 34.96	1763.49 ± 37.43	1809.60 ± 16.19
	RCP6.0	1049.94 ± 680.86	1587.04 ± 30.61	1677.63 ± 32.01	1797.12 ± 40.37	1876.04 ± 24.76
	RCP4.5	1038.10 ± 672.92	1530.38 ± 31.55	1655.46 ± 47.88	1754.23 ± 39.99	1879.75 ± 31.97
	RCP2.6	1036.50 ± 671.92	1540.80 ± 33.28	1668.84 ± 29.21	1778.32 ± 35.28	1891.61 ± 26.16
Gg NH_3 $year^{-1}$	**Historical**	1378.72 ± 8.47	n.a	n.a	n.a	n.a
	RCP8.5	1392.15 ± 16.45	1459.96 ± 37.33	1576.96 ± 33.31	1680.09 ± 35.67	1724.03 ± 15.42
	RCP6.0	1400.39 ± 27.06	1511.98 ± 29.15	1598.28 ± 30.51	1712.12 ± 38.45	1787.30 ± 23.59
	RCP4.5	1384.62 ± 16.06	1458.00 ± 30.05	1577.17 ± 45.62	1671.25 ± 38.11	1790.83 ± 30.45
	RCP2.6	1382.46 ± 18.54	1467.91 ± 31.71	1589.90 ± 27.83	1694.20 ± 33.61	1802.13 ± 24.92
Gg HCN $year^{-1}$	**Historical**	396.00 ± 2.43	n.a	n.a	n.a	n.a
	RCP8.5	399.86 ± 4.73	419.34 ± 10.74	452.95 ± 9.57	482.56 ± 10.25	495.19 ± 4.44
	RCP6.0	402.21 ± 7.77	434.28 ± 8.38	459.08 ± 8.77	491.78 ± 11.05	513.37 ± 6.76
	RCP4.5	397.69 ± 4.61	418.77 ± 8.66	453.02 ± 13.09	480.04 ± 10.94	514.39 ± 8.74
	RCP2.6	397.07 ± 5.32	421.63 ± 9.11	456.67 ± 7.99	486.65 ± 9.65	517.64 ± 7.16
M E K_2 ye ar-	**Historical**	73.26 ± 0.46	n.a	n.a	n.a	n.a

sp.	Year	2000 - 2020	2021 - 2040	2041 - 2060	2061 - 2080	2081 - 2100
	RCP8.5	74.00 ± 0.88	77.61 ± 1.99	83.83 ± 1.77	89.34 ± 1.90	91.67 ± 0.82
	RCP6.0	74.43 ± 1.44	80.38 ± 1.55	84.97 ± 1.64	91.03 ± 2.05	95.03 ± 1.26
	RCP4.5	73.59 ± 0.85	77.49 ± 1.60	83.85 ± 2.43	88.86 ± 2.03	95.22 ± 1.62
	RCP2.6	73.47 ± 0.99	78.02 ± 1.69	84.52 ± 1.48	90.07 ± 1.79	95.82 ± 1.32
Gg CH_3CN $year^{-1}$	**Historical**	146.65 ± 0.88	n.a	n.a	n.a	n.a
	RCP8.5	148.06 ± 1.75	155.28 ± 3.97	167.73 ± 3.55	178.71 ± 3.79	183.38 ± 1.64
	RCP6.0	148.94 ± 2.88	160.82 ± 3.11	170.00 ± 3.25	182.12 ± 4.08	190.13 ± 2.51
	RCP4.5	147.26 ± 1.70	155.08 ± 3.21	167.76 ± 4.85	177.77 ± 4.07	190.49 ± 3.24
	RCP2.6	147.03 ± 1.98	156.12 ± 3.37	169.13 ± 2.96	180.24 ± 3.59	191.70 ± 2.67

4. DISCUSSION

4.1. Feasibility of fire simulation

According to the default module, the fires spread throughout almost all of Siberia (S4.a-d, 4.a-d) because the module considered only the fuel amount and fuel moisture content. Thus, if the fuel load met the threshold requirement in any random grid, a fire appeared and could spread to other areas. Furthermore, the spatial distribution and trend of burned biomass under all of the RCP scenarios in the default fire module were not consistent with the burned fraction data. Areas with high burned fraction values should also have high burned biomass, and vice versa.

However, in the improved module, the fires ignited only in areas that were covered in the lightning ignition and population ignition datasets based on the calculation of each ignition factor. This is confirmed by the comparison of the fire variable with the ignition factor variables, the comparison of the burned fraction variable with the lightning flash strikes variable shows a strong correlation of 0.68 (R^2=0.45), and the comparison of the burned fraction variable with the population density variable shows a correlation of 0.24 (R^2=0.06) (Figure 34). These relatively low correlation values are due to the fact that the presence of an ignition factor does not guarantee that a fire will start; the area needs to have sufficient dry litter to feed the fire. Apart from these variables in the improved model, other factors also influence fire occurrence and spread in real life, such as slope and solar aspect (Rothermell, 1972), but their inclusion at this point was not possible due to the limitations of the model. In addition, when comparing the fire and AGB distributions, the SEIB-DGVM SPITFIRE showed greater agreement than did the default fire module.

Furthermore, differences remained between the spatial distribution patterns of the simulated fires and the GFED4s data in eastern Siberia. We believe that the main reason for the lack of simulated fires in eastern Siberia was the scarcity of available fuel and biomass for the ignition and spread of fires. We found that the AGB in these areas (130-142°E and 65-80°N; Figure 46) was very low, averaging 65.59 g C m^{-2}. This value was far below the model minimum fuel load threshold requirement of 200 g C m^{-2} (Sato et al., 2007) for fire ignition or spread. All three benchmark datasets, the ESA Biomass CCI (aboveground biomass), GFED4 (burned area), and GFED4s (burned fraction), indicate that fire is present in this area, with ESA Biomass CCI showing an AGB of 2,309.67 g DM m^{-2}. It is challenging to produce a model product that precisely predicts observations, as the simulations are highly dependent

on the input data and dynamics, while the benchmark datasets were obtained from satellite image estimations that are able to capture natural conditions and events in real time. Even predictions based on satellite observations can differ significantly from field-based observations. For example, the International Forest Fire News (IFFN) Russian Federation reported that 2003 had extremely severe fires in Siberia based both on ground and aerial observation. However, the burnt area was determined to be 2,654,000 ha based on field observations and 17,406,900 ha based on satellite-derived observations (NOAA AVHRR) (IFFN, 2003; Siegert and Huang, 2005). The difference between ground observation data and satellite-derived data is due to differences in the data collection time and continuity. Ground-based observations are carried out only for a short time due to technical difficulties, while observations based on satellite data are carried out without any significant difficulties (IFFN, 2003). In this case, the SEIB-DGVM SPITFIRE model reported a burned area of 7,969,785 ha, an estimation centered between the observational and satellite data.

Overall, based on the fire variable outputs (burned fraction and burned area) from the improved model generated and validated with benchmark data, we project that Siberia will have an increasing trend until 2100 (Figure 31.d, Figure 33.b, and Figure 36.d). Yasunari et al., (2024) in a comprehensive assessment of the impacts of the Siberian wildfire using MIROC5 stated that there is high probability of increased Siberian wildfires in the future, and this estimate implies that worse air quality due to wildfires is predicted in the future, with frequent exceedances of air quality environmental standards (ES).

Kasischke and Bruhwiler, (2003) stated that the level of uncertainty in the burned area parameter for estimating fire emissions in the Russian boreal forest is ± 30% for satellite imagery, while the uncertainty of the parameter is -300% according to official government statistics, resulting in fires being largely underestimated. This difference in uncertainty was caused by the diverse parameters/equations used for estimation, the varying levels of detail of the analysis, and other factors, such as forest type, location, fuel load, fire type, and aboveground biomass density. Differences are also extrapolated when estimations for large areas are based on individual fires (Kasischke and Bruhwiler, 2003; Kukavskaya et al., 2013). Therefore, uncertainties will inevitably persist in model- or simulation-based research when comparing model- or simulation-based data with direct observations.

4.2. Forest resilience under fire and climate change

Terrestrial NPP is an essential element of the carbon cycle and global climate dynamics, as it directly affects the CO_2 content of the atmosphere, resulting in delayed climatic changes (Running, 2022). If NPP decreases, the land's ability to absorb CO_2 will decrease, causing atmospheric CO_2 to increase faster and thereby contributing climate change (Running, 2022). Based on the comparison between fire-on and fire-off simulation, under RCP8.5 scenario, from 2000 to 2100 the NPP will decrease by 385.11 ± 40.4 g C m^{-2} (5.03 ± 1.5 g C m^{-2} $year^{-1}$) due to wildfires until 2100. Satellite observations one year after boreal forest fires in Alaska and Canada recorded a 60–260 g C m^{-2} loss of NPP (Hicke et al., 2003). In the coniferous forests of the western United States, postfire NPP loss was also recorded and ranged from 67 to 312 g C m^{-2} $year^{-1}$ (Sparks et al., 2018). These data indicate that the NPP simulation results of the SEIB-DGVM SPITFIRE model are also consistent with some observational data in different areas.

NPP and NBP, both are significant elements of the global C cycle and are used as indicators of ecosystem function and are linked to biodiversity, biogeochemical cycling, ecosystem resilience, and other aspects of ecosystem services (Pan et al., 2007; Richmond et al., 2007; Ito, 2011). However specifically, the mitigation ability of ecosystems is determined by net biome productivity (NBP) (Chapin et al., 2006; Fisher et al., 2014)(Chapin et al., 2006; Fisher et al., 2014), and climate-driven large anomalies in NBP could impact the structure, composition, and function of terrestrial ecosystems (Frank et al., 2015). The twenty-year average NBP from 2000-2100 shows a carbon sink in Siberia with a increasing trend (Figure 50). Overall, from 2000 to 2100, RCP8.5 produces the highest value, then RCP6.0, RCP4.5 and RCP2.6 with values of 304.61 ± 11.77, 286.78 ± 10.64, 286.17 ± 10.99, and 274.95 ± 9.36 Tg C $year^{-1}$, respectively (Table 9). The historical annual mean value of NBP in Siberia for 2000-2021 of 136.39 ± 83.4 Tg C $year^{-1}$ is also similar to the CLM4CN simulations (annual average 1981-2006) in Eurasia and Boreal and Arctic of 204 and 284 Tg C $year^{-1}$, respectively (Kantzas et al., 2013).

Under all climate scenarios from 2000 to 2100, we estimate that the net biome productivity (NBP) will continue to increase, indicating a continued flux of CO_2 from the atmosphere to the land (Figure 50). The classification of NBP variables based on climate input data also shows the correct order, from the smallest under RCP2.6 to the largest under RCP8.5 (Figure 51). This is because climate factors, such as temperature and precipitation, have a positive impact on vegetation (Yuan et al., 2021). On average, from 2000 to 2100, under the RCP8.5

climate scenario, the NBP in Siberia is estimated at 301.3 ± 49.1 Tg C (equivalent to 3.01 ± 0.5 Tg C $year^{-1}$). Other studies have similar estimation that the NBP across northern peatlands, including the Russian Far East (RFE) and West Siberian Lowlands (WSL), ranges from 10 to 220 Tg C $year^{-1}$ (Qiu et al., 2022). Additionally, we estimate that the heterotrophic respiration (HTR) in Siberia will continue to increase until 2100. On average under RCP8.5, from 2000 to 2100, HTR value in Siberia is estimated at 4,002.7 ± 967.7 Tg C (equivalent to an increase of 40 ± 9.7 Tg C $year^{-1}$) (Figure 52, Table 10). We suggest that the high HTR values during those years were attributable to an elevated fuel load (Figure 53.a) followed by significant precipitation (Figure 53.b), which increased litter moisture content (Figure 54) and consequently accelerated the decomposition rates of litter and soil organic carbon. Increased of heterotrophic respiration, tree mortality and increased disturbance (drought and fire) contribute significantly to negative carbon fluxes from the ecosystem due to increased temperature and atmospheric CO_2 (Sharma et al., 2023). Overall, SEIB-DGVM SPITFIRE simulates that until the end of the 21st century, there will continue to be a strengthening of the land carbon sink in Siberia under all RCP scenarios. Boreal forests (1135 Mha) consistently acted as an average carbon sink of 0.5 ± 0.1 Pg C $year^{-1}$ over the two decades from 1990 to 2010. Furthermore, Asian Russia had the largest boreal carbon sink, which showed no overall change despite increased emissions from wildfire disturbances (Pan et al., 2007).

Boreal forest vegetation is naturally influenced by a variety of periodic disturbances, such as wildfires (Kasischke et al., 1995), insect outbreaks, and windthrow. Wildfires and insect outbreaks are not necessarily independent, there is a likelihood of wildfires often increasing or decreasing after insect outbreaks (Meigs et al., 2015, 2016). However, wildfires are among the main disturbances that drive forest dynamics, shape forest composition and structure, and affect biomass and productivity (Burns and Honkala, 1990; Greene and Johnson, 1999). Circumpolar northern boreal forests and tundra are likely to continue to warm more than most other terrestrial biomes according to available data from models and observations (Chapin et al., 2005; Foley, 2005; Meehl et al., 2007; Trenberth et al., 2007; Lee et al., 2021). Based on the observations and changes in regional attributes from 1950 to the present, it is projected that during 2071-2100, the WSB (West Siberia), ESB (East Siberia), and RFE (Russian Far East) will experience an increase in extreme temperatures with high confidence of more than 7 °C for all seasons under the RCP8.5 scenario. Projected warming is most evident on the large continental Siberian Plateau, which has boreal and subboreal climates and biomes (i.e., taiga forests and tundra), during the winter season (Ozturk et al., 2017; IPCC, 2021). Such

changes in climatic extreme scenarios and seasonality are also likely to have multiple effects, including extended but drier growing seasons, the occurrence of more intense convective storms leading to more lightning-caused fires (Hessilt et al., 2021; Kharuk et al., 2022), and decreased forest productivity (Orangeville et al., 2018); additionally, longer, warmer, and drier summers may cause an increase in fire frequency and size in some areas of boreal forests (Krawchuk et al., 2009; Flannigan et al., 2016; Wotton et al., 2017). This finding is in line with our results, which show that the assessment of forest ecology variables indicates tree mortality due to fire and succession as well as postfire vegetation (Figure 42.c) and affects NPP dynamics in Siberia (Figure 42.a).

Under the RCP2.6 scenario, the SEIB-DGVM estimated the average tree density to be 2,166 tree ha^{-1} between 200 and 2023 in Siberia. The tree density is greater in northeastern Siberia (1,197 tree ha^{-1}) than in southern Siberia (Miesner et al., 2022). Our simulation resulted in higher tree densities than did the observations in northeastern Siberia, as we covered a larger area of forest at 60°-180°E and 45°-80°N. The number of trees is affected by the frequency of fires at a certain location. Additionally, the number of trees destroyed by wildfires depended upon the climate scenario used in the simulations but naturally increased with fire frequency and size. In all the RCP scenarios, the number of destroyed trees was greater than that in the historical simulation, and the number of destroyed trees increased annually, indicating that changes in climatic factors affected the surviving tree density. The projected increase in the number of trees destroyed annually is consistent with the modeled fire product data, which exhibit an increasing trend until 2100. The difference in tree mortality data between climate scenarios is because each climate scenario has a different projected temperature increase. In Siberia, under the RCP8.5 scenario, we simulate that the 2-meter surface temperature will increase by 4.67°C by 2100 (Figure 55). This estimate aligns with the IPCC projections, which predict air temperature increases by 2100 ranging from 0.3-1.7°C (average 1.0°C) under the RCP2.6 scenario, 1.1-2.6°C (average 1.8°C) under the RCP4.5 scenario, 1.4-3.1°C (average 2.2°C) under the RCP6.0 scenario, and 2.6-4.8°C (average 3.7°C) under the RCP8.5 scenario (IPCC, 2021).

The DBH ranges of the trees in the fire-on and fire-off simulations were comparable to those in northeastern Siberia, where the DBH ranged up to 71.6 cm, the tree height up to 28.5 m, and the crown area averaged 4.77 m^2 (Miesner et al., 2022). As the average DBH variable was similar in the fire-on and fire-off simulations, trees with large DBHs are resistant to fire. This was also confirmed based on observational research in Yenisei Siberia, where trees with

a DBH greater than 18.1 cm were the most resistant to further postfire succession (Bryukhanov et al., 2018). Specifically, based on the division of regions, we found an interesting pattern, that in Siberia the eastern region has the highest value of allometry variables (tree height, tree DBH and crown area), then the central region and lowest is the west region (Figure 43, Figure 44, and Figure 45). An interesting pattern was observed in western Siberia, where trees with high height and large DBH but low crown area were detected in some locations (Figure 41.a). We suggest that this happens because of the wildfire, the Siberian central region has the highest wildfire frequency followed by the west region, then the east region. The major Siberian Forest types are formed by larch (*Larix sibirica, L. gmelinii, and L. cajanderi*) and majority distributed in western and central Siberia (Figure 1, and Figure 1 in Kharuk et al., (2021)). Furthermore, larch is classified as pyrophytic species, that have adapted or evolved under conditions of periodic forest fires, they have adapted and gaining a competitive edge over non-fire adapted species in regenerating and growing in burned areas (Kharuk et al., 2021). The abundance of species and high frequency of wildfires in the Siberian central and western regions led to excellent larch succession and regeneration as evidenced by the high tree allometry variables and on the other hand the projected continuity of wildfires led to a downward trend. On the other hand, in the eastern region, very few wildfires are simulated, partly due to the low aboveground biomass available in some areas, which affects ignition and fire spread (Figure 46). However, due to the low frequency of wildfires, allometric variables are projected to have an increasing trend until 2100 in the Siberian east region. The unique relationship between allometric variables, which are naturally distributed without a wide gap between grid plots (Figure 41.c), in the eastern region is also due to the area's low wildfire frequency. The forest in the Siberian east region appears to grow and spread naturally without having high impact from the wildfire. While the majority tree species in Siberia: larch, regenerates extremely well on post-fire-mineralized soil, however on contrast, they regenerate very slowly over a ground floor covered in lichen and moss (where the soil's surface is tough for sapling roots to reach) (Kharuk et al., 2016).

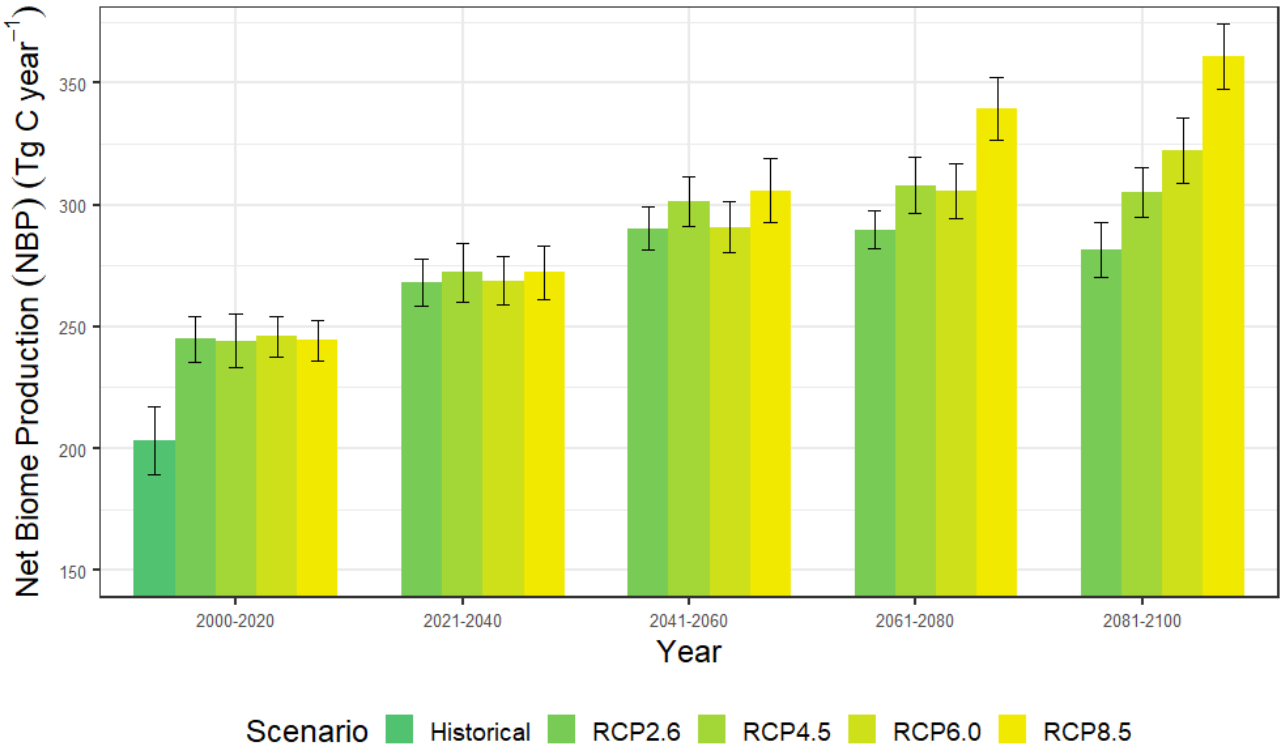

Figure 50. Temporal variation of projected Net Biome Production (NBP) from 2000 to 2100 under different RCPs scenarios. The standard deviation is obtained from the annual average data of each climate scenario.

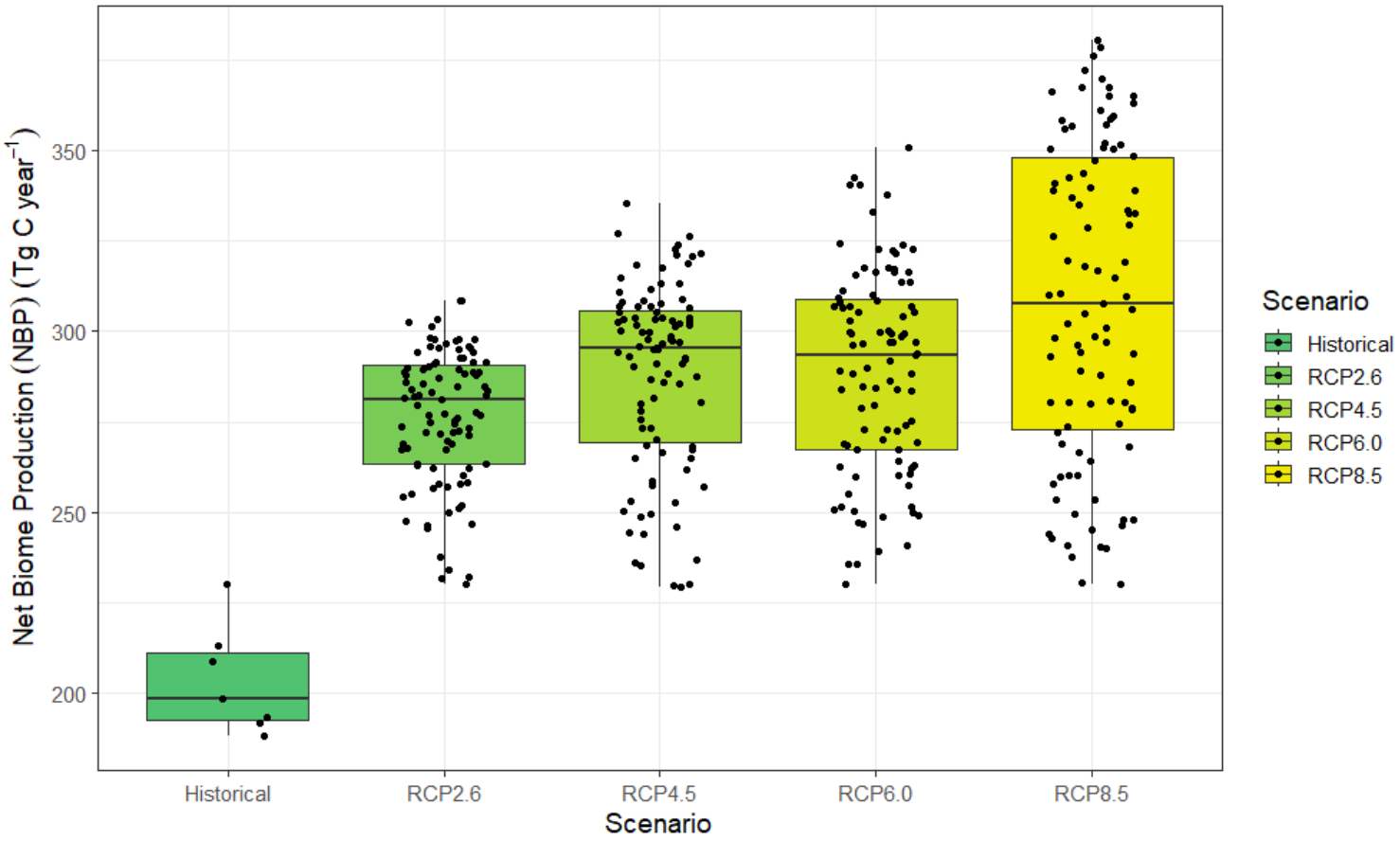

Figure 51. Comparison of annual averaged simulated NBP variables between different climate scenarios from 2000 to 2100.

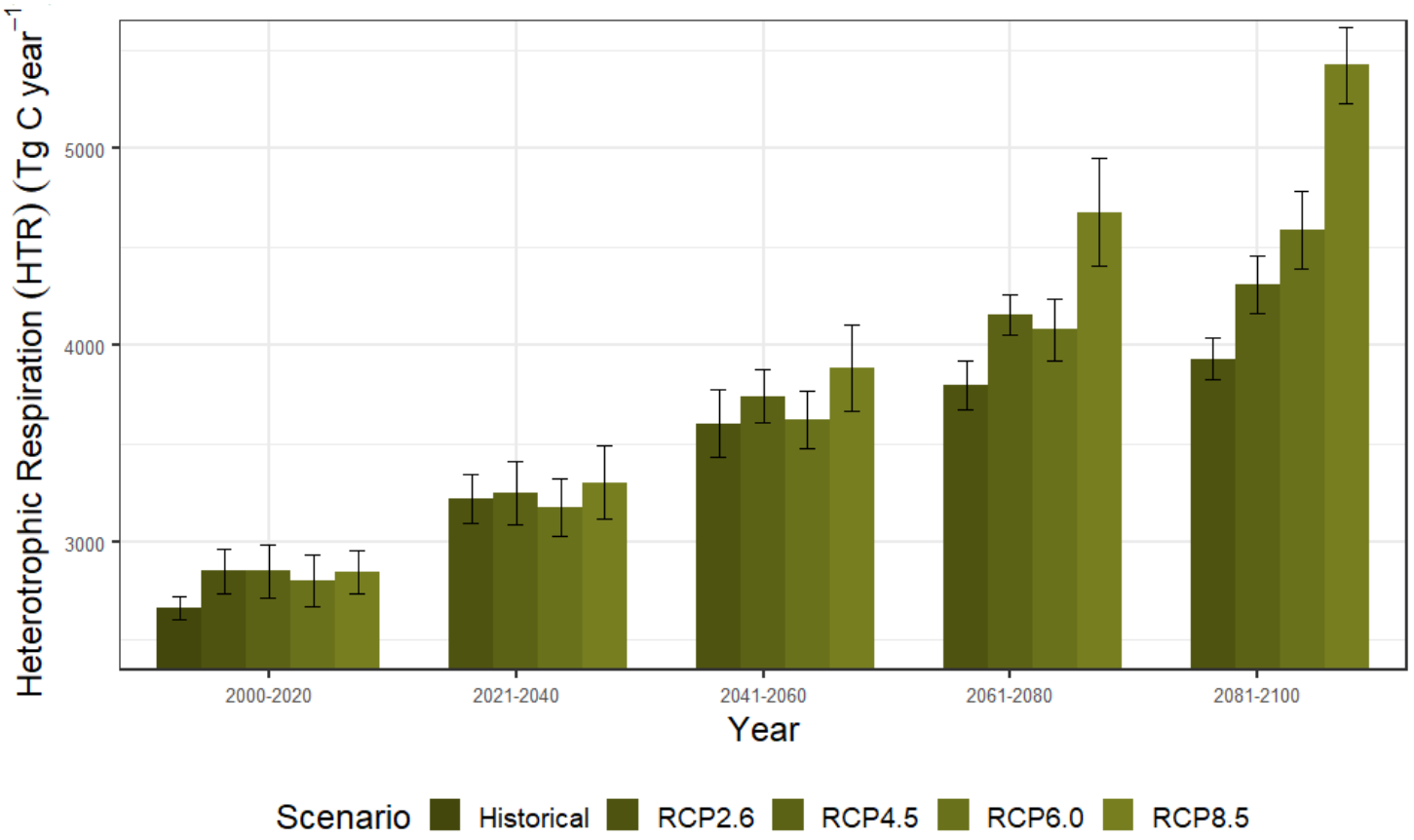

Figure 52. Temporal variation of projected Heterotrophic Respiration (HTR) from 2000 to 2100 under different RCPs scenarios. The standard deviation is obtained from the annual average data of each climate scenario.

Table 9. Twenty-year average NBP from 2000-2100 from model simulations in Siberia

Year	Historical	RCP8.5	RCP6.0	RCP4.5	RCP2.6
2000-2020	203.27 ± 13.78	244.41 ± 8.35	246.14 ± 8.31	244.17 ± 11.09	244.97 ± 9.26
2021-2040	n.a	272.33 ± 10.98	268.85 ± 9.94	272.27 ± 12.06	268.23 ± 9.57
2041-2060	n.a	305.86 ± 13.32	290.89 ± 10.27	301.17 ± 10.13	290.21 ± 8.80
2061-2080	n.a	339.55 ± 13.00	305.65 ± 11.43	308.01 ± 11.62	289.69 ± 7.77
2081-2100	n.a	360.90 ± 13.22	322.39 ± 13.27	305.22 ± 10.04	281.66 ± 11.39
Average	203.27 ± 13.78	304.61 ± 11.77	286.78 ± 10.64	286.17 ± 10.99	274.95 ± 9.36

Table 10. Twenty-year average HR from 2000-2100 from model simulations in Siberia

Year	Historical	RCP8.5	RCP6.0	RCP4.5	RCP2.6
2000-2020	2664.51 ± 59.17	2847.17 ± 111.36	2802.51 ± 130.57	2852.31 ± 135.54	2852.44 ± 114.02
2021-2040	n.a	3303.00 ± 183.68	3176.25 ± 144.19	3248.85 ± 160.10	3218.30 ± 122.48
2041-2060	n.a	3882.35 ± 218.50	3622.35 ± 147.67	3741.40 ± 137.27	3601.80 ± 171.54
2061-2080	n.a	4674.90 ± 275.01	4078.75 ± 158.01	4154.75 ± 100.30	3796.20 ± 126.33
2081-2100	n.a	5423.50 ± 191.02	4583.85 ± 196.23	4307.30 ± 147.47	3930.50 ± 106.95

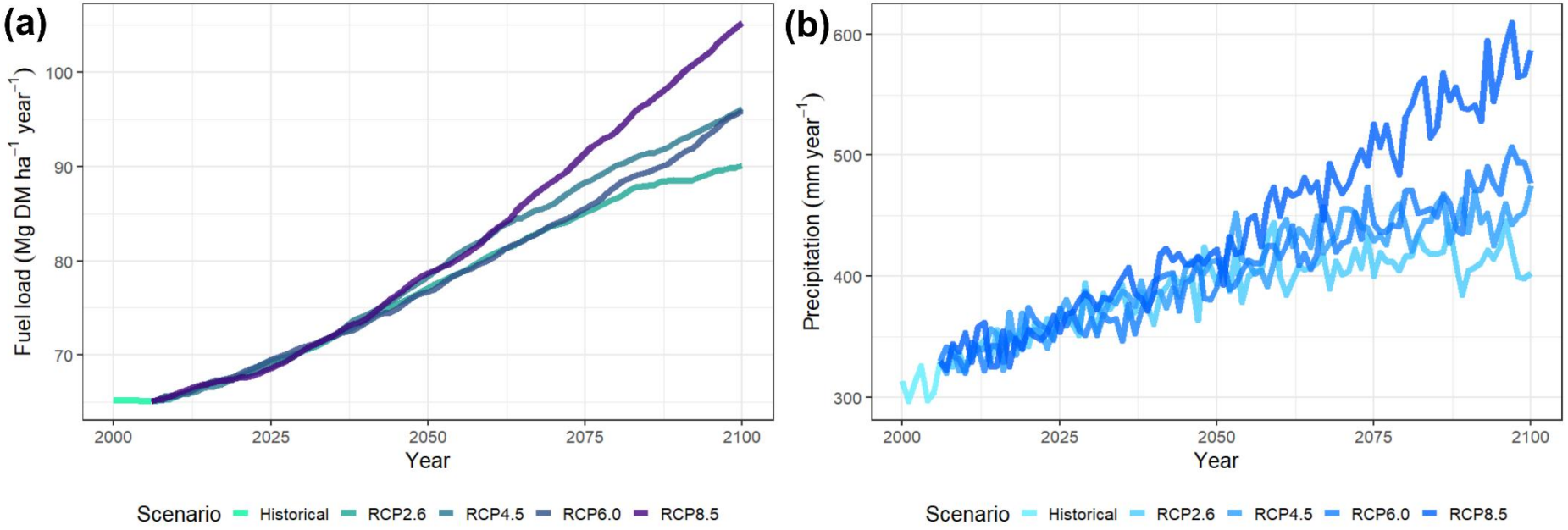

Figure 53. (a) Temporal variation of simulated SEIB-DGVM SPITFIRE fuel load in Siberia under different RCPs climate scenarios from 2000 to 2100. **(b)** Temporal variation of precipitation under different RCPs climate scenarios in Siberia from 2000 to 2100

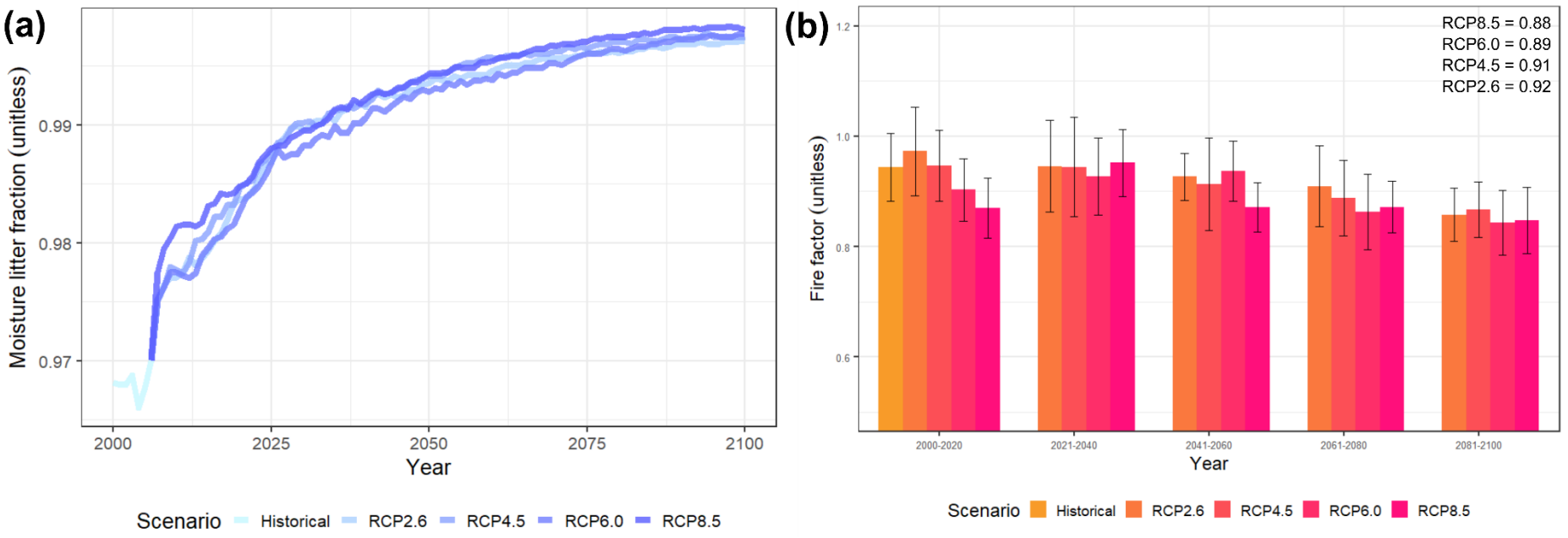

Figure 54. (a) Temporal variation of simulated SEIB-DGVM SPITFIRE moisture litter fraction in Siberia under different RCPs climate scenarios from 2000 to 2100. **(b)** Temporal variation of fire factor under different RCPs climate scenarios in Siberia from 2000 to 2100

4.3. Spatial distribution and temporal variation of biomass burning emissions under climate change scenarios

The spatiotemporal dynamics of the biomass burning emissions under all RCP scenarios had similar patterns and trends, but they had slightly different variations in dynamics because climate affects the frequency and distribution of fires. This is evidenced by all fire variables produced by the model, from burned fraction to burned biomass emissions. In the last 20 years of the projection (2080-2100), the highest values were obtained from simulations using climate inputs RCP2.6, RCP4.5, RCP6.0, and RCP8.5. This occurs because each RCP scenario exhibits varying radiative forcing, with RCP8.5 notably experiencing the highest temperature increase (Figure 55) and also projecting the highest precipitation levels (Figure 53.b). The fuel load variable follows a corresponding order reflective of RCP forcing levels, with RCP8.5 showing the highest and RCP2.6 the lowest (Figure 53.a). However, due to increased precipitation and temperature-induced snowmelt, the moisture content of litter fractions in RCP8.5 simulations attains the highest values, contrasting with the lowest values in RCP2.6. Consequently, available fuel loads may not ignite in areas with high moisture content, leading to projections of the highest burned biomass emissions in the last 20 years of RCP climate projections (2080-2100) for RCP2.6, RCP4.5, RCP6.0, and RCP8.5, respectively. The difference in emission values between climate scenarios in the same year shows that temperature has an impact on vegetation succession and climate-sensitive emission production from wildfires (Gutierrez et al., 2021; Stocker et al., 2021). Thus, the model is able to simulate and integrate fire disturbance, forest dynamics or vegetation succession, and burned biomass emissions well.

Over a 20-year average from 2080 to 2100, under RCP6.0 in Siberia, our simulation predicts that forest fires will emit CO2, CO, PM2.5, TPM, and TPC in amounts of 989.93 ± 13.72, 79.24 ± 1.10, 12.91 ± 0.18, 9.78 ± 0.14, and 6.77 ± 0.09 Tg, respectively (Table 6). Spatially, the projections depict heterogeneous patterns of burned biomass emissions, with regions of high emissions intensity concentrated in areas of larch forest (*Larix spp*.), consistent with Figure 1 and our simulation results, where the fire and emission variables show high values in central to southern Siberia (Figure 31.b, Figure 36.b, and Figure 33.b). This is reinforced by field-based estimation data, that fires in this region result in high tree mortality 76%, Siberian larch forests experience greater aboveground carbon loss after fire than do North American forests, both in absolute and relative levels (Webb et al., 2024). We also visualized all the 33

graphs depicting projected burned biomass emissions, offering valuable insights into the future dynamics of the burned biomass emissions in Siberia. Across these graphs, we observe distinct temporal patterns, revealing trends in burned biomass emissions over time. Under the RCP8.5 to RCP2.6 scenarios, the twenty-year average comparison of overall burned biomass emissions data from 2080-2100, compared to data from 2000-2020, shows projected increases of 23.87%, 27.63%, 29.34%, and 30.36%, respectively (Figure 56). The twenty-year dynamics are summarized in Table 6 and Table 7. Furthermore, each year, various climate scenarios predicted differing emissions based on the respective radiative forcing values (from lowest to highest). The RCP8.5, RCP6.0, RCP4.0, and RCP2.6 scenarios exhibited average annual increases of 0.295%, 0.354%, 0.358%, and 0.361% $year^{-1}$, respectively, from 2000 to 2100.

Under the RCP4.5 scenario, radiative forcing stabilized until 2100 (Thomson et al., 2011), which is consistent with our results, as emissions under the RCP4.5 scenario were more stable than those under the other RCP scenarios. Therefore, its indicated that the trend in fire emissions is consistent with the different scenario-dependent trends in radiative forcings. Overall, based on the RCPs climate scenario data used (MirocAR5), the emission scenario projected an increase in global mean surface temperature in the range of 1.0-3.7 (0.3~4.8) ^{o}C (IPCC, 2014), and currently ranges between 1.5 and 6.0 ^{o}C by 2100 compared to 1850-1900 mean value (Lee et al., 2021). One of the impacts of rising global temperatures is the increased occurrence and severity of forest fires, which lead to a greater prevalence of wildfire (Schoennagel et al., 2017; Haider et al., 2019). The global land area burned by wildfires is expected to increase by 35% if the global temperature increases by 2 °C and precipitation patterns change (Pörtner et al., 2022). Extremely high temperature increase the frequency of severe droughts and proliferate wildfires in several regions, such as southern Europe, northern Eurasia, the USA, and Australia (IPCC, 2021). These frequent and severe wildfires will inevitably lead to an increase in the atmospheric concentration of biomass burning products (Marlon et al., 2008; Amiro et al., 2009; Tian et al., 2023).

Forests in Siberia are very important to monitor and assess continuously because they have a significant impact on regional (short-term) and global (long-term) air quality and human health due to the large amounts of carbon emissions, smoke aerosols, and trace gases in the atmosphere. In addition to the observed amount of emissions, organic carbon (OC)/ elemental carbon (EC) emissions exceeded 3 times, and emissions of inorganic ions (SO_4^{2-} and NH_4^{+}) were found to be 5 times greater than the annual average wildfire emissions from August

2010 to August 2011 (Popovicheva et al., 2014). Increased Siberian wildfire aerosols would significantly degrade air quality, particularly in the surrounding and downwind regions of Siberia (Yasunari et al., 2024). The emitted substances can be transported over long distances and affect air quality in other regions, including North America and Northeast China (Teakles et al., 2017; Johnson et al., 2021; Sun et al., 2023).

Estimating future fire emissions and their impact on air quality is challenging due to model limitations and uncertainties in estimation methods, potential mixing of emissions in the atmosphere, climate radiative forcing factors, and emission transport (Winiger et al., 2017; Schacht et al., 2019). The SEIB-DGVM SPITFIRE was not able to reproduce the events in the validation data for the same year or month but simulated similar dynamic patterns and values. This difference occurs because the benchmark data obtained from satellite image data closely follow natural conditions, while the model accumulates uncertainties due to its long simulation period. The emission estimation method used in the model refers to the dry matter variable and the emission factor from Andreae and Merlet, (2001) and Andreae, (2019), where the emission factors are obtained from laboratory and small field experiments. Each species has specific characteristics that require different assessment methods, and the combustion characteristics can be very different from those of large-scale open biomass burning and wildfires. Kasischke and Bruhwiler, (2003) reported that the level of uncertainty in the emission factor parameters for estimating emissions from fires in Russian boreal forests was ±20-50%, which agrees with the ±50% uncertainty level for major emissions presented by Andreae and Merlet, (2001). However, in the SEIB-DGVM SPITFIRE, we also used the latest emission factor from Andreae, (2019), which was developed for oxygenated volatile organic compounds and for HCN; this approach improved all assessment compound emissions significantly with more accurate measurements and has been widely used by various dynamic global vegetation models to estimate biomass burning emissions globally. Overall, the comparison between different climate RCP scenarios provides further insight into uncertainties and variability in the projections, offering valuable information for understanding the potential impacts of future burned biomass emissions on air quality, climate dynamics, and ecosystem health. Through this analysis, our study contributes to a better understanding of the drivers and implications of burned biomass emissions, informing policy decisions and management strategies aimed at mitigating their environmental and societal impacts.

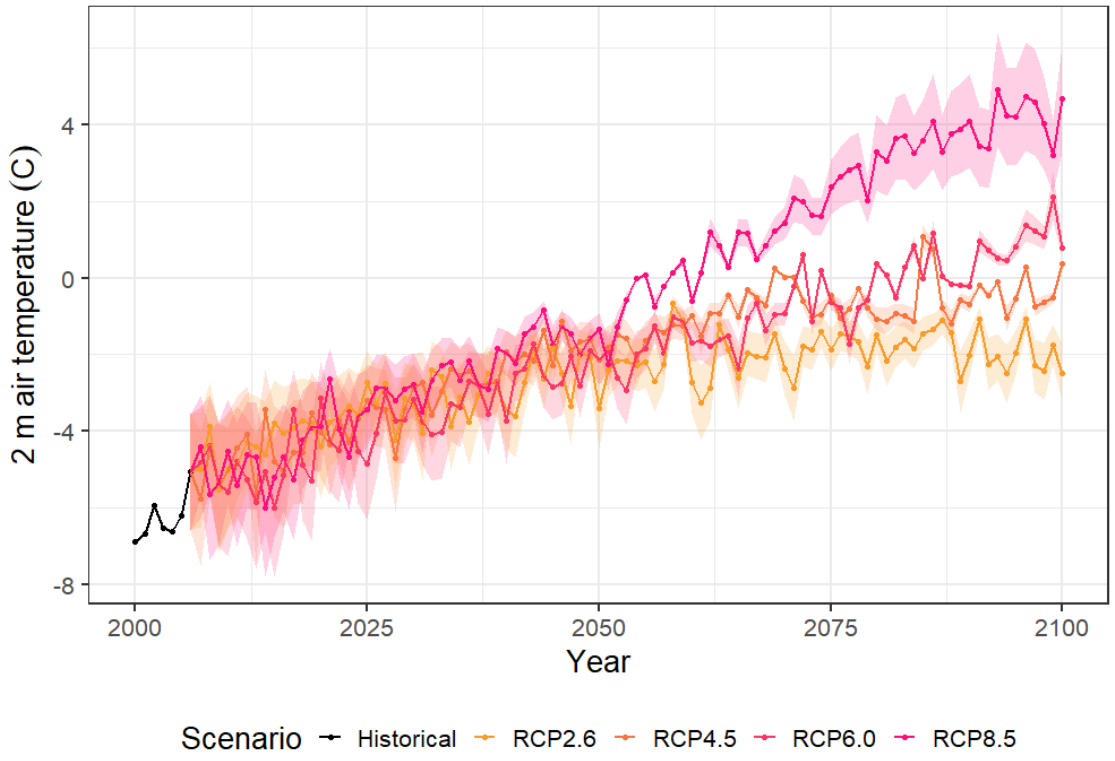

Figure 55. Temporal variation of average 2 m air temperature in Siberia under different RCPs climate scenarios from 2000 to 2100

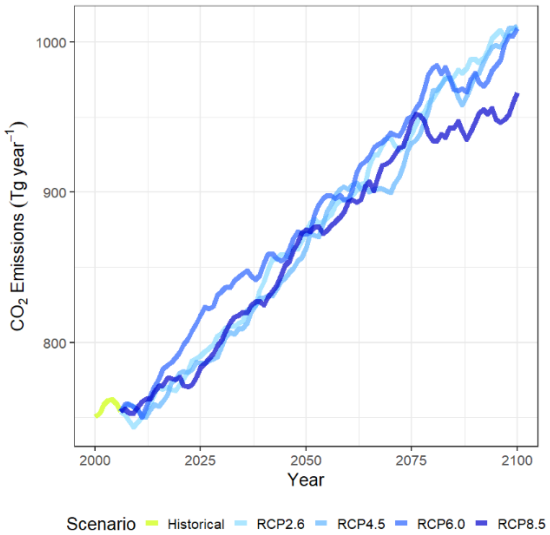
1000
900
800
CO_2 Emissions (Tg year^{-1})
2000
2025
2050
2075
2100
Year
Scenario
Historical
RCP2.6
RCP4.5
RCP6.0
RCP8.5

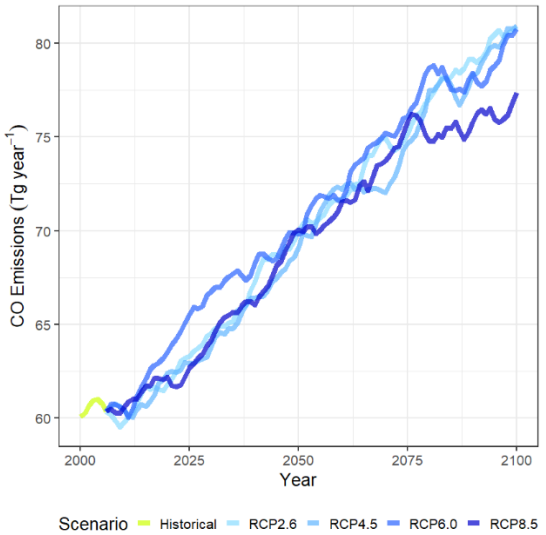
80
75
70
65
60
CO Emissions (Tg year^{-1})
2000
2025
2050
2075
2100
Year
Scenario
Historical
RCP2.6
RCP4.5
RCP6.0
RCP8.5

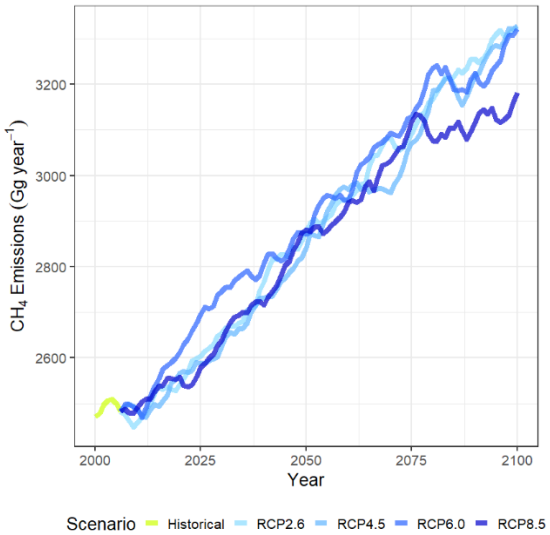
3200
3000
2800
2600
CH_4 Emissions (Gg year^{-1})
2000
2025
2050
2075
2100
Year
Scenario
Historical
RCP2.6
RCP4.5
RCP6.0
RCP8.5

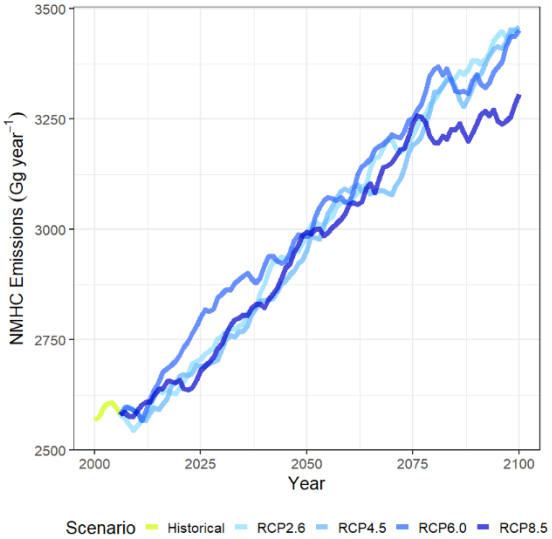
3500
3250
3000
2750
2500
NMHC Emissions (Gg year^{-1})
2000
2025
2050
2075
2100
Year
Scenario
Historical
RCP2.6
RCP4.5
RCP6.0
RCP8.5

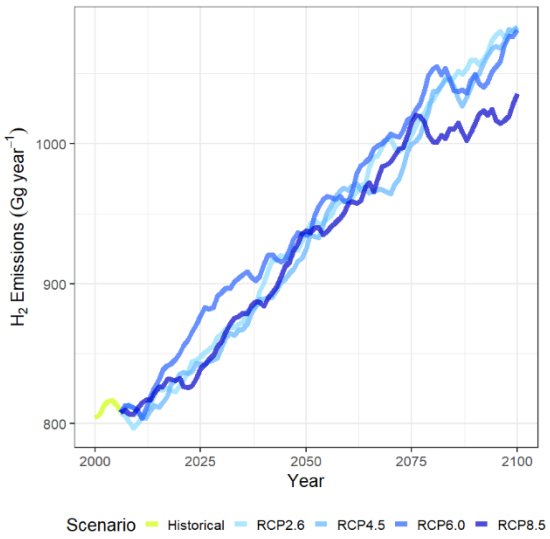
1000
900
800
H_2 Emissions (Gg year^{-1})
2000
2025
2050
2075
2100
Year
Scenario
Historical
RCP2.6
RCP4.5
RCP6.0
RCP8.5

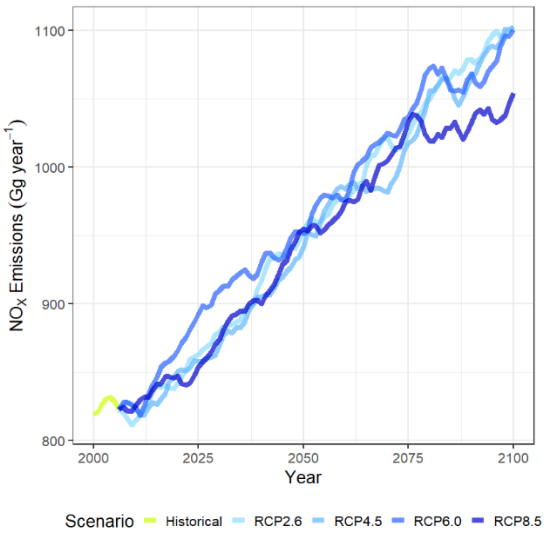
1100
1000
900
800
NO_X Emissions (Gg year^{-1})
2000
2025
2050
2075
2100
Year
Scenario
Historical
RCP2.6
RCP4.5
RCP6.0
RCP8.5

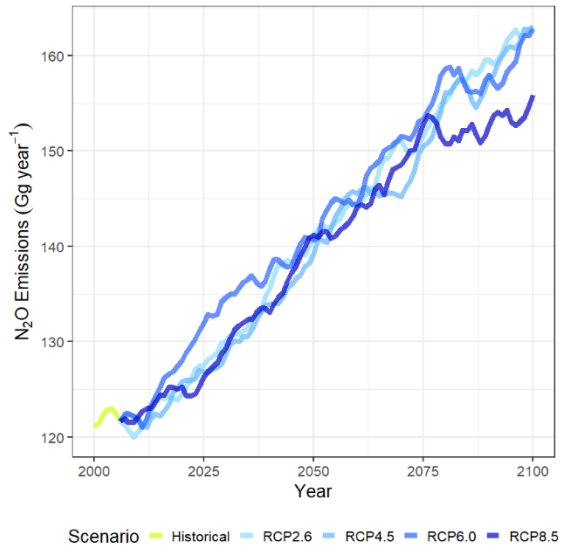
N_2O Emissions (Gg year^{-1})
160
150
140
130
120
2000
2025
2050
2075
2100
Year
Scenario
Historical
RCP2.6
RCP4.5
RCP6.0
RCP8.5

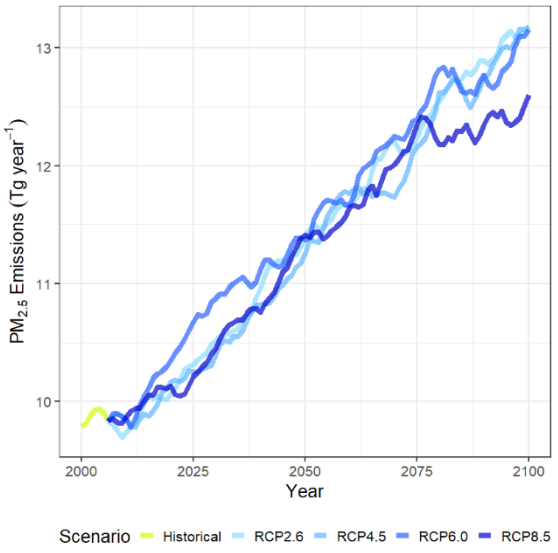
$PM_{2.5}$ Emissions (Tg year^{-1})
13
12
11
10
2000
2025
2050
2075
2100
Year
Scenario
Historical
RCP2.6
RCP4.5
RCP6.0
RCP8.5

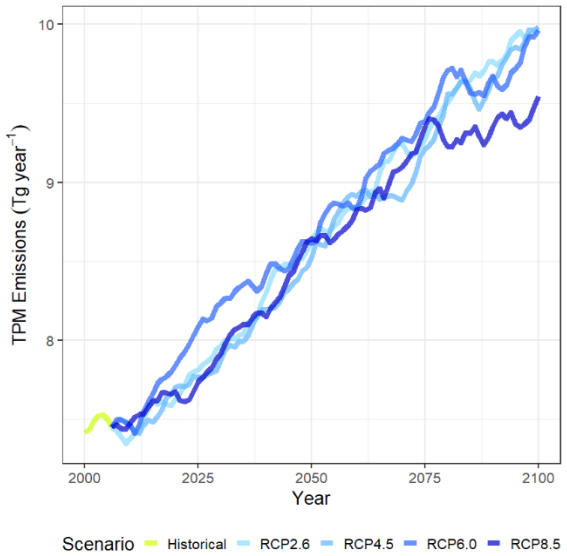
TPM Emissions (Tg year^{-1})
10
9
8
2000
2025
2050
2075
2100
Year
Scenario
Historical
RCP2.6
RCP4.5
RCP6.0
RCP8.5

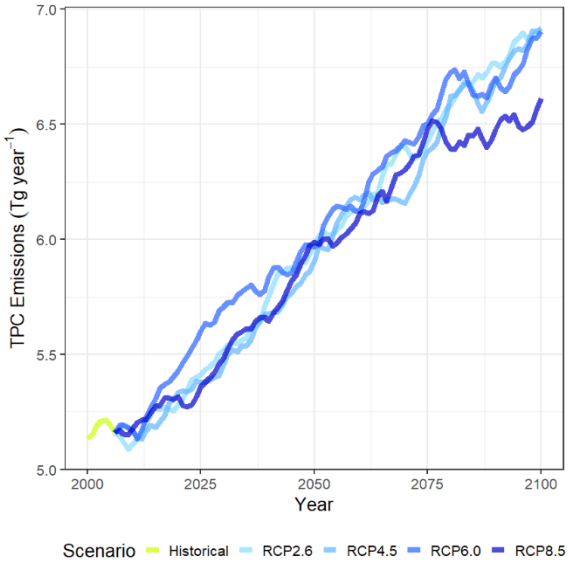
TPC Emissions (Tg year^{-1})
7.0
6.5
6.0
5.5
5.0
2000
2025
2050
2075
2100
Year
Scenario
Historical
RCP2.6
RCP4.5
RCP6.0
RCP8.5

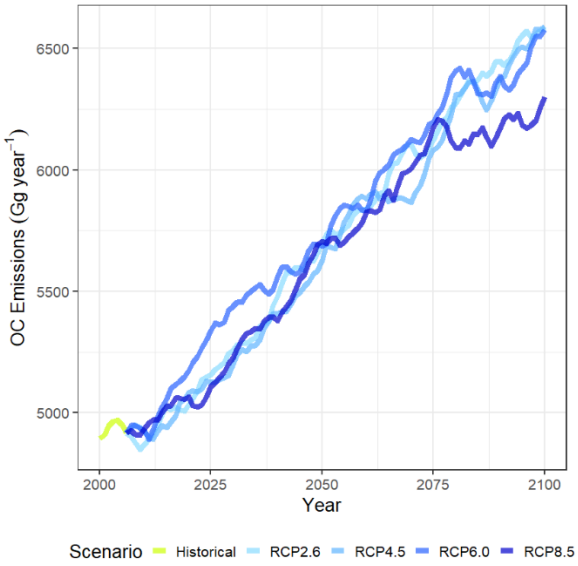
OC Emissions (Gg year^{-1})
6500
6000
5500
5000
2000
2025
2050
2075
2100
Year
Scenario
Historical
RCP2.6
RCP4.5
RCP6.0
RCP8.5

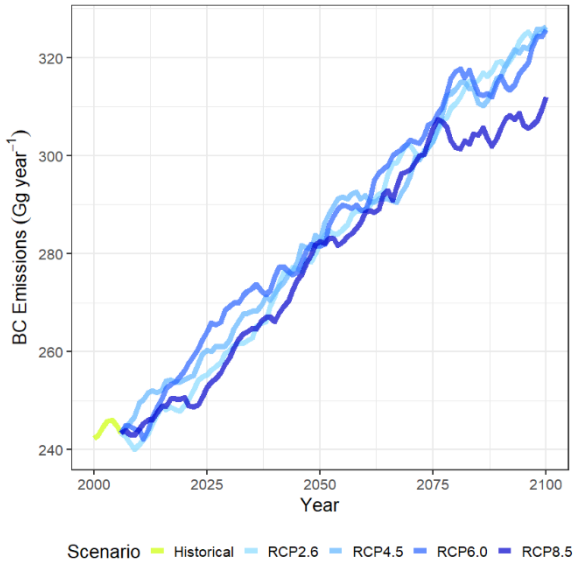
BC Emissions (Gg year^{-1})
320
300
280
260
240
2000
2025
2050
2075
2100
Year
Scenario
Historical
RCP2.6
RCP4.5
RCP6.0
RCP8.5

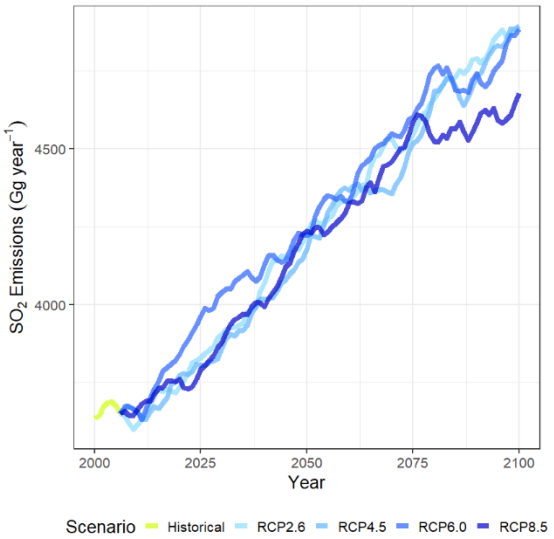
SO2 Emissions (Gg year−1)
4500
4000
2000
2025
2050
2075
2100
Year
Scenario
Historical
RCP2.6
RCP4.5
RCP6.0
RCP8.5

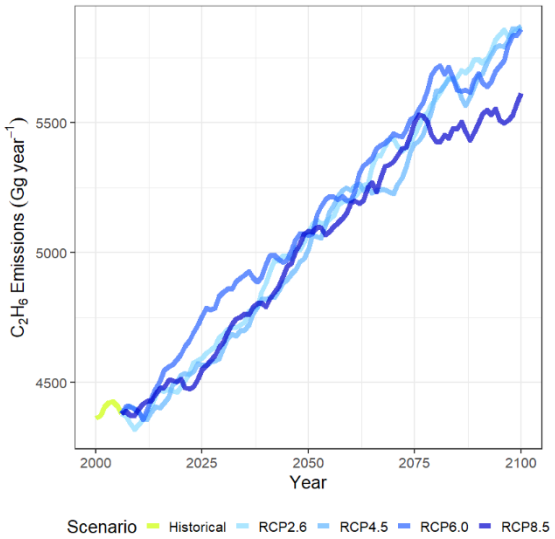
C2H6 Emissions (Gg year−1)
5500
5000
4500
2000
2025
2050
2075
2100
Year
Scenario
Historical
RCP2.6
RCP4.5
RCP6.0
RCP8.5

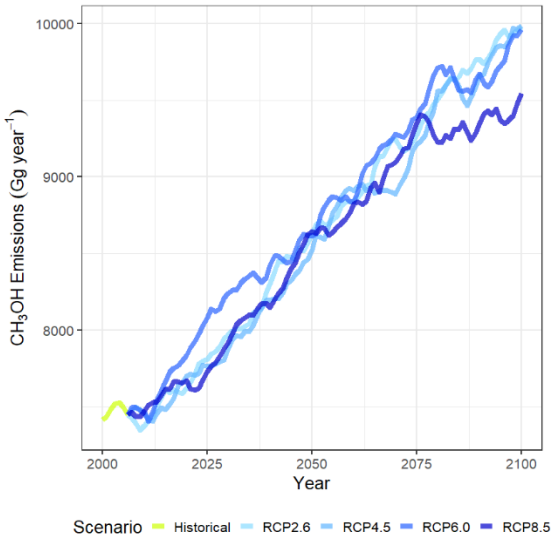
CH3OH Emissions (Gg year−1)
10000
9000
8000
2000
2025
2050
2075
2100
Year
Scenario
Historical
RCP2.6
RCP4.5
RCP6.0
RCP8.5

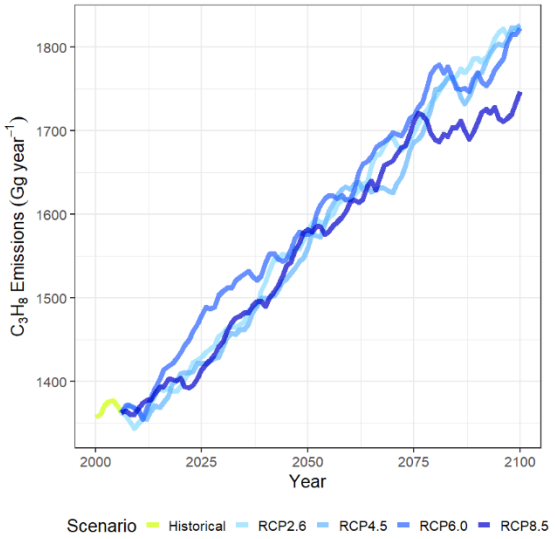
C3H8 Emissions (Gg year−1)
1800
1700
1600
1500
1400
2000
2025
2050
2075
2100
Year
Scenario
Historical
RCP2.6
RCP4.5
RCP6.0
RCP8.5

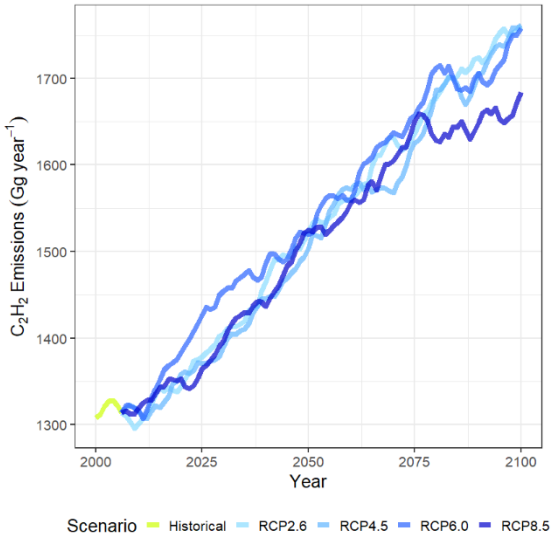
C2H2 Emissions (Gg year−1)
1700
1600
1500
1400
1300
2000
2025
2050
2075
2100
Year
Scenario
Historical
RCP2.6
RCP4.5
RCP6.0
RCP8.5

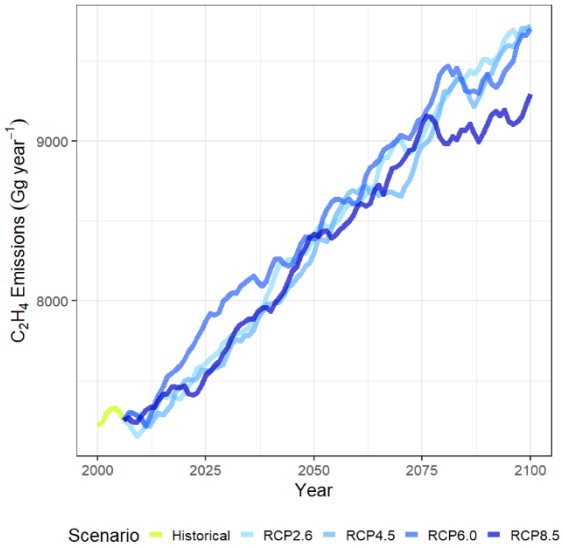
C2H4 Emissions (Gg year−1)
9000
8000
2000
2025
2050
2075
2100
Year
Scenario
Historical
RCP2.6
RCP4.5
RCP6.0
RCP8.5

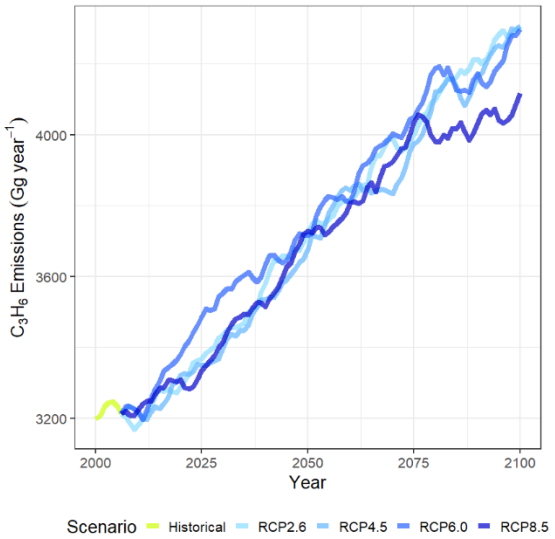
C_3H_6 Emissions (Gg year^{-1})
4000
3600
3200
2000
2025
2050
2075
2100
Year
Scenario Historical RCP2.6 RCP4.5 RCP6.0 RCP8.5

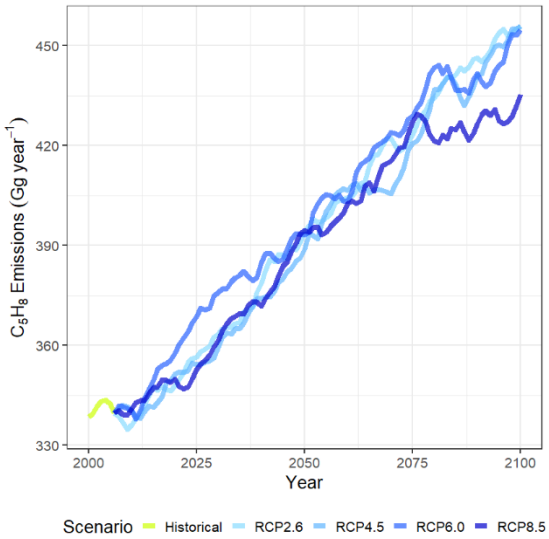
C_5H_8 Emissions (Gg year^{-1})
450
420
390
360
330
2000
2025
2050
2075
2100
Year
Scenario Historical RCP2.6 RCP4.5 RCP6.0 RCP8.5

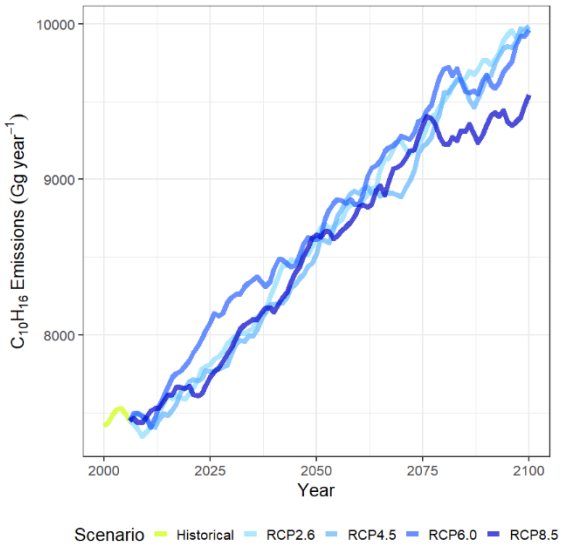
$C_{10}H_{16}$ Emissions (Gg year^{-1})
10000
9000
8000
2000
2025
2050
2075
2100
Year
Scenario Historical RCP2.6 RCP4.5 RCP6.0 RCP8.5

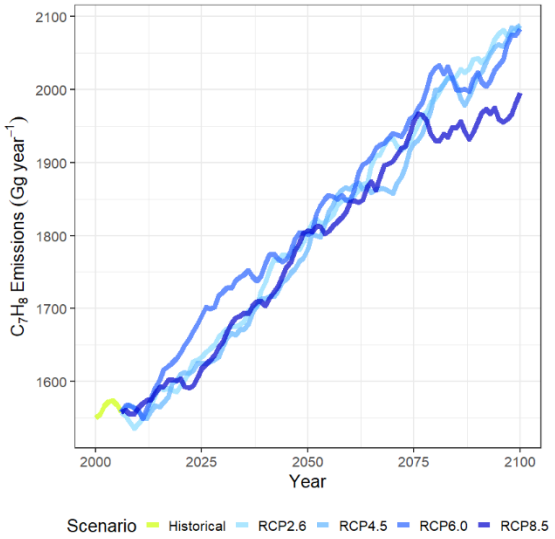
C_7H_8 Emissions (Gg year^{-1})
2100
2000
1900
1800
1700
1600
2000
2025
2050
2075
2100
Year
Scenario Historical RCP2.6 RCP4.5 RCP6.0 RCP8.5

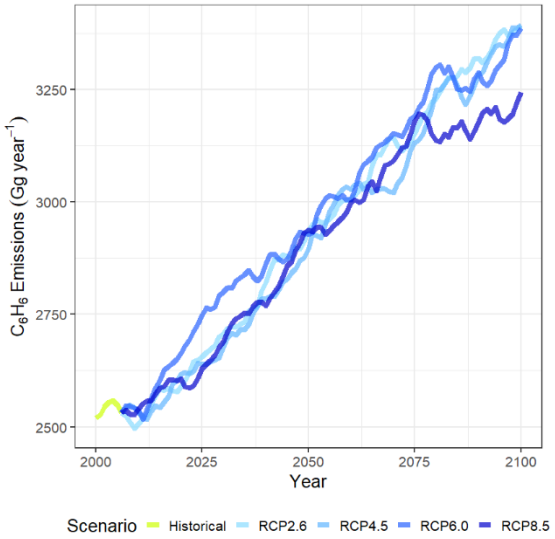
C_6H_6 Emissions (Gg year^{-1})
3250
3000
2750
2500
2000
2025
2050
2075
2100
Year
Scenario Historical RCP2.6 RCP4.5 RCP6.0 RCP8.5

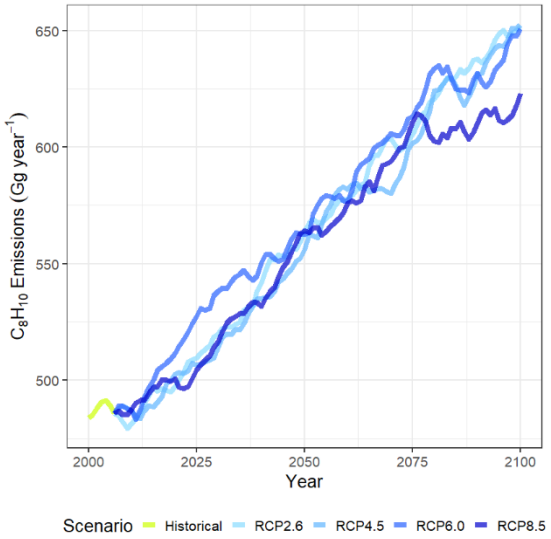
C_8H_{10} Emissions (Gg year^{-1})
650
600
550
500
2000
2025
2050
2075
2100
Year
Scenario Historical RCP2.6 RCP4.5 RCP6.0 RCP8.5

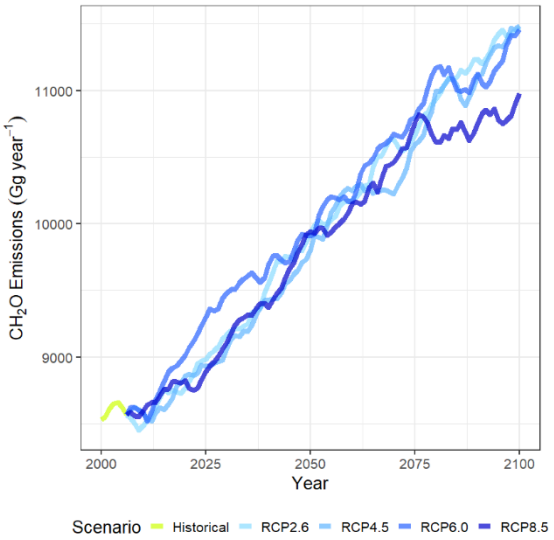
CH_2O Emissions (Gg year^{-1})
11000
10000
9000
2000
2025
2050
2075
2100
Year
Scenario Historical RCP2.6 RCP4.5 RCP6.0 RCP8.5

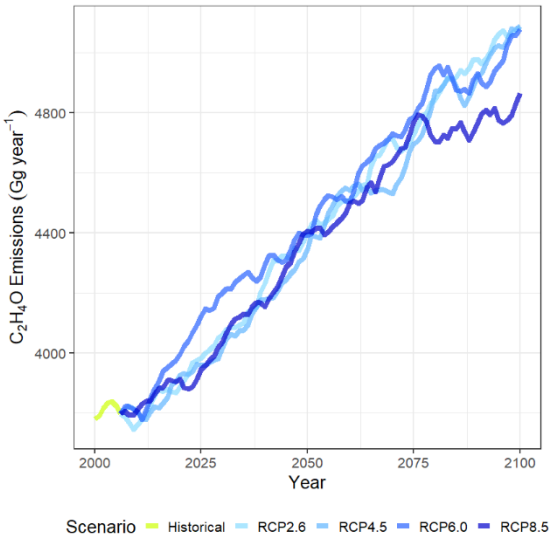
C_2H_4O Emissions (Gg year^{-1})
4800
4400
4000
2000
2025
2050
2075
2100
Year
Scenario Historical RCP2.6 RCP4.5 RCP6.0 RCP8.5

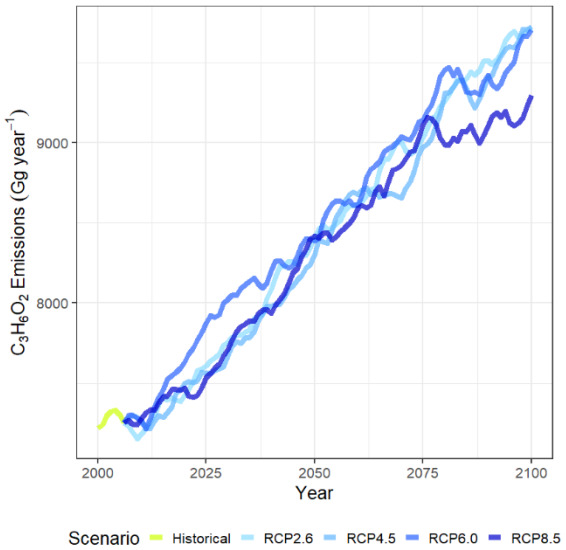
$C_3H_6O_2$ Emissions (Gg year^{-1})
9000
8000
2000
2025
2050
2075
2100
Year
Scenario Historical RCP2.6 RCP4.5 RCP6.0 RCP8.5

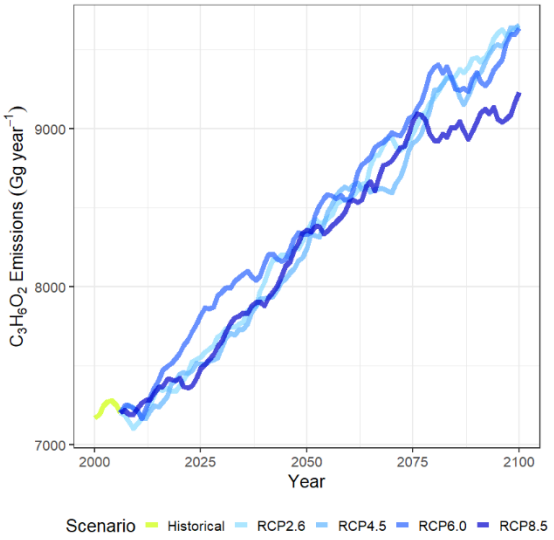
$C_3H_6O_2$ Emissions (Gg year^{-1})
9000
8000
7000
2000
2025
2050
2075
2100
Year
Scenario Historical RCP2.6 RCP4.5 RCP6.0 RCP8.5

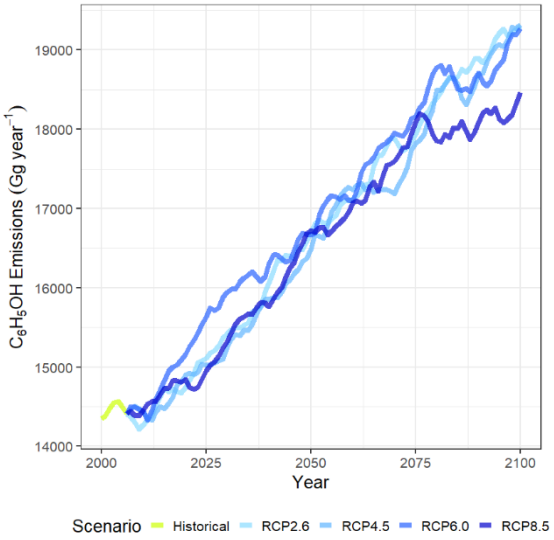
C_6H_5OH Emissions (Gg year^{-1})
19000
18000
17000
16000
15000
14000
2000
2025
2050
2075
2100
Year
Scenario Historical RCP2.6 RCP4.5 RCP6.0 RCP8.5

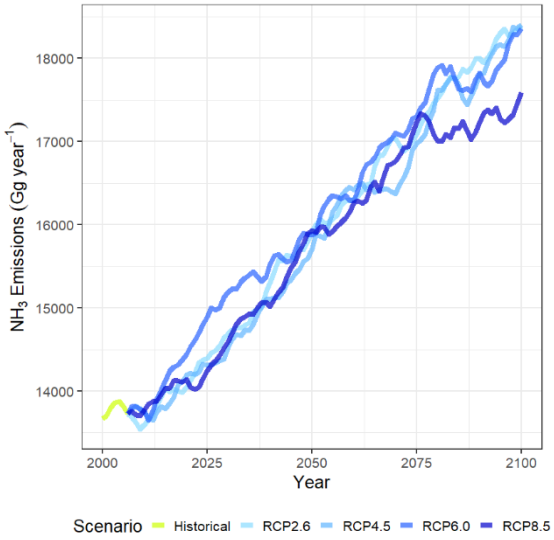
NH_3 Emissions (Gg year^{-1})
18000
17000
16000
15000
14000
2000
2025
2050
2075
2100
Year
Scenario Historical RCP2.6 RCP4.5 RCP6.0 RCP8.5

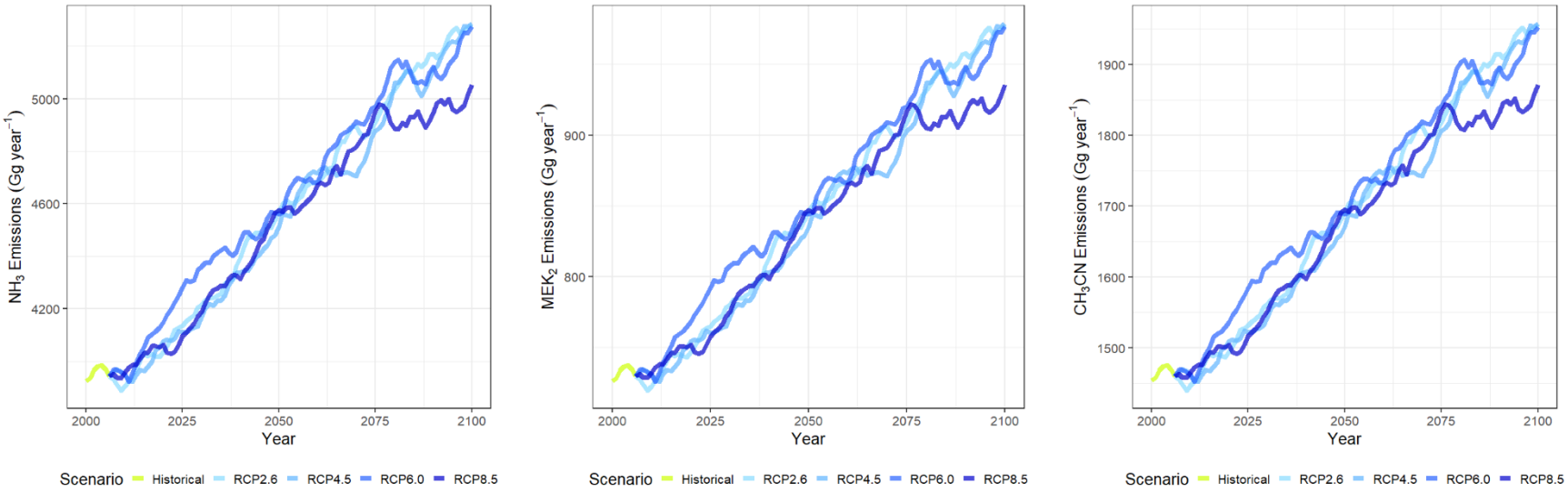

Figure 56. Projected annual emissions of 33 gaseous species from forest fires in Siberia (2000-2100)

4.4. Model uncertainty

We introduced the SPITFIRE fire module into the SEIB-DGVM and achieved a better representation of fire dynamics in Siberia between 1996 and 2100 by creating monthly outputs and producing several new outputs related to fires at a 0.5° spatial resolution, such as vegetation and burned biomass emission variables. Our modifications have led to a more realistic depiction of fire frequency, intensity, and extent, aligning the model outputs more closely with benchmark datasets. The major variables related to fire (vegetation, CO_2 and $PM_{2.5}$ emissions, burned area, burned fraction, aboveground biomass, and dry matter) all reached an agreement of 70.7 % or greater with the observations. Additionally, the improved model accurately simulated forest structure, increasing the agreement between the simulated and observed dataset patterns and further emphasizing the reliability of our model and its emission projections. Under the RCP2.6 scenario, we estimated that the CO_2, CO, $PM_{2.5}$, total particulate matter (TPM), and total particulate carbon (TPC) emissions in Siberia will continue to increase annually until 2100 by an average of 2.71 ± 0.87, 0.22 ± 0.07, 0.04 ± 0.01, 0.03 ± 0.01, and 0.02 ± 0.01 Tg species $year^{-1}$, respectively. Moreover, forest fires in Siberia in 2100 are projected to emit all five of these compounds under the RCP8.5 scenario, amounting to 1010.00 ± 82.64, 80.84 ± 6.61, 13.17 ± 1.08, 9.97 ± 0.82, and 6.91 ± 0.57 Tg, respectively.

Although our research has made significant steps, there are several limitations that require further research. Future studies should minimize the uncertainty of the simulations and achieve better fits with benchmark datasets on fire, vegetation, and emission products. Specific parameter settings need to also be developed to emphasize regional and seasonal differences. Continued improvement in the fire module and consideration of feedback loops will be crucial to continuously enhancing the accuracy of our models. Our work contributes to a more comprehensive understanding of the intricate interactions between fire dynamics, ecosystems, and climate, creating a new path for informed decision-making and broadening the field of biogeochemistry, global elemental cycles, and the importance of accurate vegetation dynamic modeling.

5. CONCLUSIONS AND RECOMMENDATIONS

We introduced the SPITFIRE fire module into the SEIB-DGVM and achieved a better representation of fire dynamics in Siberia between 1996 and 2100 by creating monthly outputs and producing several new outputs related to fires at a 0.5° spatial resolution, such as vegetation and burned biomass emission variables. Our modifications have led to a more realistic depiction of fire frequency, intensity, and extent, aligning the model outputs more closely with benchmark datasets. Compared to the default model, the improved model (SEIB-DGVM SPITFIRE) demonstrates a higher accuracy in simulating the burned fraction, achieving a 75% agreement with the GFED4s data, whereas the default model only shows a 68% agreement. Overall, the major fire-related variables (vegetation, CO_2 and $PM_{2.5}$ emissions, burned area, burned fraction, aboveground biomass, and dry matter) all achieved an average spatial agreement of 70.7% or higher with the observational data. Additionally, the improved model accurately simulated forest structure, increasing the agreement between the simulated and observed dataset patterns and further emphasizing the reliability of our model and its emission projections. Under the RCP2.6 scenario, we estimated that the CO_2, CO, $PM_{2.5}$, total particulate matter (TPM), and total particulate carbon (TPC) emissions in Siberia will continue to increase annually until 2100 by an average of 2.71 ± 0.87, 0.22 ± 0.07, 0.04 ± 0.01, 0.03 ± 0.01, and 0.02 ± 0.01 Tg species $year^{-1}$, respectively. Moreover, forest fires in Siberia in 2100 are projected to emit all five of these compounds under the RCP8.5 scenario, amounting to 1010.00 ± 82.64, 80.84 ± 6.61, 13.17 ± 1.08, 9.97 ± 0.82, and 6.91 ± 0.57 Tg, respectively.

Although our research has made significant steps, there are several limitations that require further research. Future studies should minimize the uncertainty of the simulations and achieve better fits with benchmark datasets on fire, vegetation, and emission products. Specific parameter settings need to also be developed to emphasize regional and seasonal differences. Continued improvement in the fire module and consideration of feedback loops will be crucial to continuously enhancing the accuracy of our models. Our work contributes to a more comprehensive understanding of the intricate interactions between fire dynamics, ecosystems, and climate, creating a new path for informed decision-making and broadening the field of biogeochemistry, global elemental cycles, and the importance of accurate vegetation dynamic modeling.

APPENDIX A

A.1. Input and outputs of the improved SEIB-DGVM

A.1.1. Input

1) Location: Latitude and altitude.
2) Soil (fixed in time): Soil moisture at saturation point, field capacity, matrix potential, wilting point, and albedo.
3) Climatic data (daily): Air temperature, soil temperature, fraction of cloud cover, precipitation, humidity, and wind velocity.
4) Atmospheric Carbon dioxide (CO_2) concentrations
5) Fire ignition factors: population density (GPWv4), and lightning flash rate (LIS/OTD HRFC)

A.1.2. Output

1) Carbon dynamics (daily–yearly): Terrestrial carbon pool (woody biomass, grass biomass, litter, soil organic matter), CO_2 absorption and emission rates.
2) Water dynamics (daily): Soil moisture content (three layers), interception rate, evaporation rate, transpiration rate, interception rate, and runoff rate.
3) Radiation (daily): Albedo from the terrestrial surface.
4) Properties of vegetation (daily–yearly): Vegetation type, dominant plant functional type, leaf area index, tree density, size distribution of trees, age distribution of trees, woody biomass for each tree, and grass biomass per unit area.
5) Disturbances (monthly-yearly): fire fraction, burned area, burned biomass, FDI, complete SPITFIRE variables, and 33 type of burned biomass emissions.

A.2. Processes in the SEIB–DGVM improved fire module, and the approaches used to represent each process

Process	Approach	References
Disturbance	Fire as an empirical function of fuel (litter and aboveground biomass), fuel moisture, and ignition factor (human and lightning caused)	(Thonicke et al., 2001, 2010)
Biogeochemical	Trace gas emissions as an empirical function of the total amount of biomass burning and emission factor of each trace gas species	(Andreae and Merlet, 2001)

A.3. Variables, parameters, and constants in the model's equations

Abbreviation	Description	Unit
TrBE	Tropical broad-leaved evergreen	-
TrBR	Tropical broad-leaved raingreen	-
TeNE	Temperate needle-leaved evergreen	-
TeBE	Temperate broad-leaved evergreen	-
TeBS	Temperate broad-leaved summergreen	-
BoNE	Boreal needle-leaved evergreen	-
BoNS	Boreal needle-leaved summergreen	-
BoBS	Boreal broad-leaved summergreen	-
TeH	Temperate herbaceous (C_3 grass)	-
TrH	Tropical herbaceous (C_4 grass)	-
M3	Probability of each PFTs survival after fire (varying 0.0–1.0)	-
$pool\ w$	The soil water content of each soil layer	mm/day
$Depth$	Depth of each soil layer	meter
Wfi	Field capacity	$m^3\ m^{-3}$
Ab	Area burnt	ha/time unit
A	Grid cell area	ha
ρ_b	Fuel bulk density	$kg\ m^{-3}$

Abbreviation	Description	Unit
FDI	Fire Danger Index (0.0 – 1.0)	-
L_B	Length to breadth ratio for woody and grass PFTs	-
$U_{forward}$	Forward wind speed	m/s
$E(N_{ig})$	Expected number of fire ignition event (sum of population and lightning ignitions)	km^2/time unit
$E(N_{ih})$	Expected number of human-caused fire ignition	km^2/time unit
$E(N_{il})$	Expected number of lightning-caused fire ignition	km^2/time unit
Ip	Ignition parameter: define the power of lightning caused ignition (0.0 – 1.0)	-
ω_o	Relative moisture content	-
NI	Nesterov Index	$^oC^2$
Tmax	Maximum temperature	^oC
Tmin	Minimum temperature	^oC
Tdew	Dew-point temperature	^oC
m_e	Moisture extinction	-
α_{av}	Drying parameters for 1-, 10- and 100-h fuel classes	$^oC^{-2}$
$ROS_{f,\ surface}$	Forward rate of spread of surface fire	m min^{-1}
$ROS_{b,\ surface}$	Backward rate of spread of a surface fire	m min^{-1}
I_R	Reaction intensity	kJ m^{-2} min^{-1}
ξ	Propagating flux ratio	-
ϕ_w	Wind factor	-
P_b	Probability of fire per unit time	Time $unit^{-1}$
ε	Effective heating number	-
Q_{ig}	Heat of pre-ignition	kJ kg^{-1}
t_{fire}	Fire duration	min
$I_{surface}$	Surface fire intensity	kW m^{-1}
SH	Schorch Height	m
F	PFT-parameter in crown scorch equation	-

Abbreviation	Description	Unit
CK	Fraction of crown scorch	-
T_H	Tree height	m
CL	Crown length of woody PFT	m
P_m	Probability of post-fire mortality	-
$P_m(CK)$	Probability of mortality as a result of crown scorching	-
$P_m(\tau)$	Probability of mortality by cambial damage	-
p	Parameter for woody PFTs used in $P_m(CK)$ equation	-
τ_l	Residence time of the fire	min
τ_c	Critical time for cambial damage	min
BT	Bark thickness	cm
par1, par2	Parameters for woody PFTs used in bark thickness calculation	-
DBH	Diameter at breast high	m
$E_{i,j}$	fire emissions of trace gas and aerosol species i and the PFT j	g species m^{-2} s^{-1}
$EF_{i,j}$	PFT-specific emission factor	g species (kg dry matter (DM))$^{-1}$
CE_j	combusted biomass of PFT_j due to the fire	g C m^{-2}
C	unit conversion factor from carbon to dry matter	g C (kg DM)$^{-1}$
D_T	Distance Traveled	m
$U_{forward}$	Forward wind speed	m min^{-1}

Additional equations and variables of the implemented SPITFIRE module are referred to with adjustments to Thonicke *et al.*, (2010) Table A1 and Appendix A-B respectively.

This research was published as

Nurrohman, R. K., Kato, T., Ninomiya, H., Végh, L., Delbart, N., Miyauchi, T., Sato, H., Shiraishi, T., and Hirata, R.: Future projections of Siberian wildfire and aerosol emissions, Biogeosciences, 21, 4195–4227, https://doi.org/10.5194/bg-21-4195-2024, 2024.

ACKNOWLEDGEMENT

In the name of Allah, the Most Gracious, the Most Merciful. Alhamdulillah for the countless blessings and unwavering spirit that have guided me throughout this academic journey.

First, I would like extend my deepest gratitude to Prof. Tomomichi Kato, who provided enormous support for me in my studies at the Terrestrial Ecosystem Modeling Laboratory, Faculty of Agriculture, Hokkaido University. Indeed, I am just an ordinary student who is lucky to be able to continue my Ph.D. study under his supervision. Since I was in Indonesia, due to the limited resources I had, he supported our research preparation process, sending a new personal computer for the model learning process. I am very grateful because it is very useful until now and I hope that I can use it for the research process in the future. During the early days of learning in the lab, he was very patient in teaching me some of the basics code, modeling and related environmental sciences. However, for some things, not everything I asked was easily answered, but he just guided me and asked me to try to find answers myself through all the resources I had. In the beginning, it felt a little hard, but I felt the benefits when we are able to solve our own problems. Since then, I have been able to answer my own questions by searching for many sources of information, on a big thing it is not easy, it takes a long time because the solution is to understand the basics and do trials until you get good results. I learned a lot from him, to be an independent person who is able to solve problems independently. Then conduct short and regular scientific discussions to strengthen and form accurate study results. During the manuscript preparation, he also provided many fundamental inputs. How to write a manuscript for publication in a highly reputable journal and explain the benefits for us as researchers. He is a great researcher who has a strong character and is able to teach many students with many different characters, and I hope I can become a good researcher like him in the future.

I would like to express my gratitude to Prof. Takashi Hirano for the opportunities and guidance that enabled me to successfully complete my studies. During the presentation process at the seminar group, he gave me a lot of useful feedback and comments. Also, I would like to express my sincere gratitude to Prof. Hisashi Sato who developed the SEIB-DGVM program, which I used in this study. We first met at the Japan Geoscience Union (JpGU) event, he gave me some suggestions. In the beginning, I had no idea that he was the developer of the model I used, after finding out, I was like wow! I asked for a group photo with him and with Kato Sensei. It was a memorable meeting for me. He also provided many constructive suggestions and comments during the discussion of research progress in the laboratory, and during the preparation of manuscripts for submission to journals.

I would like to express my special thanks to Hideki Ninomiya, Dr. Lea Végh for the support, insight and suggestions, information during research discussion, and during manuscript preparation for journal publication. Their contributions have been invaluable in the experiments conducted during this research. Also I would like to express my special thanks to Dr. Tatsuya Miyauchi, for the technical support provided, several times helping to solve problems on the server when I was doing simulations. Then, special thanks to Dr. Tomohiro Shiraishi, I first met him during his Ph.D. defense at the Faculty of Agriculture, then he

provided a lot of support for my research process, and they also provided valuable input on manuscripts in preparation for publication in journals. I would like to express my gratitude for all of the co-authors of my manuscript, for the insights given, then have significantly contributed to the refinement of my manuscripts, and I am grateful for the learning experience.

A heartfelt thank you to all of the current and past members of the Laboratory of Terrestrial Ecosystem Modeling. Your friendly welcome, attention, support, and enthusiasm created a fun, enjoyable, and positive learning environment that enhanced my academic experience.

I would also like to thank the Ministry of Education, Culture, Sports, Science and Technology (MEXT) for the scholarship support given to me to pursue my Ph.D. program at Hokkaido University. In addition, I would like extend my gratitude to Assoc. Prof. Bayu Dwi Apri Nugroho for the support from the beginning to continue the Ph.D. program to complete it at this time. Also, I would like extend my gratitude to Mr. Murad, S.P., MP., and Assoc. Prof. Baiq Rien Handayani, for the study permit granted, although administratively it cannot be processed due to existing regulations. To date, they and their staff are still taking care of the administrative process for me regarding this matter in University of Mataram. Hopefully I can contribute to the advancement of science in Indonesia and also globally.

I am grateful to my family for their continuous encouragement throughout my studies at Hokkaido University. Their unwavering support has been an additional source of strength to get through the tough times during the study process.

Lastly, I express my appreciation to everyone, all of my friends who supported and coloured my academic journey at Hokkaido University, Sapporo, Japan.

Hopefully, this thesis will be beneficial to all of the readers.

REFERENCES

Abaimov, A. P. and Sofronov, M. A.: The Main Trends of Post-Fire Succession in Near-Tundra Forests of Central Siberia, 372–386, https://doi.org/10.1007/978-94-015-8737-2_33, 1996.

Abaimov, A. P., Lesinski, J. A., Martinsson, O., and Milyutin, L. I.: Variability and ecology of Siberian larch species, 1998.

Agee, J.K. (1997) 'Fire Ecology of Pacific Northwest Forests', *Electronic Green Journal*, 1(7). Available at: https://doi.org/10.5070/g31710279.

Amiro, B. D., Cantin, A., Flannigan, M. D., and De Groot, W. J.: Future emissions from Canadian boreal forest fires, Can. J. For. Res., 39, 383–395, https://doi.org/10.1139/X08-154, 2009.

Andreae, M.: Emission of trace gases and aerosols from biomass burning. Global Biogeochemical, At. Chem. Phys., 15 (4), 955–966, 2019.

Andreae, M. O. and Merlet, P.: Emission of trace gases and aerosols from biomass burning, 15, 955–966, 2001.

Arakida, H., Kotsuki, S., Otsuka, S., Sawada, Y., and Miyoshi, T.: Regional-scale data assimilation with the Spatially Explicit Individual-based Dynamic Global Vegetation Model (SEIB-DGVM) over Siberia, Prog. Earth Planet. Sci., 8, https://doi.org/10.1186/s40645-021-00443-6, 2021.

Archibald, S., Roy, D.P., van Wilgen, B.W. and Scholes, R.J. (2009) 'What limits fire? An examination of drivers of burnt area in Southern Africa', *Global Change Biology*, 15(3), pp. 613–630. Available at: https://doi.org/10.1111/j.1365-2486.2008.01754.x.

Archibald, S., Lehmann, C. E. R., Gómez-Dans, J. L., and Bradstock, R. A.: Defining pyromes and global syndromes of fire regimes, Proc. Natl. Acad. Sci. U. S. A., 110, 6442–6447, https://doi.org/10.1073/pnas.1211466110, 2013.

Aurell, J., Mitchell, B., Greenwell, D., Holder, A., Tabor, D., Kiros, F., and Gullett, B.: Measuring emission factors from open fires and detonations, AQM 2019 - Air Qual. Meas. Methods Technol. Conf. 2019, 2019.

Bartalev, S. A., Belward, A. S., Erchov, D. V., and Isaev, A. S.: A new SPOT4-VEGETATION derived land cover map of Northern Eurasia, Int. J. Remote Sens., 24, 1977–1982, https://doi.org/10.1080/0143116031000066297, 2003.

Bergeron, Y., Gauthier, S., Flannigan, M., and Kafka, V.: Fire regimes at the transition between mixedwood and coniferous boreal forest in northwestern Quebec, Ecology, 85, 1916–1932, https://doi.org/10.1890/02-0716, 2004.

Bonan, G. B.: Forests and climate change: Forcings, feedbacks, and the climate benefits of forests, Science (80-.)., 320, 1444–1449, https://doi.org/10.1126/science.1155121, 2008.

Bond, T. C., Doherty, S. J., Fahey, D. W., Forster, P. M., Berntsen, T., Deangelo, B. J., Flanner, M. G., Ghan, S., Kärcher, B., Koch, D., Kinne, S., Kondo, Y., Quinn, P. K., Sarofim, M. C., Schultz, M. G., Schulz, M., Venkataraman, C., Zhang, H., Zhang, S., Bellouin, N.,

Guttikunda, S. K., Hopke, P. K., Jacobson, M. Z., Kaiser, J. W., Klimont, Z., Lohmann, U., Schwarz, J. P., Shindell, D., Storelvmo, T., Warren, S. G., and Zender, C. S.: Bounding the role of black carbon in the climate system: A scientific assessment, J. Geophys. Res. Atmos., 118, 5380–5552, https://doi.org/10.1002/jgrd.50171, 2013.

Bowman, D. M. J. S., Balch, J. K., Artaxo, P., Bond, W. J., Carlson, J. M., Cochrane, M. A., D'Antonio, C. M., DeFries, R. S., Doyle, J. C., Harrison, S. P., Johnston, F. H., Keeley, J. E., Krawchuk, M. A., Kull, C. A., Marston, J. B., Moritz, M. A., Prentice, I. C., Roos, C. I., Scott, A. C., Swetnam, T. W., Van Der Werf, G. R., and Pyne, S. J.: Fire in the earth system, Science (80-.)., 324, 481–484, https://doi.org/10.1126/science.1163886, 2009.

Bryukhanov, A. V., Panov, A. V., Ponomarev, E. I., and Sidenko, N. V.: Wildfire Impact on the Main Tree Species of the Near-Yenisei Siberia, Izv. - Atmos. Ocean Phys., 54, 1525–1533, https://doi.org/10.1134/S0001433818110026, 2018.

Burns, R. M. and Honkala, B. H.: Silvics of North America: Volume 2. Hardwoods, Agric. Handb. 654, 2, 877, 1990.

Byram, G.M. (1959) 'Combustion of forest fuels', in K.P. Davis (ed.) *Forest Fire Control and Use*. New York: McGraw-Hill, pp. 61–89. Available at: https://doi.org/10.2307/1932261.

Carnicer, J., Alegria, A., Giannakopoulos, C., Di Giuseppe, F., Karali, A., Koutsias, N., Lionello, P., Parrington, M., and Vitolo, C.: Global warming is shifting the relationships between fire weather and realized fire-induced CO2 emissions in Europe, Sci. Rep., 12, 8–13, https://doi.org/10.1038/s41598-022-14480-8, 2022.

Cecil and Daniel, J.: LIS/OTD 0.5 Degree High Resolution Full Climatology (HRFC) V2.3.2015, https://doi.org/http://dx.doi.org/10.5067/LIS/LIS-OTD/DATA302, 2001.

Chapin, F. S., Sturm, M., Serreze, M. C., McFadden, J. P., Key, J. R., Lloyd, A. H., McGuire, A. D., Rupp, T. S., Lynch, A. H., Schimel, J. P., Beringer, J., Chapman, W. L., Epstein, H. E., Euskirchen, E. S., Hinzman, L. D., Jia, G., Ping, C. L., Tape, K. D., Thompson, C. D. C., Walker, D. A., and Welker, J. M.: Role of Land-Surface Changes in Arctic Summer Warming, Sci. Reports, 657, https://doi.org/10.1126/science.1117368, 2005.

Chapin, F. S., Woodwell, G. M., Randerson, J. T., Rastetter, E. B., Lovett, G. M., Baldocchi, D. D., Clark, D. A., Harmon, M. E., Schimel, D. S., Valentini, R., Wirth, C., Aber, J. D., Cole, J. J., Goulden, M. L., Harden, J. W., Heimann, M., Howarth, R. W., Matson, P. A., McGuire, A. D., Melillo, J. M., Mooney, H. A., Neff, J. C., Houghton, R. A., Pace, M. L., Ryan, M. G., Running, S. W., Sala, O. E., Schlesinger, W. H., and Schulze, E. D.: Reconciling carbon-cycle concepts, terminology, and methods, Ecosystems, 9, 1041–1050, https://doi.org/10.1007/s10021-005-0105-7, 2006.

Christian, T. J., Kleiss, B., Yokelson, R. J., Holzinger, R., Crutzen, P. J., Hao, W. M., Saharjo, B. H., and Ward, D. E.: Comprehensive laboratory measurements of biomass-burning emissions: 1. Emissions from Indonesian, African, and other fuels, J. Geophys. Res. Atmos., 108, https://doi.org/10.1029/2003jd003704, 2003.

Chylek, P., Folland, C., Klett, J. D., Wang, M., Hengartner, N., Lesins, G., and Dubey, M. K.: Annual Mean Arctic Amplification 1970–2020: Observed and Simulated by CMIP6 Climate Models, Geophys. Res. Lett., 49, 1–8, https://doi.org/10.1029/2022GL099371, 2022.

CIESIN: Gridded Population of the World, Version 4.11 (GPWv4): Population Count, Revision 11, https://doi.org/https://doi.org/10.7927/H4JW8BX5, 2018.

Clark, J. S. and Richard, P. J. H.: The Role of Paleofire in Boreal and Other Cool-Coniferous Forests, 65–89, https://doi.org/10.1007/978-94-015-8737-2_5, 1996.

Cleve, K. V. and Viereck, L. A.: Forest Succession in Relation to Nutrient Cycling in the Boreal Forest of Alaska, 185–211, https://doi.org/10.1007/978-1-4612-5950-3_13, 1981.

Cochrane, M. A.: Fire science for rainforests, Nature, 421, 913–919, https://doi.org/10.1038/nature01437, 2003.

Cramer, W., Bondeau, A., Woodward, F. I., Prentice, I. C., Betts, R. A., Brovkin, V., Cox, P. M., Fisher, V., Foley, J. A., Friend, A. D., Kucharik, C., Lomas, M. R., Ramankutty, N., Sitch, S., Smith, B., White, A., and Young-Molling, C.: Global response of terrestrial ecosystem structure and function to CO2 and climate change: Results from six dynamic global vegetation models, Glob. Chang. Biol., 7, 357–373, https://doi.org/10.1046/j.1365-2486.2001.00383.x, 2001.

Crutzen, P. J. and Goldammer, J. G.: Fire in the Environment The Ecological, Atmospheric, and Climatic Importance of Vegetation Fires, High Throughput Screen., 573–577, https://doi.org/10.1201/9781482269802-30, 1993.

Dickinson, M. B. and Johnson, E. A.: Fire Effects on Trees, in: Forest Fires, 477–525, https://doi.org/10.1016/b978-012386660-8/50016-7, 2001.

Dixon, A. R. K., Brown, S., Houghton, R. A., Solomon, A. M., and Trexler, M. C.: Carbon Pools and Flux of Global Forest Ecosystems Published by : American Association for the Advancement of Science Stable URL : http://www.jstor.org/stable/2882371, Adv. Sci., 263, 185–190, 1994.

Fisher, J. B., Huntzinger, D. N., Schwalm, C. R., and Sitch, S.: Modeling the terrestrial biosphere, Annu. Rev. Environ. Resour., 39, 91–123, https://doi.org/10.1146/annurev-environ-012913-093456, 2014.

Flannigan, M., Stocks, B., Turetsky, M., and Wotton, M.: Impacts of climate change on fire activity and fire management in the circumboreal forest, Glob. Chang. Biol., 15, 549–560, https://doi.org/10.1111/j.1365-2486.2008.01660.x, 2009.

Flannigan, M. D., Wotton, B. M., Marshall, G. A., Groot, W. J. de, Johnston, J., Jurko, N., and Cantin, A. S.: Fuel moisture sensitivity to temperature and precipitation: climate change implications, Clim. Change, 59–71, https://doi.org/10.1007/s10584-015-1521-0, 2016.

Foley, J. A.: Tipping Points in the Tundra, 310, 627–628, 2005.

Forster, P., V. Ramaswamy, P. Artaxo, T. Berntsen, R. Betts, D.W. Fahey, J. Haywood, J. Lean, D.C. Lowe, G. Myhre, J. Nganga, R. Prinn, G. Raga, M. Schulz, and R. Van Dorland: Changes in Atmospheric Constituents and in Radiative Forcing, Cancer Biol. Med., 15, 228–237, https://doi.org/10.20892/j.issn.2095-3941.2017.0150, 2018.

Frank, D., Reichstein, M., Bahn, M., Thonicke, K., Frank, D., Mahecha, M. D., Smith, P., van der Velde, M., Vicca, S., Babst, F., Beer, C., Buchmann, N., Canadell, J. G., Ciais, P., Cramer,

W., Ibrom, A., Miglietta, F., Poulter, B., Rammig, A., Seneviratne, S. I., Walz, A., Wattenbach, M., Zavala, M. A., and Zscheischler, J.: Effects of climate extremes on the terrestrial carbon cycle: Concepts, processes and potential future impacts, Glob. Chang. Biol., 21, 2861–2880, https://doi.org/10.1111/gcb.12916, 2015.

Freeborn, P. H., Wooster, M. J., Hao, W. M., Ryan, C. A., Nordgren, B. L., Baker, S. P., and Ichoku, C.: Relationships between energy release, fuel mass loss, and trace gas an aerosol emissions during laboratory biomass fires, J. Geophys. Res. Atmos., 113, 1–17, https://doi.org/10.1029/2007JD008679, 2008.

Friedlingstein, P., O'Sullivan, M., Jones, M., Andrew, R., Hauck, J., Olsen, A., Peters, G., Peters, W., Pongratz, J., Sitch, S., Le Quéré, C., Canadell, J., Ciais, P., Jackson, R., Alin, S., Aragão, L., Arneth, A., Arora, V., Bates, N., Becker, M., Benoit-Cattin, A., Bittig, H., Bopp, L., Bultan, S., Chandra, N., Chevallier, F., Chini, L., Evans, W., Florentie, L., Forster, P., Gasser, T., Gehlen, M., Gilfillan, D., Gkritzalis, T., Gregor, L., Gruber, N., Harris, I., Hartung, K., Haverd, V., Houghton, R., Ilyina, T., Jain, A., Joetzjer, E., Kadono, K., Kato, E., Kitidis, V., Korsbakken, J. I., Landschützer, P., Lefèvre, N., Lenton, A., Lienert, S., Liu, Z., Lombardozzi, D., Marland, G., Metzl, N., Munro, D., Nabel, J., Nakaoka, S.-I., Niwa, Y., O'Brien, K., Ono, T., Palmer, P., Pierrot, D., Poulter, B., Resplandy, L., Robertson, E., Rödenbeck, C., Schwinger, J., Séférian, R., Skjelvan, I., Smith, A., Sutton, A., Tanhua, T., Tans, P., Tian, H., Tilbrook, B., van der Werf, G., Vuichard, N., Walker, A., Wanninkhof, R., Watson, A., Willis, D., Wiltshire, A., Yuan, W., Yue, X., and Zaehle, S.: Global Carbon Budget 2020, Earth Syst. Sci. Data Discuss., 1–3, https://doi.org/10.5194/essd-2020-286, 2020.

Galanter, M., Levy II, H., and Carmichael, G. R.: Impact of biomass burning of tropospheric CO, NOx, and O3, https://doi.org/https://doi.org/10.1029/1999JD901113, 2000.

Gauthier, S., Bernier, P., Kuuluvainen, T., Shvidenko, A. Z., and Schepaschenko, D. G.: Boreal forest health and global change, Science (80-.)., 349, 819–822, https://doi.org/10.1126/science.aaa9092, 2015.

Giglio, L., Randerson, J. T., and Van Der Werf, G. R.: Analysis of daily, monthly, and annual burned area using the fourth-generation global fire emissions database (GFED4), J. Geophys. Res. Biogeosciences, 118, 317–328, https://doi.org/10.1002/jgrg.20042, 2013.

Goldammer, J. G. and Furyaev, V. V: Fire in ecosystems of boreal Eurasia, Fire Ecosyst. boreal Eurasia, 1–2, 1996.

Greene, D. F. and Johnson, E. A.: Modelling recruitment of *Populus tremuloides*, *Pinus banksiana*, and *Picea mariana* following fire in the mixedwood boreal forest, Can. J. For. Res., 29, 462–473, https://doi.org/10.1139/cjfr-29-4-462, 1999.

De Groot, W. J., Cantin, A. S., Flannigan, M. D., Soja, A. J., Gowman, L. M., and Newbery, A.: A comparison of Canadian and Russian boreal forest fire regimes, For. Ecol. Manage., 294, 23–34, https://doi.org/10.1016/j.foreco.2012.07.033, 2013.

Gutierrez, A. A., Hantson, S., Langenbrunner, B., Chen, B., Jin, Y., Goulden, M. L., and Randerson, J. T.: Wildfire response to changing daily temperature extremes in California's Sierra Nevada, Sci. Adv., 7, 1–11, https://doi.org/10.1126/sciadv.abe6417, 2021.

Haider, W., Knowler, D., Trenholm, R., Moore, J., Bradshaw, P., and Lertzman, K.: Climate change, increasing forest fire incidence, and the value of visibility: Evidence from British Columbia, Canada, Can. J. For. Res., 49, 1242–1255, https://doi.org/10.1139/cjfr-2018-0309, 2019.

Hantemirov, R. M., Corona, C., Guillet, S., Shiyatov, S. G., Stoffel, M., Osborn, T. J., Melvin, T. M., Gorlanova, L. A., Kukarskih, V. V., Surkov, A. Y., von Arx, G., and Fonti, P.: Current Siberian heating is unprecedented during the past seven millennia, Nat. Commun., 13, 1–8, https://doi.org/10.1038/s41467-022-32629-x, 2022.

Hantson, S., Arneth, A., Harrison, S. P., Kelley, D. I., Colin Prentice, I., Rabin, S. S., Archibald, S., Mouillot, F., Arnold, S. R., Artaxo, P., Bachelet, D., Ciais, P., Forrest, M., Friedlingstein, P., Hickler, T., Kaplan, J. O., Kloster, S., Knorr, W., Lasslop, G., Li, F., Mangeon, S., Melton, J. R., Meyn, A., Sitch, S., Spessa, A., Van Der Werf, G. R., Voulgarakis, A., and Yue, C.: The status and challenge of global fire modelling, Biogeosciences, 13, 3359–3375, https://doi.org/10.5194/bg-13-3359-2016, 2016.

Heĺy, C., Flannigan, M., and Bergeron, Y.: Modeling tree mortality following wildfire in the southeastern Canadian mixed-wood boreal forest, For. Sci., 49, 566–576, 2003.

Hély, C., Bergeron, Y., and Flannigan, M. D.: Effects of stand composition on fire hazard in mixed-wood Canadian boreal forest, J. Veg. Sci., 11, 813–824, https://doi.org/10.2307/3236551, 2000.

Hessilt, T. D., Werf, G. Van Der, Abatzoglou, J. T., and Scholten, R. C.: Future increases in lightning-ignited boreal fires from conjunct increases in dry fuels and lightning, Proc. 23rd EGU Gen. Assem., 2021.

Hicke, J. A., Asner, G. P., Kasischke, E. S., French, N. H. F., Randerson, J. T., Collatz, G. J., Stocks, B. J., Tucker, C. J., Los, S. O., and Field, C. B.: Postfire response of North American boreal forest net primary productivity analyzed with satellite observations, Glob. Chang. Biol., 9, 1145–1157, https://doi.org/10.1046/j.1365-2486.2003.00658.x, 2003.

Ichoku, C., Giglio, L., Wooster, M. J., and Remer, L. A.: Global characterization of biomass-burning patterns using satellite measurements of fire radiative energy, Remote Sens. Environ., 112, 2950–2962, https://doi.org/10.1016/j.rse.2008.02.009, 2008.

IFFN: The Current Fire Situation in the Russian Federation : Implications for Enhancing International and Regional Cooperation in the UN Framework and the Global Programs on Fire Monitoring and Assessment, International Forest Fire News (IFFN), 89–111 pp., 2003.

IPCC: Climate Change 2014, 259–264 pp., 2014.

IPCC: Climate Change 2021, Phys. Sci. Basis. Contrib. Work. Gr. 1 to Sixth Assess. Rep. Intergov. Panel Clim. Chang., In Press, 2021.

Ito, A.: Mega fire emissions in Siberia: Potential supply of bioavailable iron from forests to the ocean, Biogeosciences, 8, 1679–1697, https://doi.org/10.5194/bg-8-1679-2011, 2011.

Ivanova, G.A. and Ivanov, V.A. (2005) ‘Fire Regimes in Siberian Forests’, *International Forest Fire News (IFFN)*, 32(1), pp. 67–69.

Ivanov, V., Milyaev, I., Konstantinov, A., and Loiko, S.: Land-Use Changes on Ob River

Floodplain (Western Siberia, Russia) in Context of Natural and Social Changes over Past 200 Years, Land, 11, https://doi.org/10.3390/land11122258, 2022.

Jacobson, T. A., Kler, J. S., Hernke, M. T., Braun, R. K., Meyer, K. C., and Funk, W. E.: Direct human health risks of increased atmospheric carbon dioxide, Nat. Sustain., 2, 691–701, https://doi.org/10.1038/s41893-019-0323-1, 2019.

Johnson, M. S., Strawbridge, K., Knowland, K. E., Keller, C., and Travis, M.: Long-range transport of Siberian biomass burning emissions to North America during FIREX-AQ, Atmos. Environ., 252, https://doi.org/10.1016/j.atmosenv.2021.118241, 2021.

Jones, P.W. (1999) 'First- and second-order conservative remapping schemes for grids in spherical coordinates', *Monthly Weather Review*, 127(9), pp. 2204–2210. Available at: https://doi.org/10.1175/1520-0493(1999)127<2204:FASOCR>2.0.CO;2.

Kaiser, J. W., Heil, A., Andreae, M. O., Benedetti, A., Chubarova, N., Jones, L., Morcrette, J. J., Razinger, M., Schultz, M. G., Suttie, M., and Van Der Werf, G. R.: Biomass burning emissions estimated with a global fire assimilation system based on observed fire radiative power, Biogeosciences, 9, 527–554, https://doi.org/10.5194/bg-9-527-2012, 2012.

Kantzas, E., Lomas, M., and Quegan, S.: Fire at high latitudes: Data-model comparisons and their consequences, Global Biogeochem. Cycles, 27, 677–691, https://doi.org/10.1002/gbc.20059, 2013.

Kasischke, E. S.: Boreal Ecosystems in the Global Carbon Cycle, 19–30, https://doi.org/10.1007/978-0-387-21629-4_2, 2000.

Kasischke, E. S. and Bruhwiler, L. P.: Emissions of carbon dioxide, carbon monoxide, and methane from boreal forest fires in 1998, J. Geophys. Res. Atmos., 108, https://doi.org/10.1029/2001jd000461, 2003.

Kasischke, E. S., Christensen, N. L., and Stocks, B. J.: Fire, global warming, and the carbon balance of boreal forests, Ecol. Appl., 5, 437–451, https://doi.org/10.2307/1942034, 1995.

Keane, R. E., Arno, S. F., and Brown, J. K.: Simulating Cumulative Fire Effects in Ponderosa Pine / Douglas-Fir Forests Author (s): Robert E . Keane , Stephen F . Arno , James K . Brown Published by : Ecological Society of America Stable URL : http://www.jstor.org/stable/1940259 . SIMULATING CUMUL, America (NY)., 71, 189–203, 1990.

Kharuk, V. I., Ranson, K. J., Dvinskaya, M. L., and Im, S. T.: Wildfires in northern Siberian larch dominated communities, Environ. Res. Lett., 6, https://doi.org/10.1088/1748-9326/6/4/045208, 2011.

Kharuk, V. I., Mariya, L. D., Ilya, A. P., Sergei, T. I., and Kenneth, J. R.: Larch Forests of Middle Siberia: Long-Term Trends in Fire Return Intervals, Reg. Environ. Chang., 16, 2389–2397, https://doi.org/doi:10.1007/s10113-016-0964-9, 2016.

Kharuk, V. I., Ponomarev, E. I., Ivanova, G. A., Dvinskaya, M. L., Coogan, S. C. P., and Flannigan, M. D.: Wildfires in the Siberian taiga, Ambio, 50, 1953–1974, https://doi.org/10.1007/s13280-020-01490-x, 2021.

Kharuk, V. I., Dvinskaya, M. L., Im, S. T., Golyukov, A. S., and Smith, K. T.: Wildfires in the

Siberian Arctic, Fire, 5, 1–16, https://doi.org/10.3390/fire5040106, 2022.

Kimball, B. A. and Idso, S. B.: Increasing atmospheric CO2: effects on crop yield, water use and climate, Agric. Water Manag., 7, 55–72, https://doi.org/10.1016/0378-3774(83)90075-6, 1983.

Knorr, W., Kaminski, T., Arneth, A. and Weber, U. (2014) 'Impact of human population density on fire frequency at the global scale', *Biogeosciences*, 11(4), pp. 1085–1102. Available at: https://doi.org/10.5194/bg-11-1085-2014.

Krawchuk, M. A., Cumming, S. G., and Flannigan, M. D.: Predicted changes in fire weather suggest increases in lightning fire initiation and future area burned in the mixedwood boreal forest, Clim. Change, 83–97, https://doi.org/10.1007/s10584-008-9460-7, 2009.

Krylov, A., McCarty, J. L., Potapov, P., Loboda, T., Tyukavina, A., Turubanova, S., and Hansen, M. C.: Remote sensing estimates of stand-replacement fires in Russia, 2002-2011, Environ. Res. Lett., 9, https://doi.org/10.1088/1748-9326/9/10/105007, 2014.

Kukavskaya, E. A., Soja, A. J., Petkov, A. P., Ponomarev, E. I., Ivanova, G. A., and Conard, S. G.: Fire emissions estimates in siberia: Evaluation of uncertainties in area burned, land cover, and fuel consumption, Can. J. For. Res., 43, 493–506, https://doi.org/10.1139/cjfr-2012-0367, 2013.

Landrum, L. and Holland, M. M.: Extremes become routine in an emerging new Arctic, Nat. Clim. Chang., 10, 1108–1115, https://doi.org/10.1038/s41558-020-0892-z, 2020.

Latham, D. and Schlieter, J. (1989) 'Ignition probabilities of wildland fuels based on simulated lightning discharges', *United States Department of Agriculture, Forest Service*, (Research Paper INT-411), p. 16. Available at: http://www.firemodels.org/downloads/behaveplus/publications/Latham_and_Schlieter_INT-411_1989_ocr.pdf.

Latham, D. and Williams, E. (2001) 'Lightning and Forest Fires', *Monthly Weather Review*, 51(11), pp. 566–567. Available at: https://doi.org/10.1175/1520-0493(1923)51<566:laffic>2.0.co;2.

Lee, J.-Y., J. Marotzke, G. Bala, L. Cao, S. Corti, J.P. Dunne, F. Engelbrecht, E. Fischer, J.C. Fyfe, C. Jones, A. Maycock, J. Mutemi, O. Ndiaye, S. Panickal, and T. Zhou: Future Global Climate: Scenario-based Projections and Near-term Information, 553–672 pp., https://doi.org/10.1017/9781009157896.006, 2021.

Li, F., Val Martin, M., Andreae, M. O., Arneth, A., Hantson, S., Kaiser, J. W., Lasslop, G., Yue, C., Bachelet, D., Forrest, M., Kluzek, E., Liu, X., Mangeon, S., Melton, J. R., Ward, D. S., Darmenov, A., Hickler, T., Ichoku, C., Magi, B. I., Sitch, S., Van Der Werf, G. R., Wiedinmyer, C., and Rabin, S. S.: Historical (1700-2012) global multi-model estimates of the fire emissions from the Fire Modeling Intercomparison Project (FireMIP), Atmos. Chem. Phys., 19, 12545–12567, https://doi.org/10.5194/acp-19-12545-2019, 2019.

Lin, N. H., Tsay, S. C., Maring, H. B., Yen, M. C., Sheu, G. R., Wang, S. H., Chi, K. H., Chuang, M. T., Ou-Yang, C. F., Fu, J. S., Reid, J. S., Lee, C. Te, Wang, L. C., Wang, J. L., Hsu, C. N., Sayer, A. M., Holben, B. N., Chu, Y. C., Nguyen, X. A., Sopajaree, K., Chen, S. J., Cheng, M. T., Tsuang, B. J., Tsai, C. J., Peng, C. M., Schnell, R. C., Conway, T., Chang, C. T.,

Lin, K. S., Tsai, Y. I., Lee, W. J., Chang, S. C., Liu, J. J., Chiang, W. L., Huang, S. J., Lin, T. H., and Liu, G. R.: An overview of regional experiments on biomass burning aerosols and related pollutants in Southeast Asia: From BASE-ASIA and the Dongsha Experiment to 7-SEAS, Atmos. Environ., 78, 1–19, https://doi.org/10.1016/j.atmosenv.2013.04.066, 2013.

Liousse, C., Guillaume, B., Grégoire, J. M., Mallet, M., Galy, C., Pont, V., Akpo, A., Bedou, M., Castéra, P., Dungall, L., Gardrat, E., Granier, C., Konaré, A., Malavelle, F., Mariscal, A., Mieville, A., Rosset, R., Serça, D., Solmon, F., Tummon, F., Assamoi, E., Yoboué, V., and Van Velthoven, P.: Updated African biomass burning emission inventories in the framework of the AMMA-IDAF program, with an evaluation of combustion aerosols, Atmos. Chem. Phys., 10, 9631–9646, https://doi.org/10.5194/acp-10-9631-2010, 2010.

Lobert, J. M., Scharffe, D. H., Hao, W. M., Kuhlbusch, T. A., Seuwen, R., Warneck, P., and Crutzen, P. J.: Experimental Evaluation of Biomass Burning Emissions: Nitrogen and Carbon Containing Compounds, Glob. Biomass Burn. Atmos. Clim. Biosph. Implic., 289–304, https://doi.org/10.7551/mitpress/3286.003.0041, 1991.

Marlon, J. R., Bartlein, P. J., Carcaillet, C., Gavin, D. G., Harrison, S. P., Higuera, P. E., Joos, F., Power, M. J., and Prentice, I. C.: Climate and human influences on global biomass burning over the past two millennia, Nat. Geosci., 1, 697–702, https://doi.org/10.1038/ngeo313, 2008.

Meehl, G. A., T.F., S., W.D., C., P., F., A.T., G., J.M., G., A., K., R., K., J.M., M., A., N., S.C.B., R., I.G., W., A.J., W., and Zhao, Z.-C.: Global Climate Projections, Glob. Clim. Proj. Clim. Chang. 2007 Phys. Sci. Basis, 2007.

Meigs, G. W., Campbell, J. L., Zald, H. S. J., Bailey, J. D., Shaw, D. C., and Kennedy, R. E.: Does wildfire likelihood increase following insect outbreaks in conifer forests?, Ecosphere, 6, 1–24, https://doi.org/10.1890/ES15-00037.1, 2015.

Meigs, G. W., Zald, H. S. J., Campbell, J. L., Keeton, W. S., and Kennedy, R. E.: Do insect outbreaks reduce the severity of subsequent forest fires?, Environ. Res. Lett., 11, https://doi.org/10.1088/1748-9326/11/4/045008, 2016.

Melillo, J. M., A. David, M., David, W. K., Berrien M. I., Charles J. V., and Annette L. S.: Global climate change and terrestrial net primary production, Nature, 8, 312, https://doi.org/10.2307/2800863, 1993.

Miesner, T., Herzschuh, U., Pestryakova, L. A., Wieczorek, M., Zakharov, E. S., Kolmogorov, A. I., Davydova, P. V., and Kruse, S.: Forest structure and individual tree inventories of northeastern Siberia along climatic gradients, Earth Syst. Sci. Data, 14, 5695–5716, https://doi.org/10.5194/essd-14-5695-2022, 2022.

Miller, C. and Urban, D. L.: Interactions between forest heterogeneity and surface fire regimes in the southern Sierra Nevada, Can. J. For. Res., 29, 202–212, https://doi.org/10.1139/x98-188, 1999.

Morton, D. C., Defries, R. S., Randerson, J. T., Giglio, L., Schroeder, W., and van der Werf, G. R.: Agricultural intensification increases deforestation fire activity in Amazonia, Glob. Chang. Biol., 14, 2262–2275, https://doi.org/10.1111/j.1365-2486.2008.01652.x, 2008.

Mouillot, F., Schultz, M. G., Yue, C., Cadule, P., Tansey, K., Ciais, P., and Chuvieco, E.: Ten years of global burned area products from spaceborne remote sensing-A review: Analysis of

user needs and recommendations for future developments, Int. J. Appl. Earth Obs. Geoinf., 26, 64–79, https://doi.org/10.1016/j.jag.2013.05.014, 2014.

Natali, S. M., Watts, J. D., Rogers, B. M., Potter, S., Ludwig, S. M., Selbmann, A. K., Sullivan, P. F., Abbott, B. W., Arndt, K. A., Birch, L., Björkman, M. P., Bloom, A. A., Celis, G., Christensen, T. R., Christiansen, C. T., Commane, R., Cooper, E. J., Crill, P., Czimczik, C., Davydov, S., Du, J., Egan, J. E., Elberling, B., Euskirchen, E. S., Friborg, T., Genet, H., Göckede, M., Goodrich, J. P., Grogan, P., Helbig, M., Jafarov, E. E., Jastrow, J. D., Kalhori, A. A. M., Kim, Y., Kimball, J. S., Kutzbach, L., Lara, M. J., Larsen, K. S., Lee, B. Y., Liu, Z., Loranty, M. M., Lund, M., Lupascu, M., Madani, N., Malhotra, A., Matamala, R., McFarland, J., McGuire, A. D., Michelsen, A., Minions, C., Oechel, W. C., Olefeldt, D., Parmentier, F. J. W., Pirk, N., Poulter, B., Quinton, W., Rezanezhad, F., Risk, D., Sachs, T., Schaefer, K., Schmidt, N. M., Schuur, E. A. G., Semenchuk, P. R., Shaver, G., Sonnentag, O., Starr, G., Treat, C. C., Waldrop, M. P., Wang, Y., Welker, J., Wille, C., Xu, X., Zhang, Z., Zhuang, Q., and Zona, D.: Large loss of CO2 in winter observed across the northern permafrost region, Nat. Clim. Chang., 9, 852–857, https://doi.org/10.1038/s41558-019-0592-8, 2019.

Neto, T. G. S., Carvalho, J. A., Veras, C. A. G., Alvarado, E. C., Gielow, R., Lincoln, E. N., Christian, T. J., Yokelson, R. J., and Santos, J. C.: Biomass consumption and CO2, CO and main hydrocarbon gas emissions in an Amazonian forest clearing fire, Atmos. Environ., 43, 438–446, https://doi.org/10.1016/j.atmosenv.2008.07.063, 2009.

Nguyen, H. M. and Wooster, M. J.: Advances in the estimation of high Spatio-temporal resolution pan-African top-down biomass burning emissions made using geostationary fire radiative power (FRP) and MAIAC aerosol optical depth (AOD) data, https://doi.org/10.1016/j.rse.2020.111971, 2020.

Ninomiya, H., Kato, T., Végh, L., and Wu, L.: Modeling of non-structural carbohydrate dynamics by the spatially explicitly individual-based dynamic global vegetation model SEIB-DGVM (SEIB-DGVM-NSC ver1.0), 1–33, 2023.

Nitzbon, J., Westermann, S., Langer, M., Martin, L. C. P., Strauss, J., Laboor, S., and Boike, J.: Fast response of cold ice-rich permafrost in northeast Siberia to a warming climate, Nat. Commun., 11, 1–11, https://doi.org/10.1038/s41467-020-15725-8, 2020.

Orangeville, L. D., Houle, D., Duchesne, L., Phillips, R. P., Bergeron, Y., and Kneeshaw, D.: Beneficial effects of climate warming on boreal tree growth may be transitory, Nat. Commun., 1–10, https://doi.org/10.1038/s41467-018-05705-4, 2018.

Ozturk, T., Turp, M. T., Türke, M., and Kurnaz, M. L.: Projected changes in temperature and precipitation climatology of Central Asia CORDEX Region 8 by using RegCM4.3.5, 183, 296–307, https://doi.org/10.1016/j.atmosres.2016.09.008, 2017.

Pan, X., Chin, M., Gautam, R., Bian, H., Kim, D., Colarco, P. R., Diehl, T. L., Takemura, T., Pozzoli, L., Tsigaridis, K., Bauer, S., and Bellouin, N.: A multi-model evaluation of aerosols over South Asia: Common problems and possible causes, Atmos. Chem. Phys., 15, 5903–5928, https://doi.org/10.5194/acp-15-5903-2015, 2015.

Pan, X., Ichoku, C., Chin, M., Bian, H., Darmenov, A., Colarco, P., Ellison, L., Kucsera, T., Da Silva, A., Wang, J., Oda, T., and Cui, G.: Six global biomass burning emission datasets: Intercomparison and application in one global aerosol model, Atmos. Chem. Phys., 20, 969–

994, https://doi.org/10.5194/acp-20-969-2020, 2020.

Pan, Y., Birdsey, R. ., Fang, J., Houghton, R., Kauppi, P. ., Kurz, W. A., Phillips, O. ., Shvidenko, A., Lewis, S. ., Canadell, J. ., Ciais, P., Jackson, R. B., Pacala, S. W., McGuire, A. D., Piao, S., Rautiainen, A., Sitch, S., and Daniel, H.: A Large and Persistent Carbon Sink in the World's Forests, Science (80-.)., 317, 4, 2007.

Pastor, J. and Post, W. M.: Influence of climate, soil moisture, and succession on forest carbon and nitrogen cycles, 3–27, 1986.

Pellegrini, A. F. A., Harden, J., Georgiou, K., Hemes, K. S., Malhotra, A., Nolan, C. J., and Jackson, R. B.: Fire effects on the persistence of soil organic matter and long-term carbon storage, Nat. Geosci., 15, https://doi.org/10.1038/s41561-021-00867-1, 2021.

Pereira, G., Siqueira, R., Rosário, N. E., Longo, K. L., Freitas, S. R., Cardozo, F. S., Kaiser, J. W., and Wooster, M. J.: Assessment of fire emission inventories during the South American Biomass Burning Analysis (SAMBBA) experiment, Atmos. Chem. Phys., 16, 6961–6975, https://doi.org/10.5194/acp-16-6961-2016, 2016.

Peterson, D.L. and Ryan, K.C. (1986) 'Modeling postfire conifer mortality for long-range planning', *Environmental Management*, 10(6), pp. 797–808. Available at: https://doi.org/10.1007/BF01867732.

Petrenko, M., Kahn, R., Chin, M., Soja, A., Kucsera, T., and Harshvardhan: The use of satellite-measured aerosol optical depth to constrain biomass burning emissions source strength in the global model GOCART, J. Geophys. Res. Atmos., 117, https://doi.org/10.1029/2012JD017870, 2012.

Petrenko, M., Kahn, R., Chin, M., and Limbacher, J.: Refined Use of Satellite Aerosol Optical Depth Snapshots to Constrain Biomass Burning Emissions in the GOCART Model, J. Geophys. Res. Atmos., 122, 10,983-11,004, https://doi.org/10.1002/2017JD026693, 2017.

Pickett, S. T., Wu, J., and Cadenasso., M. L.: Patch dynamics and the ecology of disturbed ground: a framework for synthesis., Ecosyst. Disturb. Gr., 707–722, 1999.

Popovicheva, O., Kistler, M., Kireeva, E., Persiantseva, N., Timofeev, M., Kopeikin, V., and Kasper-Giebl, A.: Physicochemical characterization of smoke aerosol during large-scale wildfires: Extreme event of August 2010 in Moscow, Atmos. Environ., 96, 405–414, https://doi.org/10.1016/j.atmosenv.2014.03.026, 2014.

Pörtner, H.-O., Roberts, D. C., Adams, H., Adelekan, I., Adler, C., Adrian, R., Aldunce, P., Ali, E., Begum, R. A., BednarFriedl, B., Kerr, R. B., Biesbroek, R., Birkmann, J., Bowen, K., Caretta, M. A., Carnicer, J., Castellanos, E., Cheong, T. S., Chow, W., Cissé, G., Clayton, S., Constable, A., Cooley, S. R., Costello, M. J., Craig, M., Cramer, W., Dawson, R., Dodman, D., Efitre, J., Garschagen, M., Gilmore, E. A., Glavovic, B. C., Gutzler, D., Haasnoot, M., Harper, S., Hasegawa, T., Hayward, B., Hicke, J. A., Hirabayashi, Y., Huang, C., Kalaba, K., Kiessling, W., Kitoh, A., Lasco, R., Lawrence, J., Lemos, M. F., Lempert, R., Lennard, C., Ley, D., Lissner, T., Liu, Q., Liwenga, E., Lluch-Cota, S., Löschke, S., Lucatello, S., Luo, Y., Mackey, B., Mintenbeck, K., Mirzabaev, A., Möller, V., Vale, M. M., Morecroft, M. D., Mortsch, L., Mukherji, A., Mustonen, T., Mycoo, M., Nalau, J., New, M., Okem, A., Ometto, J. P., O'Neill, B., Pandey, R., Parmesan, C., Pelling, M., Pinho, P. F., Pinnegar, J.,

Poloczanska, E. S., Prakash, A., Preston, B., Racault, M.-F., Reckien, D., Revi, A., Rose, S. K., Schipper, E. L. F., Schmidt, D. N., Schoeman, D., Shaw, R., Simpson, N. P., Singh, C., Solecki, W., Stringer, L., Totin, E., Trisos, C. H., Trisurat, Y., Aalst, M. van, Viner, D., M.Wairiu, R.Warren, P.Wester, et al.: Technical Summary of IPCC Sixth Assessment Report, 35–74 pp., 2022.

Pyne, S.J., Andrews, P.L. and Laren, R.D. (1996) 'Introduction to Wildland Fire'. Canada: John Wiley & Sons, Inc.

Qiu, C., Ciais, P., Zhu, D., Guenet, B., Chang, J., Chaudhary, N., Kleinen, T., Li, X. Y., Müller, J., Xi, Y., Zhang, W., Ballantyne, A., Brewer, S. C., Brovkin, V., Charman, D. J., Gustafson, A., Gallego-Sala, A. V., Gasser, T., Holden, J., Joos, F., Kwon, M. J., Lauerwald, R., Miller, P. A., Peng, S., Page, S., Smith, B., Stocker, B. D., Sannel, A. B. K., Salmon, E., Schurgers, G., Shurpali, N. J., Wårlind, D., and Westermann, S.: A strong mitigation scenario maintains climate neutrality of northern peatlands, One Earth, 5, 86–97, https://doi.org/10.1016/j.oneear.2021.12.008, 2022.

Rabin, S. S., Melton, J. R., Lasslop, G., Bachelet, D., Forrest, M., Hantson, S., Kaplan, J. O., Li, F., Mangeon, S., Ward, D. S., Yue, C., Arora, V. K., Hickler, T., Kloster, S., Knorr, W., Nieradzik, L., Spessa, A., Folberth, G. A., Sheehan, T., Voulgarakis, A., Kelley, D. I., Colin Prentice, I., Sitch, S., Harrison, S., and Arneth, A.: The Fire Modeling Intercomparison Project (FireMIP), phase 1: Experimental and analytical protocols with detailed model descriptions, Geosci. Model Dev., 10, 1175–1197, https://doi.org/10.5194/gmd-10-1175-2017, 2017.

Randerson, J. T., Liu, H., Flanner, M. G., Chambers, S. D., Jin, Y., Hess, P. G., Pfister, G., Mack, M. C., Treseder, K. K., Welp, L. R., Chapin, F. S., Harden, J. W., Goulden, M. L., Lyons, E., Neff, J. C., Schuur, E. A. G., and Zender, C. S.: The impact of boreal forest fire on climate warming, Science (80-.)., 314, 1130–1132, https://doi.org/10.1126/science.1132075, 2006.

Randerson, J. T., Chen, Y., Van Der Werf, G. R., Rogers, B. M., and Morton, D. C.: Global burned area and biomass burning emissions from small fires, J. Geophys. Res. G Biogeosciences, 117, https://doi.org/10.1029/2012JG002128, 2012.

Reddington, C. L., Spracklen, D. V., Artaxo, P., Ridley, D. A., Rizzo, L. V., and Arana, A.: Analysis of particulate emissions from tropical biomass burning using a global aerosol model and long-term surface observations, Atmos. Chem. Phys., 16, 11083–11106, https://doi.org/10.5194/acp-16-11083-2016, 2016.

Reinhardt, E. D., Keane, R. E., and Brown, J. K.: First order fire effects model: FOFEM 4.0, user's guide, USDA For. Serv. Intermt. Res. Stn., INT-GTR-344, 1997.

Richmond, A., Kaufmann, R. K., and Myneni, R. B.: Valuing ecosystem services: A shadow price for net primary production, Ecol. Econ., 64, 454–462, https://doi.org/10.1016/j.ecolecon.2007.03.009, 2007.

Ritchie, H., Roser, M., and Rosado, P.: CO2 and Greenhouse Gas Emissions, ourworldindata.org, 2020.

Romanov, A. A., Tamarovskaya, A. N., Gusev, B. A., Leonenko, E. V., Vasiliev, A. S., and

Krikunov, E. E.: Catastrophic PM2.5 emissions from Siberian forest fires: Impacting factors analysis, Environ. Pollut., 306, https://doi.org/10.1016/j.envpol.2022.119324, 2022.

Romps, D.M., Seeley, J.T., Vollaro, D. and Molinari, J. (2014) 'Projected increase in lightning strikes in the united states due to global warming', *Science*, 346(6211), pp. 851–854. Available at: https://doi.org/10.1126/science.1259100.

Rothermell, R. C.: A Mathematical Model for Predicting Fire Spread, United States Dep. Agric. For. Serv. Res. Pap., 46, 1972.

Running, S. W.: GLOBAL ARIDIFICATION AND THE DECLINE OF NPP: A COMMENTARY on Projected increases in global terrestrial net primary productivity loss caused by drought under climate change by Dan Cao, Jiahua Zhang, Jiaqi Han, Tian Zhang, Shanshan Yang, Jingwen Wang, Foyez, Earth's Futur., 10, 1–3, https://doi.org/10.1029/2022EF003113, 2022.

Santoro, M. and Cartus, O.: ESA Biomass Climate Change Initiative (Biomass_cci): Global datasets of forest above-ground biomass for the years 2010, 2017 and 2018, v3, https://doi.org/http://dx.doi.org/10.5285/5f331c418e9f4935b8eb1b836f8a91b8, 2021.

Santoro, M., Cartus, O., Carvalhais, N., Rozendaal, D. M. A., Avitabile, V., Araza, A., De Bruin, S., Herold, M., Quegan, S., Rodríguez-Veiga, P., Balzter, H., Carreiras, J., Schepaschenko, D., Korets, M., Shimada, M., Itoh, T., Moreno Martínez, Á., Cavlovic, J., Gatti, R. C., Da Conceição Bispo, P., Dewnath, N., Labrière, N., Liang, J., Lindsell, J., Mitchard, E. T. A., Morel, A., Pacheco Pascagaza, A. M., Ryan, C. M., Slik, F., Vaglio Laurin, G., Verbeeck, H., Wijaya, A., and Willcock, S.: The global forest above-ground biomass pool for 2010 estimated from high-resolution satellite observations, Earth Syst. Sci. Data, 13, 3927–3950, https://doi.org/10.5194/essd-13-3927-2021, 2021.

Sato, H. and Kobayashi, H.: Topography Controls the Abundance of Siberian Larch Forest, J. Geophys. Res. Biogeosciences, 123, 106–116, https://doi.org/10.1002/2017JG004096, 2018.

Sato, H., Itoh, A., and Kohyama, T.: SEIB-DGVM: A new Dynamic Global Vegetation Model using a spatially explicit individual-based approach, Ecol. Modell., 200, 279–307, https://doi.org/10.1016/j.ecolmodel.2006.09.006, 2007.

Sato, H., Kobayashi, H., and Delbart, N.: Simulation study of the vegetation structure and function in eastern Siberian larch forests using the individual-based vegetation model SEIB-DGVM, For. Ecol. Manage., 259, 301–311, https://doi.org/10.1016/j.foreco.2009.10.019, 2010.

Sato, H., Kobayashi, H., Iwahana, G., and Ohta, T.: Endurance of larch forest ecosystems in eastern Siberia under warming trends, Ecol. Evol., 6, 5690–5704, https://doi.org/10.1002/ece3.2285, 2016.

Sato, H., Kobayashi, H., Beer, C., and Fedorov, A.: Simulating interactions between topography, permafrost, and vegetation in Siberian larch forest, Environ. Res. Lett., 15, https://doi.org/10.1088/1748-9326/ab9be4, 2020.

Schacht, J., Heinold, B., Quaas, J., Backman, J., Cherian, R., Ehrlich, A., Herber, A., Ting Katty Huang, W., Kondo, Y., Massling, A., Sinha, P. R., Weinzierl, B., Zanatta, M., and Tegen, I.: The importance of the representation of air pollution emissions for the modeled

distribution and radiative effects of black carbon in the Arctic, Atmos. Chem. Phys., 19, 11159–11183, https://doi.org/10.5194/acp-19-11159-2019, 2019.

Schimel, D. S., House, J. I., Hibbard, K. A., Bousquet, P., Ciais, P., Peylin, P., Braswell, B. H., Apps, M. J., Baker, D., Bondeau, A., Canadell, J., Churkina, G., Cramer, W., Denning, A. S., Field, C. B., Friedlingstein, P., Goodale, C., Heimann, M., Houghton, R. A., Melillo, J. M., Moore, B., Murdiyarso, D., Noble, I., Pacala, S. W., Prentice, I. C., Raupach, M. R., Rayner, P. J., Scholes, R. J., Steffen, W. L., and Wirth, C.: Recent patterns and mechanisms of carbon exchange by terrestrial ecosystems, Nature, 414, 169–172, https://doi.org/10.1038/35102500, 2001.

Schoennagel, T., Balch, J. K., Brenkert-Smith, H., Dennison, P. E., Harvey, B. J., Krawchuk, M. A., Mietkiewicz, N., Morgan, P., Moritz, M. A., Rasker, R., Turner, M. G., and Whitlock, C.: Adapt tomore wildfire in western North American forests as climate changes, Proc. Natl. Acad. Sci. U. S. A., 114, 4582–4590, https://doi.org/10.1073/pnas.1617464114, 2017.

Schultz, M. G., Heil, A., Hoelzemann, J. J., Spessa, A., Thonicke, K., Goldammer, J. G., Held, A. C., Pereira, J. M. C., and van Het Bolscher, M.: Global wildland fire emissions from 1960 to 2000, Global Biogeochem. Cycles, 22, 1–17, https://doi.org/10.1029/2007GB003031, 2008.

Schulzweida, U. (2019) 'CDO User Guide', (August). Available at: https://doi.org/10.5281/zenodo.3539275.

Schuur, E. A. G., McGuire, A. D., Schädel, C., Grosse, G., Harden, J. W., Hayes, D. J., Hugelius, G., Koven, C. D., Kuhry, P., Lawrence, D. M., Natali, S. M., Olefeldt, D., Romanovsky, V. E., Schaefer, K., Turetsky, M. R., Treat, C. C., and Vonk, J. E.: Climate change and the permafrost carbon feedback, Nature, 520, 171–179, https://doi.org/10.1038/nature14338, 2015.

Seiler, W. and Crutzen, P.: Estimates of Gross and Net Fluxes of Carbon Between, Clim. Change, 2, 207–247, 1980.

Sharma, B., Kumar, J., Ganguly, A. R., and Hoffman, F. M.: Carbon cycle extremes accelerate weakening of the land carbon sink in the late 21st century, Biogeosciences, 20, 1829–1841, https://doi.org/10.5194/bg-20-1829-2023, 2023.

Shiraishi, T., Hirata, R., and Hirano, T.: New inventories of global carbon dioxide emissions through biomass burning in 2001–2020, Remote Sens., 13, https://doi.org/10.3390/rs13101914, 2021.

Shorohova, E., Kuuluvainen, T., Kangur, A., and Jõgiste, K.: Natural stand structures, disturbance regimes and successional dynamics in the Eurasian boreal forests: A review with special reference to Russian studies, Ann. For. Sci., 66, 201–201, https://doi.org/10.1051/forest/2008083, 2009.

Shorohova, E., Kneeshaw, D., Kuuluvainen, T., and Gauthier, S.: Variability and dynamics of old- growth forests in the circumboreal zone: Implications for conservation, restoration and management, Silva Fenn., 45, 785–806, https://doi.org/10.14214/sf.72, 2011.

Shvidenko, A. and Nilsson, S.: A synthesis of the impact of Russian forests on the global carbon budget for 1961–1998, Tellus B Chem. Phys. Meteorol., 55, 391, https://doi.org/10.3402/tellusb.v55i2.16722, 2003.

Siegert, F. and Huang, S.: Large-Scale Forest Fires in Siberia Analysed by MODIS, MERIS and ASTER Multiresolution Satellite Imagery, Prociding 2004 Envisat ERS Symp. Salzburg, Austria, 2005.

Sofronov, M.A., Volokitina, A.V. and Shvidenko, A.Z. (1998) 'Wildland fires in the north of Central Siberia', *The Commonwealth Forestry Review*, 77(2), pp. 124–127.

Sparks, A. M., Kolden, C. A., Smith, A. M. S., Boschetti, L., Johnson, D. M., and Cochrane, M. A.: Fire intensity impacts on post-fire temperate coniferous forest net primary productivity, Biogeosciences, 15, 1173–1183, https://doi.org/10.5194/bg-15-1173-2018, 2018.

Stocker, M., Ladstädter, F., and Steiner, A. K.: Observing the climate impact of large wildfires on stratospheric temperature, Sci. Rep., 11, 1–11, https://doi.org/10.1038/s41598-021-02335-7, 2021.

Sun, L., Yang, L., Wang, D., and Zhang, T.: Influence of the Long-Range Transport of Siberian Biomass Burnings on Air Quality in Northeast China in June 2017, Sensors, 23, 1–13, https://doi.org/10.3390/s23020682, 2023.

Teakles, A. D., So, R., Ainslie, B., Nissen, R., Schiller, C., Vingarzan, R., McKendry, I., Marie Macdonald, A., Jaffe, A. D., Bertram, K. A., Strawbridge, B. K., Richard Leaitch, W., Hanna, S., Toom, D., Baik, J., and Huang, L.: Impacts of the July 2012 Siberian fire plume on air quality in the Pacific Northwest, Atmos. Chem. Phys., 17, 2593–2611, https://doi.org/10.5194/acp-17-2593-2017, 2017.

Thomson, A. M., Calvin, K. V., Smith, S. J., Kyle, G. P., Volke, A., Patel, P., Delgado-Arias, S., Bond-Lamberty, B., Wise, M. A., Clarke, L. E., and Edmonds, J. A.: RCP4.5: A pathway for stabilization of radiative forcing by 2100, Clim. Change, 109, 77–94, https://doi.org/10.1007/s10584-011-0151-4, 2011.

Thonicke, K., Venevsky, S., and Sitch, S.: The role of fire disturbance for global vegetation dynamics: coupling fire into a Dynamic Global Vegetation Model, Glob. Ecol. Biogeogr., 10, 661–677, 2001.

Thonicke, K., Spessa, A., Prentice, I. C., Harrison, S. P., Dong, L., and Carmona-Moreno, C.: The influence of vegetation, fire spread and fire behaviour on biomass burning and trace gas emissions: Results from a process-based model, Biogeosciences, 7, 1991–2011, https://doi.org/10.5194/bg-7-1991-2010, 2010.

Tian, C., Yue, X., Zhu, J., Liao, H., Yang, Y., Chen, L., Zhou, X., Lei, Y., Zhou, H., and Cao, Y.: Projections of fire emissions and the consequent impacts on air quality under 1.5 °C and 2 °C global warming, Environ. Pollut., 323, 121311, https://doi.org/10.1016/j.envpol.2023.121311, 2023.

Trenberth, K. E., P.D., J., P., A., R., B., D., E., A. Klein, T., D., P., F., R., J.A., R., M., R., B., S., and P., Z.: Observations: Surface and Atmospheric Climate, Clim. Chang. 2007 Phys. Sci. Basis, 2007.

University of East Anglia Climatic Research Unit; Harris, I.C.; Jones, P. D.: CRU TS3.22: Climatic Research Unit (CRU) Time-Series (TS) Version 3.22 of High Resolution Gridded Data of Month-by-month Variation in Climate (Jan. 1901- Dec. 2013), https://doi.org/https://dx.doi.org/10.5285/18BE23F8-D252-482D-8AF9-5D6A2D40990C,

2014.

Végh, L. and Kato, T.: Modified SEIB-DGVM enables simulation of masting in a temperate forest, Ecol. Modell., 488, https://doi.org/10.1016/j.ecolmodel.2023.110577, 2024.

Ward, D. E. and Hardy, C. C.: Smoke emissions from wildland fires, Environ. Int., 17, 117–134, https://doi.org/10.1016/0160-4120(91)90095-8, 1991.

Webb, E. E., Alexander, H. D., Paulson, A. K., Loranty, M. M., DeMarco, J., Talucci, A. C., Spektor, V., Zimov, N., and Lichstein, J. W.: Fire-Induced Carbon Loss and Tree Mortality in Siberian Larch Forests, Geophys. Res. Lett., 51, https://doi.org/10.1029/2023GL105216, 2024.

Van Der Werf, G. R., Randerson, J. T., Giglio, L., Collatz, G. J., Kasibhatla, P. S., and Arellano, A. F.: Interannual variability in global biomass burning emissions from 1997 to 2004, Atmos. Chem. Phys., 6, 3423–3441, https://doi.org/10.5194/acp-6-3423-2006, 2006.

Van Der Werf, G. R., Randerson, J. T., Giglio, L., Collatz, G. J., Mu, M., Kasibhatla, P. S., Morton, D. C., Defries, R. S., Jin, Y., and Van Leeuwen, T. T.: Global fire emissions and the contribution of deforestation, savanna, forest, agricultural, and peat fires (1997-2009), Atmos. Chem. Phys., 10, 11707–11735, https://doi.org/10.5194/acp-10-11707-2010, 2010.

Van Der Werf, G. R., Randerson, J. T., Giglio, L., Van Leeuwen, T. T., Chen, Y., Rogers, B. M., Mu, M., Van Marle, M. J. E., Morton, D. C., Collatz, G. J., Yokelson, R. J., and Kasibhatla, P. S.: Global fire emissions estimates during 1997-2016, Earth Syst. Sci. Data, 9, 697–720, https://doi.org/10.5194/essd-9-697-2017, 2017.

Venevsky, S., Thonicke, K., Sitch, S. and Cramer, W. (2002) 'Simulating fire regimes in human-dominated ecosystems: Iberian Peninsula case study', *Global Change Biology*, 8(10), pp. 984–998. Available at: https://doi.org/10.1046/j.1365-2486.2002.00528.x.

Viegas, D.X., Viegas, T.S.P. and Ferreira, D. (1992) 'Moisture content of fine forest fuels and fire occurrence in central portugal', *International Journal of Wildland Fire*, 2(2), pp. 69–86. Available at: https://doi.org/10.1071/WF9920069.

Westerling, A. L., Hidalgo, H. G., Cayan, D. R., and Swetnam, T. W.: Warming and earlier spring increase Western U.S. forest wildfire activity, Science (80-.)., 313, 940–943, https://doi.org/10.1126/science.1128834, 2006.

Whelan, R. J.: The ecology of fire-developments since 1995 and outstanding questions, Proc. R. Soc. Queensl., 115, 59–68, 2009.

Williams, R.J., Gill, A.M. and Moore, P.H.R. (1998) 'Seasonal changes in fire behaviour in a tropical savanna in Northern Australia', *International Journal of Wildland Fire*, 8(4), pp. 227–239. Available at: https://doi.org/10.1071/WF9980227.

Wilson, R.A. (1982) 'A Reexamination of Fire Spread in Free-Burning Porous Fuel Beds', *United States Department of Agriculture, Forest Service* [Preprint].

Winiger, P., Andersson, A., Eckhardt, S., Stohl, A., Semiletov, I. P., Dudarev, O. V., Charkin, A., Shakhova, N., Klimont, Z., Heyes, C., and Gustafsson, Ö.: Siberian Arctic black carbon sources constrained by model and observation, Proc. Natl. Acad. Sci. U. S. A., 114, E1054–E1061, https://doi.org/10.1073/pnas.1613401114, 2017.

Wotton, B. M., Flannigan, M. D., and Marshall, G. A.: Potential climate change impacts on fire intensity and key wildfire suppression thresholds in Canada, Environ. Res. Lett., 12, 13, 2017.

Wu, L., Kato, T., Sato, H., Hirano, T., and Yazaki, T.: Sensitivity analysis of the typhoon disturbance effect on forest dynamics and carbon balance in the future in a cool-temperate forest in northern Japan by using SEIB-DGVM, For. Ecol. Manage., 451, 117529, https://doi.org/10.1016/j.foreco.2019.117529, 2019.

Xu, W., Scholten, R.C., Hessilt, T.D., Liu, Y. and Veraverbeke, S. (2022) 'Overwintering fires rising in eastern Siberia', *Environmental Research Letters*, 17(4). Available at: https://doi.org/10.1088/1748-9326/ac59aa.

Yasunari, T. J., Narita, D., Takemura, T., Wakabayashi, S., and Takeshima, A.: Comprehensive Impact of Changing Siberian Wildfire Severities on Air Quality, Climate, and Economy: MIROC5 Global Climate Model's Sensitivity Assessments, Earth's Futur., 12, https://doi.org/10.1029/2023EF004129, 2024.

Yuan, Z., Wang, Y., Xu, J., and Wu, Z.: Effects of climatic factors on the net primary productivity in the source region of Yangtze River, China, Sci. Rep., 11, 1–11, https://doi.org/10.1038/s41598-020-80494-9, 2021.

Zhang, F., Wang, J., Ichoku, C., Hyer, E. J., Yang, Z., Ge, C., Su, S., Zhang, X., Kondragunta, S., Kaiser, J. W., Wiedinmyer, C., and Da Silva, A.: Sensitivity of mesoscale modeling of smoke direct radiative effect to the emission inventory: A case study in northern sub-Saharan African region, Environ. Res. Lett., 9, https://doi.org/10.1088/1748-9326/9/7/075002, 2014.

Zheng, B., Ciais, P., Chevallier, F., Chuvieco, E., Chen, Y., and Yang, H.: Increasing forest fire emissions despite the decline in global burned area, Sci. Adv., 7, https://doi.org/10.1126/sciadv.abh2646, 2021.